Manipulating the Conformational Landscape of Large Macromolecular Complexes

Dissertation

for the award of the degree
"Doctor rerum naturalium" (Dr. rer. nat.)
of the Georg-August-Universität Göttingen

within the doctoral program
Biomolecules: Structure – Function – Dynamics
of the Göttingen Graduate School for Neurosciences,
Biophysics and Molecular Biosciences (GGNB)

submitted by
Benjamin Moritz Graf
from Karlsruhe, Germany

Göttingen 2022

Thesis Advisory Committee members:

Prof. Dr. Holger Stark
Structural Dynamics, Max-Planck-Institut für Biophysikalische Chemie, Göttingen

Prof. Dr. Kai Tittmann
Molecular Enzymology, Göttinger Zentrum für Molekulare Biowissenschaften (GZMB)

Prof. Dr. Henning Urlaub
Bioanalytical Mass Spectrometry, Max-Planck-Institut für Biophysikalische Chemie / Universitätsmedizin Göttingen (UMG), Göttingen

Members of the Examination Board

1st Referee: Prof. Dr. Holger Stark
Structural Dynamics, Max-Planck-Institut für Biophysikalische Chemie (MPI-BPC), Göttingen

2nd Referee: Prof. Dr. Kai Tittmann
Molecular Enzymology, Göttinger Zentrum für Molekulare Biowissenschaften (GZMB)

Further members of the Examination Board

Prof. Dr. Henning Urlaub
Bioanalytical Mass Spectrometry, Max-Planck-Institut für Biophysikalische Chemie / Universitätsmedizin Göttingen (UMG), Göttingen

Dr. Ashwin Chari
Structural Biochemistry and Mechanisms, Max-Planck-Institut für Biophysikalische Chemie, Göttingen

Dr. Alexander Stein
Membrane Protein Biochemistry, Max-Planck-Institut für Biophysikalische Chemie, Göttingen

Dr. Alex Faesen
Biochemistry of Signal Dynamics, Max-Planck-Institut für Biophysikalische Chemie, Göttingen

Date of oral examination: 01.04.2022

Affidavit

I hereby declare that this dissertation with the title “Manipulating the Conformational Landscape of Large Macromolecular Complexes” has been written independently and with no other aids or sources than quoted. This thesis (wholly or in part) has not been submitted elsewhere for any academic award or qualification.

_____

Benjamin Moritz Graf

Abstract

De novo synthesis of fatty acids is one of the most central metabolic pathways in all forms of life. Among all known organisms, fatty acids are highly essential. Besides their role as energy resource, they are also required to maintain cellular growth, signal transduction processes and as main building block of biological membranes. Konrad Bloch and Feodor Lynen already described the metabolism of fatty acids in the early 1960s. Despite so many years of research surprisingly little is known about the enzymatic reactions involved in this process. In evolution two different fatty acid synthase (FAS) systems have evolved. Both generate fully saturated fatty-acyl chains. The type II system which can be found in plants, mitochondria, and most bacteria consists of different individual proteins. Other than that, the type I system of CMN-bacteria, higher metazoans, and fungi is a single large macromolecular protein complex that contains all required enzymatic domains. Within both systems, the growing fatty acyl chain is covalently bound to an acyl carrier protein (ACP) which mediates the transport between the different enzymatic domains. To ensure a complete processing of the covalent bound substrate, the ACP domain undergoes a highly dynamic process to interact with all distinct enzymatic domains. These ACP-enzyme interactions are transient which makes them infeasible for structure determination. However, detailed structural information of these ACP-enzyme interactions is necessary to elucidate the underlying biocatalytic mechanisms and their regulation on a molecular level. For the E. coli system other groups already successfully developed a biochemical tool that allows the specific trapping of substrate-bound ACP-enzyme interactions. Using X-ray crystallography, they managed to solve the structure of such normally transient interactions.

Within this thesis, the strategy described for the *E. coli* system was successfully transferred to the type I FAS system of the baker's yeast *Saccharomyces cerevisiae.* With a structure that shows the substrate-bound intermediate state of the transient ACP-keto synthase interaction we could proof, that this biochemical tool can also be applied to macromolecular eukaryotic FAS systems. Furthermore, the structure of this intermediate state provides an insight into the substrate binding and chain-length control mechanism within the keto synthase domain. A direct comparison with the bacterial homologue, the AcpP-FabB complex revealed several similarities between both systems. Additionally, the development of a chromatography-free purification protocol for the yeast FAS allowed us the discovery of a novel, yet unknown third subunit of the FAS complex. Structural and enzyme kinetic methods revealed that the newly discovered γ-subunit plays a role in the kinetic regulation of the FAS. The binding of the γ-subunit to the FAS molecule stabilizes a structural rearrangement of the overall complex from a non-rotated to a rotated state. In combination with steady-state enzyme kinetic measurements we showed that the γ-subunit binding regulates the NADPH turnover by inducing a kinetic hysteresis effect and suppresses an uncontrolled futile cycle reaction at the FMN-bound enoyl reductase domain. Moreover, with the help of two amino acid sequences deriving from the γ-subunit we managed to incorporate different

single proteins into the FAS complex. This reveals the potential of the γ-subunit as a biotechnological tool that could be used introduce additional fatty acyl specific activities into the FAS complex.

Acknowledgements

With the submission of this thesis, I reach another station of a journey that I started more than ten years ago at the beautiful Lake Constance. After a wonderful childhood and youth at the foot of the Black Forest, I had decided to follow the path of a scientist.

So first of all, I would like to thank my family and closest friends. Without you I would never have had the opportunity to go this way and become the person I am. Thank you, Mama. Thank you, Papa. Thank you for always removing all the obstacles and supporting me in every phase of my life. Thank you for teaching me to become a respectful, humble, sincere, and happy person. Thank you, Theresa, for being the best sister one could have. Thank you, Angelika, and Wolfgang. You have always believed in me. You always gave me support and backing. Thanks to all the Garagicrew Members. I think without any of you my youth would have never been that fun and unforgettable.

Thank you, Annie. Without the decision of becoming a scientist we would probably never have met. You are the person who gives me unconditional support and sustains me even in the most difficult phases. I can't wait to start the next journey of my life together with you. I love you.

To Ashwin, thank you for giving me your trust and teaching me so many things. Thank you, for spending hours and hours of discussing exciting ideas as well as questionable results. Thank you for giving me the opportunity to learn from you and for teaching me how to become a seasoned scientist. The opportunities that you and Holger have built for us scientists are incredible.

To Holger, thank you for giving me the opportunity to become a member of this wonderful group. Thank you, for making it possible to build up such a great environment and playground for scientists. When I first met you six years ago, I immediately felt welcome and in good hands. Even as a Badenser in a Swabian household.

To Kashish, thank you for the great cooperation and for the opportunity to learn from you during my first steps. Without our friendly relationship, constant exchange of ideas and experiences, the whole project would not have been possible at all.

To Suzan, thank you for the great support in the lab. Without your help it would have never been possible to address so many different questions at the same time.

To Kai, Fabian, Viktor, Lisa, and Sabin, thank you for the great collaboration. Working with you was very enriching and I always felt welcome when I entered your department.

To Henning, Andreas and Meina, thank you for the opportunity to clarify and address all the upcoming questions that we could have never answered ourselves.

To Elham, thank you for being a great and supportive contact for all kinds of upcoming questions and ideas that came to my mind while working on my bench.

To the whole group. Georg, Claudia, Niels, Gaby, Tobi, Mario, Alexey, Juliane, Valek, Dietmar, Leonie, Suzan, Dirk, Ka Man, Zhenwei, Cole, Fabian, Alex, Kashish, Karl, David, Steffi, Erik, Uma, Anna, Thomas, Aybeg, Kami. Thank you for the support, the great times, and the nice environment. Even during hard times as an PhD student I always felt comfortable to work with all of you.

„Bildung ist das, was übrig bleibt, wenn man alles vergessen hat, was man gelernt hat.“
(Werner Heisenberg)

Table of Contents

List of Tables

List of Figures

Introduction

1.1 The Role of Fatty Acids in Life

One of the most central and ubiquitous metabolic processes in nature is the metabolism of fatty acids. Within cells they can have manifold functions like the metabolic energy storage in the form of triacylglycerols, as precursor for the synthesis of signaling molecules like prostaglandins and as components of the phospholipid bilayer in the biological membranes (Medes et al., 1953; Sumida et al., 1993; Warburg, 1924). In all forms of life, they are known to play a role in at least one of the aforementioned processes and are thus indispensable for cell growth and survival. While metazoans only require their own fatty acid (FA) biosynthesis during embryogenesis and milk production in mammary glands, the *de novo* FA synthesis of bacteria, plants and fungi was shown to be essential during their whole lifetime (Brown et al., 2009; Chirala et al., 2003; Dibrova et al., 2014; Suburu et al., 2014).

Usually, metazoans can fulfill their fatty acid requirements by dietary uptake. An uncontrolled additional *de novo* production of fatty acids can lead to diseases such as the non-alcoholic fatty liver disease (NAFLD), obesity, and various forms of cancer (Jensen-Urstad and Semenkovich, 2012; Medes et al., 1953; Ookhtens et al., 1984; Warburg, 1924; Wu et al., 2011). Apart from their biological significance, fatty acids and their derivatives are of growing biotechnological and industrial interest. For example, the production of sustainable biofuels and fatty acid based oleochemicals for the chemical industry. Also, the broadly used palm oil and precursors for synthetic plastics are based on the biosynthetic production of saturated fatty acid chains. Some of these precursors can already be biotechnologically produced in bacteria, plants or fungi (Ducat et al.; Murphy, 1996; Sheng and Feng, 2015; Wijffels et al.; Zhou et al., 2016).

1.2 Fatty Acid Synthesis

The basic principle governing the *de novo* synthesis of fully saturated fatty acid chains remains the same for all organisms and organelles. Besides the two substrates acetyl coenzyme A (acetyl-CoA) and malonyl-CoA, the reaction requires the coenzyme nicotinamide adenine dinucleotide (phosphate) (NAD(P)H) as reducing equivalent. While acetyl-CoA is a ubiquitous substrate which is used in various metabolic reactions, malonyl-CoA is exclusively used in fatty acid synthesis. The process of fatty acid synthesis starts with a committed step in which the acetyl-CoA carboxylase (ACC) carboxylates one molecule of acetyl-CoA to produce one molecule of malonyl-CoA. The assembly of several malonyl-CoA molecules to a continuous hydro-carbon chain is catalyzed by different enzymes of the fatty acid synthase (FAS) system. A priming acetyl-group deriving from acetyl-CoA is elongated by addition of malonyl-residues from malonyl-CoA, followed by subsequent condensation, dehydration and reducing reactions. The final product of this iterative cyclic process is a fully reduced fatty acyl chain (Dietlein and Schweizer, 1975; Wakil et

al., 1964). Depending on the organism or organelle, different types of FAS systems are known. Plants, most bacteria and mitochondria rely on individual enzymes (*Figure 0.1 A*) catalyzing the different chain-elongation steps, which is denoted as the type II system (Toomey and Wakil, 1966; White et al., 2005). Metazoans, yeasts, and fungi, as well as Corynebacteria, Mycobacteria and Nocardia (CMN-bacteria) use the type I system. The type I FAS is a single macromolecular complex harboring all required enzymatic active sites for the *de novo* fatty acid synthesis (Lynen et al., 1980; Schweizer and Hofmann, 2004a). Structural investigations of the mammalian FAS revealed a X-shaped architecture (*Figure 0.1 B*) consisting of an intertwined homodimer of 540 kDa. The type I FAS from CMN-bacteria and yeast is a large ~2.6 MDa barrel-shaped molecule (*Figure 0.1 C*) (Elad et al., 2018; Leibundgut et al., 2007; Lomakin et al., 2007; Maier et al., 2008).

Although, the different FAS systems have revealed fundamental differences in their overall structure and assembly, all of them rely on a small acyl carrier protein (ACP) domain that mediates the transport of the growing fatty acyl chain to the different enzymatic domains. Therefore, the acyl chain substrate is covalently bound to the ACP (Smith and Sherman, 2008).

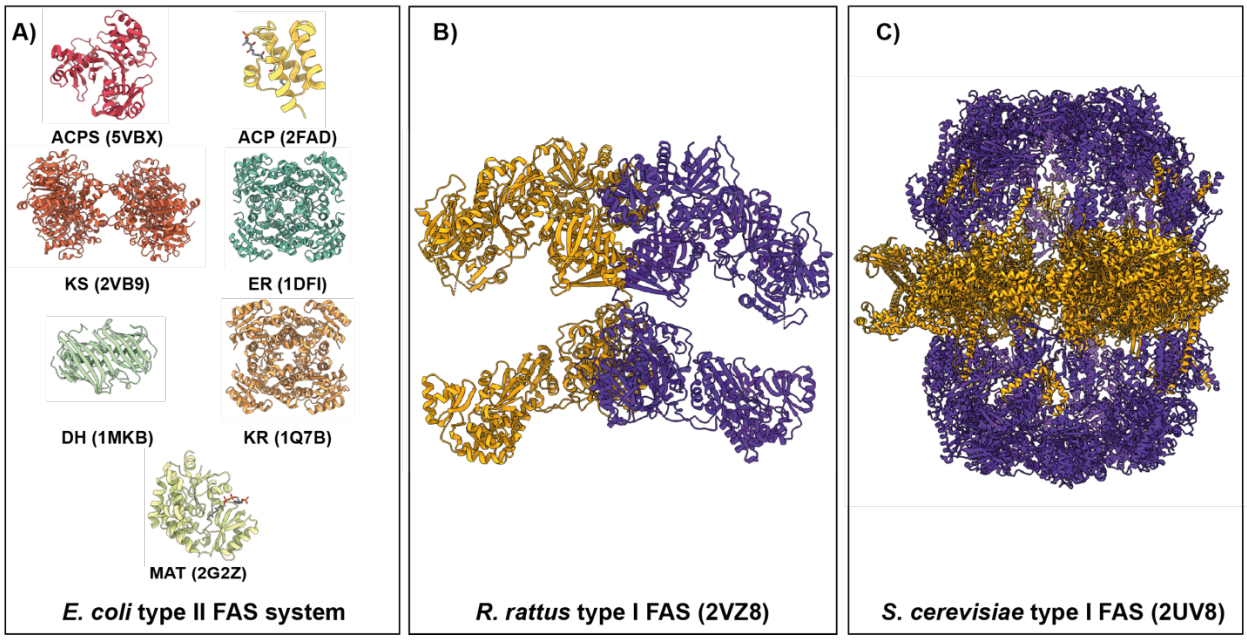

Figure 0.1: Structure of Fatty Acid Synthases. A) *Crystal structures of the individual enzymes from the bacterial E. coli type II fatty acid synthase system.* ***B)*** *Crystal structure of the mammalian (R. rattus) type I fatty acid synthase system (PDB: 2VZ8).* ***C)*** *Crystal structure of the yeast (S. cerevisiae) type I fatty acid synthase system (PDB: 2UV8).*

1.3 Structure of the Yeast Fatty Acid Synthase

Although it was known since the late 1970s that the yeast FAS is a large heterododecameric complex consisting of six α-chains and six β-chains, it took until 2007 until the first structure was solved by two independent groups (Leibundgut et al., 2007; Lomakin et al., 2007; Lynen et al., 1980; Schweizer and Hofmann, 1990; WIELAND et al., 1979). The α-chain (207 kDa) harbors the sequences of the ACP, the ketoacyl reductase (KR), the keto synthase (KS), the phosphopantetheinyl transferase (PPTase) domains, and a small part of the malonyl-palmitoyl transferase (MPT) domain. The β-chain (230 kDa) encodes for the main part of the MPT domain,

as well the acetyltransferase (AT), the enoyl reductase (ER), and the dehydratase (DH) domains (*Figure 0.2 B, left*). The overall appearance of the fully assembled complex is a barrel-shaped molecule with a three-fold radial and a two-fold equatorial symmetry axis, 250 Å in width and 270 Å in height (*Figure 0.2 A*). The barrel-like structure is formed by two half-domes each built of three β-chains and connected via an equatorial central wheel of six α-chains. This central wheel subdivides the inner cavity between the two half-domes into a lower and an upper part. Within each half-dome, three ACP-domains are located. Each of these ACP domains has access to the sixactive sites for the priming, elongation, and termination steps of iterative fatty acyl chain synthesis (*Figure 0.2 B, middle*). One ACP, together with its six accessible active sites is termed as a reaction chamber (*Figure 0.2 B, right)*. Each yeast FAS molecule contains six reaction chambers, three in each half-dome. To ensure the accessibility of the ACP to all active sites within a reaction chamber, the ACP domain is attached to flexible linker arms. After complex assembly, all active sites except those of the PPTase domain are located inside the inner cavity/reaction chamber and thus can be reached by dynamic movements of the ACP (Leibundgut et al., 2007; Lomakin et al., 2007).

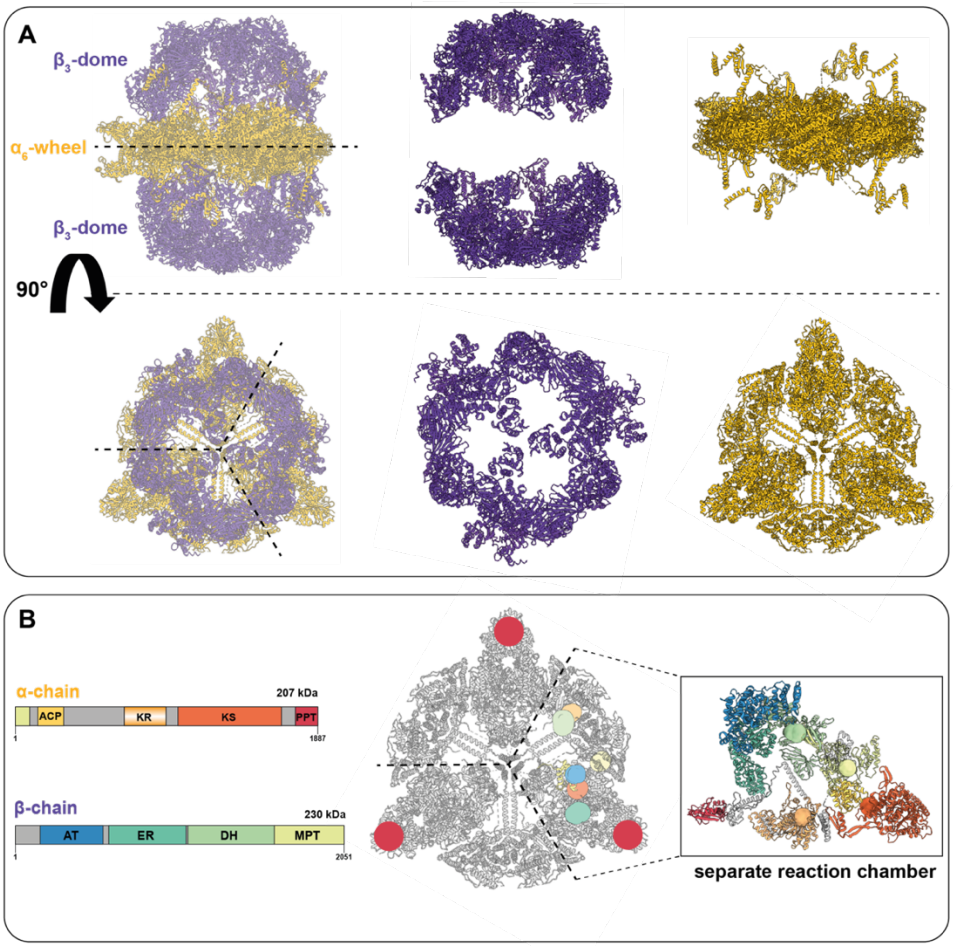

Figure 0.2: Overview of the yeast FAS complex. A) *Dissection of the yeast FAS dome into the central wheel (yellow) and the two outer domes (purple) in top and sideview.* ***B)*** *Location of the different enzymatic domains within the alpha-chain (left, yellow) and beta-chain (left, purple) and within the assembled FAS molecule. The active sites of the different domains are highlighted in the same colors as used for the alpha- and beta-chain. In the right box, one of the six reaction chambers (functional unit) with all catalytic active sites for the fatty acyl elongation is extracted.*

1.4 Fatty Acid Synthesis in Yeast

1.4.1 Production of malonyl-CoA by the acetyl-CoA carboxylase

Chain elongation in fatty acid synthesis is mediated by the condensation of single malonyl-CoA molecules. These malonyl-CoA molecules are produced by carboxylation of acetyl-CoA within the acetyl-CoA carboxylase (ACC) (*Figure 0.3*). Under consumption of one molecule adenosine triphosphate (ATP) the ACC transfers a CO_2 molecule from hydrogen carbonate to acetyl-CoA. In all organisms this reaction is the committed step for the fatty acid synthesis. In eukaryotes the ACC complex consists of a biotin carboxylase (BC) domain, a flexible biotin carboxyl carrier protein (BCCP) and carboxyl transferase (CT) domain. (Cronan and Waldrop, 2002). In the first ATP consuming step, the prosthetic biotin moiety of BCCP is carboxylated by the BC-domain, resulting in a carboxybiotin intermediate. The BCCP-carboxybiotin is then transferred to the CT-domain. At the CT active site the activated carboxylic group is transferred to an acetyl-CoA molecule, resulting in the release of one molecule malonyl-CoA (Alberts et al., 1968). Genetic and structural studies of the yeast ACC complex have shown that the enzymatic active complex is a homodimer of two 250 kDa polypeptide chains, which are encoded in the ACC1 gene (Hasslacher et al., 1993; Wei and Tong, 2015).

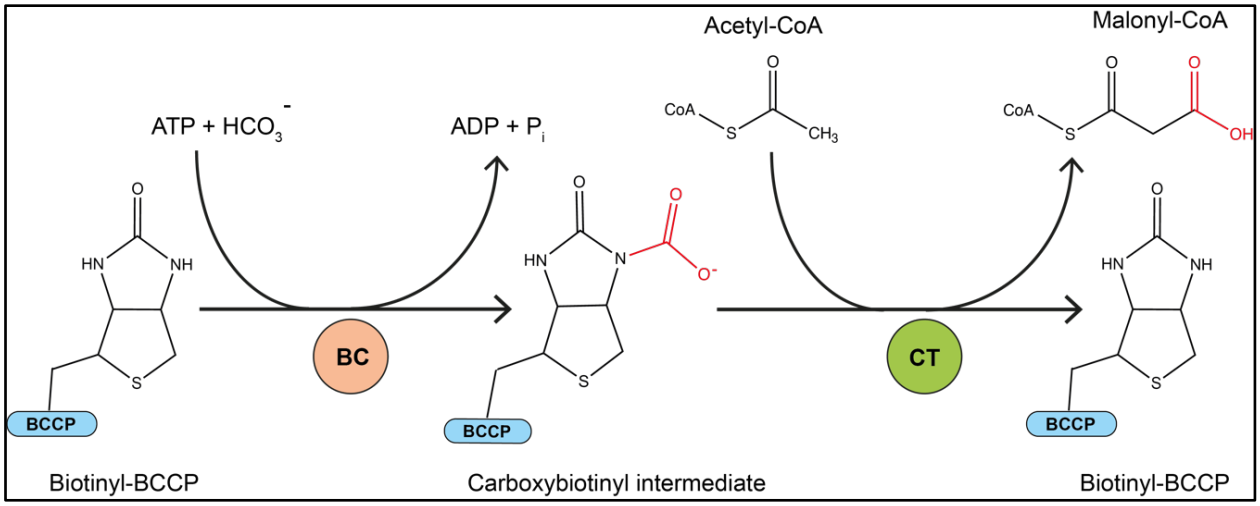

Figure 0.3: Acetyl-CoA-Carboxylase reaction. *The prosthetic biotinyl group at the BCCP domain (blue) is carboxylated by the biotin carboxylase domain (orange) under consumption of ATP. A translocation of the BCCP domain with the carboxybiotinyl intermediate to the carboxyl transferase domain (green) induces the transfer of the activated carboxylic group to its substrate acetyl-CoA, resulting in the release of malonyl-CoA.*

1.4.2 Activation of the Acyl Carrier Protein

Like all FAS systems, also the yeast type I system relies on the shuttling of the growing fatty acyl chain to its different enzymatic domains by the ACP. Former studies have shown that the fatty acyl chain is covalently bound to a prosthetic 4'-phosphopantetheine arm (PPant) of the ACP domain (Chan et al., 2010). The PPant is essential for the activity of the ACP and derives from

CoA. This post-translational activation reaction is catalyzed by the acyl carrier synthase (AcpS) in *E. coli* and by the phosphopantetheinyl transferase (PPTase) domain of the type I FAS in yeast. In all organism, the PPant is transferred to a highly conserved serine residue of the ACP. Prior to this activation reaction the ACP is inactive (apo-ACP) (*Figure 0.4*). Only the post-translational activation reaction leads to the transition into an active (holo-ACP) form. The free sulfhydryl group of the PPant allows the covalent attachment of a fatty acyl chain to the holo-ACP molecule. Thus, this activation reaction is crucial for the enzymatic activity and only activated holo-ACP molecules can contribute to the fatty acid synthesis in both FAS systems (Crosby and Crump, 2012; Mindrebo et al., 2020a).

In yeast the PPTase domain is part of the hexameric central wheel and located outside of the FAS molecule (*Figure* 0.2 *B*). Structural and enzyme kinetic studies suggest that the PPTase domain only shows enzymatic activity when it is assembled in a homo-dimeric or homo-trimeric form. This multimeric arrangements of PPTase domains can only be formed prior or during the assembly of the central wheel and before the final formation of the complete FAS barrel (Fichtlscherer et al., 2000a; Fischer et al., 2020; Johansson et al., 2009a).

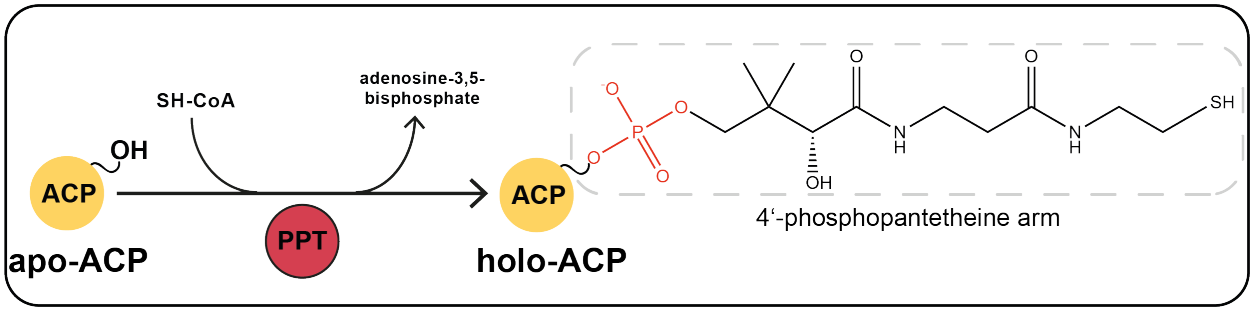

Figure 0.4: Activation reaction of the apo-ACP at the PPTase domain. *The PPant from CoA is transferred to a specific serine residue of the apo-ACP resulting in phosphopantetheinylated holo-ACP and release of adenosine-3,5-bisphosphate*

1.4.3 Iterative Fatty Acyl Chain Elongation

After the malonyl-CoA production by ACC (*Figure 0.3* and *Figure 0.5 A*), the FAS is responsible for fatty-acyl chain synthesis. In yeast, this is achieved by the 2.6 MDa type I FAS. After the ACP activation reaction, the fatty acid biosynthesis starts with a priming reaction at the sulfhydryl-group of holo-ACP. This priming reaction is catalyzed by the acetyl transferase (AT) domain (*Figure 0.5 B i*) which transfers the acetyl residue from acetyl-CoA to the free thiol group of the PPant (holo-ACP_{Ac}) (Chan et al., 2010; Schuster et al., 1995). The ACP_{Ac} transfers the acetyl group to the sulfur atom of a cysteine residue in the active site of the ketoacyl synthase (KS) domain. The resulting substrate-free holo-ACP is subsequently loaded with a malonyl residue from malonyl-CoA at the malonyl/palmitoyl transferase (MPT) domain (holo-ACP_{Mal}). After translocation back to the KS active site, the cysteine bound acetyl group is condensed with the malonyl group of the incoming holo-$ACP_{Mal.}$ Product of this reaction is a holo-ACP with a covalently bound 3-ketoacyl

chain. By further processing at three different active sites, the holo-ACP bound substrate is sequentially reduced and dehydrated. The first reduction step is performed at the ketoacyl reductase (KR) domain under consumption of one molecule NADPH resulting in β-hydroxyacyl-ACP. In the subsequent reaction at the dehydratase (DH) domain, the β-hydroxyacyl chain is dehydrated which results in α-enoylacyl-ACP. The last reaction of the chain elongation cycle is achieved by the enoyl reductase (ER) domain. In this reaction, the α-enoylacyl-ACP intermediate is further reduced under consumption of one molecule NADPH resulting in a fully saturated alky-acyl chain. The ER domain uses an additional flavin mononucleotide (FMN) as cofactor, which is specific for the type I FAS system of fungi and mycobacteria (Elad et al., 2018; Lynen, 1969; Stoops et al., 1978). After one cycle of these successive reactions, the starting product (acetyl group of acetyl-CoA; *Figure 0.5 D*) is elongated by two carbon atoms deriving from malonyl-CoA. This finally results in the production a fully saturated C4 alkyl-acyl chain attached to the holo-ACP domain (butyryl-ACP) (Oesterhelt et al., 1977; Schuster et al., 1995). For further chain elongation, the cycle starts again by addition of a new malonyl group from malonyl-CoA to butyryl-ACP in the KS active site condensation reaction (for all steps see *Figure 0.5 C*). All iterative chain elongation reactions are repeated until a fatty acyl chain length of C_{16} (palmitoyl) or C_{18} (stearoyl) is reached (*Figure 0.5 D*). For product release the alkyl-acyl chain is transferred from the PPant of ACP to the free sulfhydryl group of CoA catalyzed by the MPT domain. The resulting acyl-CoA product is released to the solvent and the empty holo-ACP domain can start with a new cycle at the AT domain with a priming reaction (Singh et al., 1985).

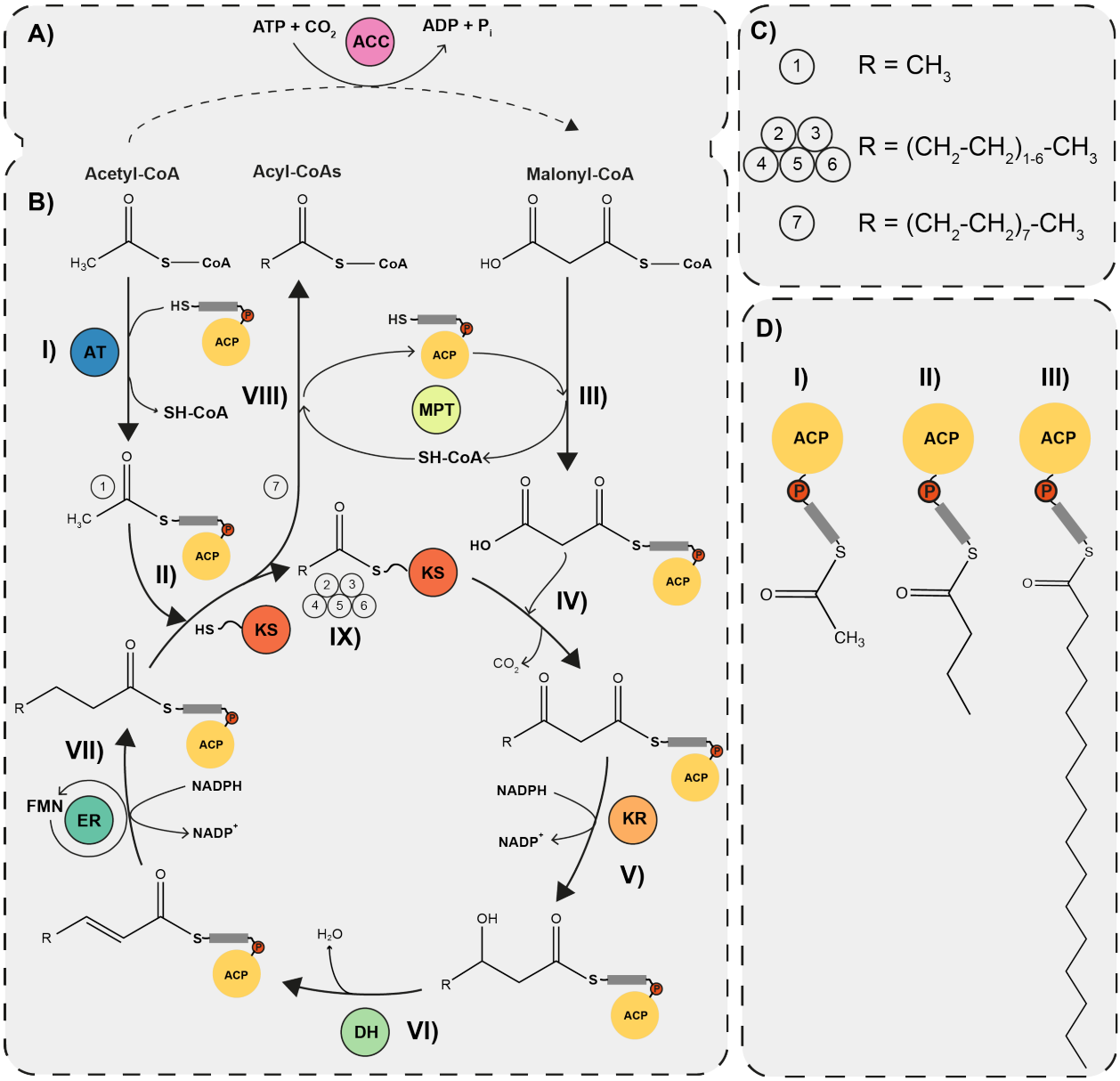

Figure 0.5: Yeast fatty acid synthesis cycle. A) *The ACC reaction is responsible for the production of malonyl-CoA. Within an ATP-dependent reaction acetyl-CoA is carboxylated resulting in the release of malonyl-CoA and ADP+P_i.* ***B)*** *Schematic representation of the iterative FAS cycle. (I) In a priming reaction at the AT-site the holo-ACP is loaded with the acetyl-residue from acetyl-CoA. (II) The acylated ACP translocates towards the KS-site, where the acyl-group is transferred to a specific cysteine residue in the KS active site. (III) At the MPT active site the malonyl-group from malonyl-CoA is loaded to the holo-ACP. After a translocation back to the KS active site (IV) the acyl-residue from the KS cysteine is condensed with the malonyl-residue of the ACP domain. (V) The resulting ACP-bound β-hydroxyacyl intermediate undergoes a first reduction step at the KR-site using NADPH as reducing equivalent. (VI) At the DH-domain a α-enoylacyl intermediate is produced by dehydration of the hydroxyacyl-ACP substrate. (VII) To end up with a fully saturated fatty acyl chain, one more reduction step is catalyzed by the ER-domain using one molecule of NADPH as reducing equivalent and FMN as cofactor. (VIII) For product release into the solvent the fatty acyl chain is transferred from the ACP domain to CoA. This reaction is also catalyzed by the MPT domain. (IX) In case of a further chain elongation, the fatty-acyl ACP enters a new elongation cycle.* ***C)*** *Sum formula of the different intermediates during the cyclic elongation reaction. The numbers indicate the total number of cyclic runs for the respective intermediate.* ***D)*** *Schematic structure of acyl-ACP (I), butanoyl-ACP (II) and palmitoyl-ACP (III).*

1.4.4 Product inhibition and product length control of FAS systems

Lynen and coworkers showed that each fatty acid synthesis cycle usually starts with a priming acetyl-CoA molecule. The growing acyl chain is sequentially elongated by addition of C_2 building blocks deriving from malonyl-CoA (Lynen, 1969). Further investigations have shown that the priming acetyl-CoA molecule can also be replaced by any acyl-CoA derivative. Depending on the chain length of the priming acyl-CoA, the enzyme activity of the FAS varies. While butyryl-CoA (C_4) resulted in a *de facto* complete inhibition, low micromolar concentrations of longer acyl-CoAs like decanoyl-CoA (C_{10}) led to similar activities like acetyl-CoA. Those findings indicate an internal acyl-CoA decarboxylation activity of the keto synthase domain within the FAS complex (Pirson et al., 1973). Apart from the ability to use different acyl-CoA derivatives as priming substrates, it was also shown that the FAS activity is strongly product chain length dependent. Addition of long chain acyl-CoAs (C_{12}-C_{18}) together with the substrates acetyl-CoA, malonyl-CoA and NADPH resulted in a strong decrease of FAS activity. This indicates product inhibition, and can be interpreted as an internal regulator of enzyme activity (Aprahamian et al., 1982; Lust and Lynen, 1968). Further detailed kinetic characterizations of FAS have shown that the substrates acetyl-CoA and malonyl-CoA, also have an inhibitory effect at micromolar concentration ranges. For all three substrates, Michaelis-Menten constants (K_m) in the lower micromolar range were reported. Notably, acetyl-CoA showed a ten times higher K_m (118 µM) than malonyl-CoA (18 µM) (Aprahamian et al., 1982).

Product analyses of different FAS systems have shown that the length of the produced acyl-CoA chains varies. In the case of yeast, *E. coli* and mammalian FAS, mainly myristoyl-CoA (C_{14}), palmitoyl-CoA (C_{16}), and stearoyl-CoA (C_{18}) where found (Tehlivets et al., 2007; Zhang et al., 2012). In yeast, a further chain elongation up to C_{26} is achieved by the elongases Elo2 and Elo3, respectively (Han et al., 2002). In contrast, the structurally homologous type I FAS from *M. tuberculosis* is able to produce acyl chains up to a length of C_{26} without any additional elongase enzymes (Schweizer and Hofmann, 2004b; Zimhony et al., 2004). Despite intensive structural and biochemical investigations, it is not fully understood how the product chain length is controlled. Since the production of fatty acids and its derivatives is of medical and biotechnological interest, a better understanding of all enzymatic reactions within the FAS system is required (Peralta-Yahya et al., 2012).

1.4.5 Acyl carrier proteins

Acyl carrier proteins are small domains with a maximum size of 100 amino acids. To date they were found to play a crucial role in two different biosynthetic pathways, the fatty acid synthesis and polyketide synthesis (PKS). While the final products of these pathways differ, their catalytic mechanism is similar. Both systems rely on the iterative processing of its substrate at different enzymatic active site domains. Instead of free diffusion, the substrate is covalently bound to the ACP domain which mediates the transient interaction with different enzymatic active sites.

Structural investigations revealed that the overall fold of ACPs is highly conserved within the FAS and PKS systems over all kingdoms of life. All of them consist of a conserved four-helix bundle including a serine residue that is post-translational activated with attachment of PPant (*Figure 0.6*) (Farmer et al., 2019; Lambalot et al., 1996). The question why such acyl carrier systems have evolved and how their transient ACP-enzyme interaction is mediated is central for the understanding of these complex enzymatic systems. The *de novo* FA synthesis for example relies on six different reactions that are catalyzed by distinct proteins/domains. To overcome a random diffusion of the growing acyl-chain within the crowded cytosol the attachment to ACP allows a specific interaction with the FA synthesis domains. Furthermore, the attachment to ACP protects the hydrophobic acyl chain from the aqueous cytosol (Chan and Vogel, 2010; Lim et al., 2011). The transfer of the substrate to different enzymatic active sites without its release into solution is also known as substrate-channeling (Huang et al., 2001). The specificity towards the different enzymatic domains is thought to be controlled by a charge-dependent ACP-enzyme interaction (Chan and Vogel, 2010; Hahn and Stachelhaus, 2004; Nguyen et al., 2014a). Proteins that are involved in the interaction with ACP possess a cationic recognition site that is thought to mediate the binding with the acyl-ACP. For the ACP itself an overall anionic surface charge, especially within its helix II region was described. It is thought that these opposite charges of enzymes and ACP are crucial for the transient interaction (Beltran-Alvarez et al., 2009; Keating and Cronan, 1996; Parris et al., 2000; Rock and Cronan, 1979; Worsham et al., 2002; Zhang et al., 2003).

Quantitative studies showed that ACP belongs to the most abundant proteins (~ 0.25 %) in *E. coli* cells reaching molar concentrations of up to 150 µM (Boom and Cronan, 1989; Jackowski and Rock, 1983). This underlines its importance for the cell and how crucial it is to maintain essential metabolic processes. As already mentioned, the iterative cycle of the FAS and PKS synthesis requires the interaction of the ACP domain with different enzymes. Therefore, it must be ensured that the ACP-enzyme interaction is transient. An interaction which is too strong or too weak would have a negative impact on the processivity if the whole catalytic process. To understand the iterative enzymatic processes, their regulation and why ACP domains evolved in exactly these systems it is crucial to gain structural information of the transient ACP-enzyme complexes. Using structural information in combination with molecular dynamic (MD) simulations, it was proposed that the dynamic movements of the ACP and its interaction with different active sites follows a stochastic manner (Anselmi et al., 2010).

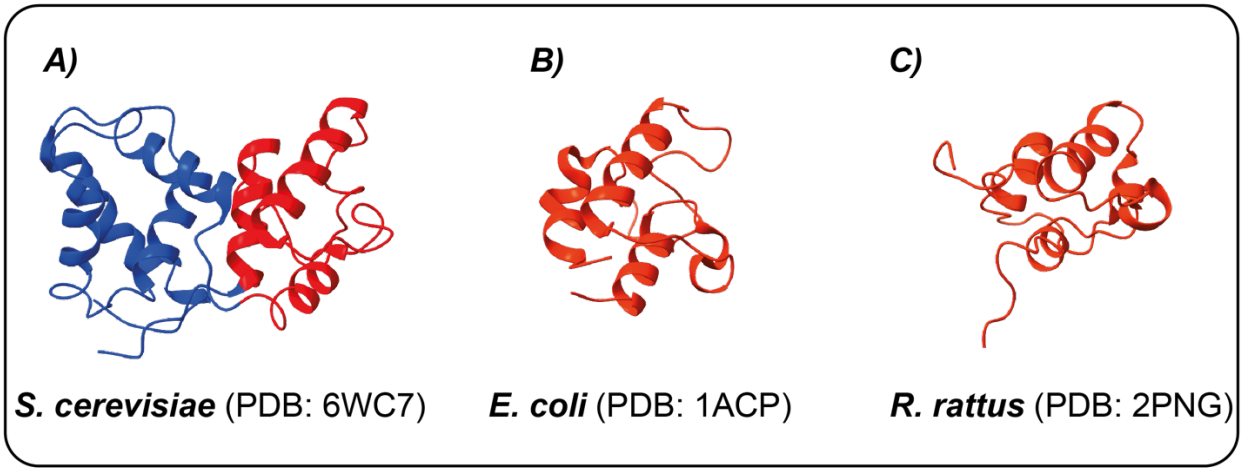

Figure 0.6: Comparison of different ACP domains. *The structures of three different ACP organisms show high structural homologies. Within all organisms, a conserved four-helix bundle (red) is found. Other than the ACP of E. coli (middle) and R. rattus (right), the ACP from the S. cerevisiae type I FAS has four additional helices (blue).*

1.4.6 Dynamics of the acyl carrier protein

In both FAS systems the ACP must interact with several different enzymatic domains during the cyclic FA synthesis. While the type II ACP is an individual protein, the ACP of the type I system is an internal part of the whole FAS complex. To allow dynamic movements between the different active sites, the yeast ACP domain is connected to flexible N- and C-terminal linker regions.

To achieve an interaction with all active site domains, the interaction with the ACP and its covalently bound acyl chain is dynamic process. Since protein structure determination methods like X-ray crystallography and Cryo-EM can only draw a picture of static states, the visualization of these transient states is one of the major challenges in the research of metabolic processes that rely on ACPs. Within the yeast FAS complex the six different enzymatic domains are distributed over the inner cavity of both halve domes. With its two linker regions the ACP can interact with all domains. Based on the proximity of the six different active sites within a single functional unit (*Figure 0.1 B*) a functional compartment with defined interaction partners of a certain ACP domain was proposed (*Figure 0.7 A*) (Leibundgut et al., 2007).

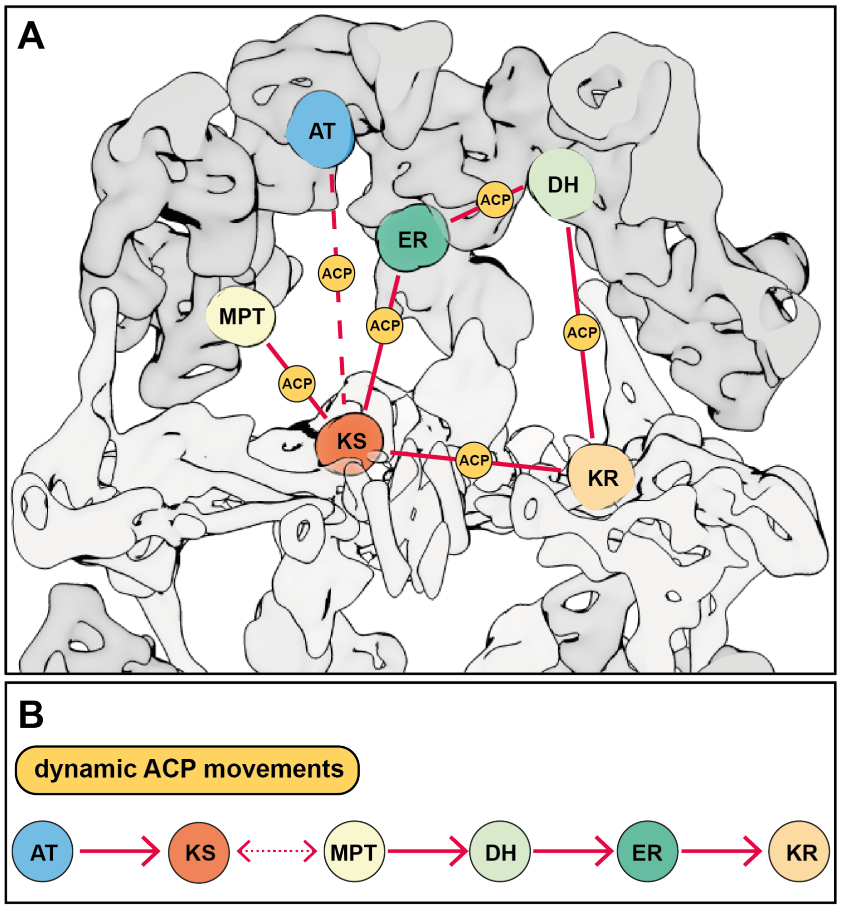

Figure 0.7: Schematic representation of the FAS ACP dynamics. A) *Schematical side-view into the FAS reaction chamber. The different active sites are highlighted in colors. With its n- an c-terminal linker regions the ACP (yellow) can reach all enzymatic domains within its defined functional compartment (red lines)* ***B)*** *The dynamics of the ACP domain are thought to start at the AT site (blue). The chain elongation is achieved by iterative translocation to the different active sites KS, MPT, DH, ER and KR. The final fatty-acyl chain is hydrolyzed and transferred to a free CoA by the MPT.*

1.4.7 Regulation of the FAS Activity in Yeast

During FA synthesis, ATP, acetyl-CoA, malonyl-CoA, CoA, and NAD(P)H are consumed. It has been shown that the total energy required for the synthesis of one molecule of palmitic acid (C_{16})is equivalent to 122 molecules of ATP (Nelson and Cox, 1993). Such high rates of energy consumption coupled with the importance of the fatty acid synthesis make a tight control of the FAS activity indispensable.

In yeast, the transcription of the ACC1 gene is regulated by the transcription factors Ino2/Ino4 and Opi1, which are involved in the biosynthesis of phospholipids (Tehlivets et al., 2007). On the protein level, the ACC activity can be controlled by its degree of biotinylation, which is essential for the function of the enzyme *(Figure 0.3)*. Additionally, the phosphorylation mediated inactivation of ACC by Snf1 has been shown (Shirra et al., 2001; Suomalainen and Keränen, 1963; Woods et al., 1994). The specific mutation of two serine residues in ACC prevents its post-translational phosphorylation by Snf1, resulting in an increase of ACC activity, and the downstream fatty acid synthesis (Shi et al., 2014).

Other than the type I FAS from CMN bacteria and Mammalia, the yeast FAS is encoded by two separate genes. The two FAS1 and FAS2 genes are located on distinct chromosomes. In

order to regulate and coordinate these separate genes, both are under control of identical upstream activating sequences (UAS_{FAS}) which are regulated by the same Ino2/Ino4 transcription factors as the ACC (Casado et al., 1999; M et al., 1986; Mondino et al., 2013; Schüller et al., 1992; Schweizer et al., 1987; Tehlivets et al., 2007). The transcription was shown to be under the tight control of the three transcription factors Rap1, Reb1 and Abf1 and, surprisingly by the FAS2 coding sequence itself. The first 66 nucleotides of the FAS2 gene turned out to be necessary for the gene expression of the FAS1 gene (Schüller et al., 1994; Wenz et al., 2001). Apart from the genetic level, the yeast FAS itself was shown to be internally controlled by product inhibition with lauryl-CoA (C_{12}), myristoyl-CoA (C_{14}), palmitoyl-CoA (C_{16}) and stearoyl-CoA (C_{18}) (Lust and Lynen, 1968).

1.5 Structural Investigation of Dynamic Processes

Intensive research in the field of structural biochemistry over the last decades has shown that the enzymatic catalysis of substrates is often a dynamic process. By movements of the substrate and/or within domains of the respective enzyme during the catalytical process, the structural architecture is arranged in a way that allows the biocatalytic processing of the substrate. Since structural investigation methods like X-ray crystallography and Cryo-EM rely on the imaging of static states, dynamic processes must be arrested or somehow controlled. Only by taking snapshots of various trapped transient states, a clear image showing detailed structural information can be acquired.

In case of the FAS systems, the ACP domain with its covalently attached fatty acyl chain undergoes such dynamic rearrangements. The transient nature of these rearrangements and ACP-enzyme interactions complicates the collection of structural information. To solve the problem of such dynamic movements and transient interactions different biochemical and biophysical tools are used and under constant development. One biochemical tool is the use of naturally occurring inhibitor molecules. Examples are α-amanitin, a polymerase II specific inhibitor from the fungus *A. phalloides,* or the antibiotic tetracycline which was isolated from the fungus *S. aureofaciens.* The tetracycline molecules specifically binds and arrests the bacterial 30S ribosomal subunit (Duggar, 1948; Lindell et al., 1970). With the help of these compounds, it was possible to stabilize the polymerase II and the 30S ribosomal subunit. Only these inhibited protein complexes could be further used to grow well diffracting crystals for X-ray crystallographic investigations (Brodersen et al., 2000; Bushnell et al., 2002).

Such compounds were also discovered for the inhibition of type I and type II fatty acid synthesis systems. Triclosan, a chemical compound was found to be a specific, reversible inhibitor of the bacterial enoyl reductase (FabI) and is broadly used as a biocide (Schweizer, 2001; Ward et al., 1999). Another FAS targeting compound is cerulenin which was first discovered and isolated from the fungus *C. ceruleans*. Biochemical studies of cerulenin showed that it irreversibly binds to the

keto synthase, where it mimics the covalently bound ketoacyl intermediate and prevents a further condensation reaction of the growing fatty acyl chain (D'Agnolo et al., 1973; Omura et al., 1967). Structural studies of cerulenin bound to the keto synthase active side of the type I and type II FAS showed, that the sulfur atom of the active side cysteine residue covalently binds to the C_2 atom of cerulenin. An unsaturated acyl-chain of cerulenin binds into an acyl-tunnel within the keto synthase domain. This tunnel is built of different hydrophobic residues (Johansson et al., 2008; Moche et al., 1999; Price et al., 2001).

1.5.1 ACP Specific Crosslinking Methods

The above-described FAS inhibitors rely on the inhibition of specific active sites. Their action of inhibition is completely independent from the dynamic ACP domain. Since the dynamics and transient interactions of the ACP domain are essential for the FAS activity, potential inhibitors should also be involved into an ACP specific inhibition mechanism.

Over the last years, Burkart and co-workers (Mindrebo et al., 2020a; Nguyen et al., 2014b; Tallorin et al., 2016a) designed a set of inhibitors that allow a mechanism-based crosslinking of the ACP domain to different enzymatic domains. Therefore, they synthesized pantetheineamide analogs with additional mechanism-based warheads. By use of a chemo-enzymatic assay these precursor molecules can be processed to reactive crypto-CoA molecules by the *E. coli* enzymes CoaA, CoaD and CoaE and ATP (*Figure 0.8*).

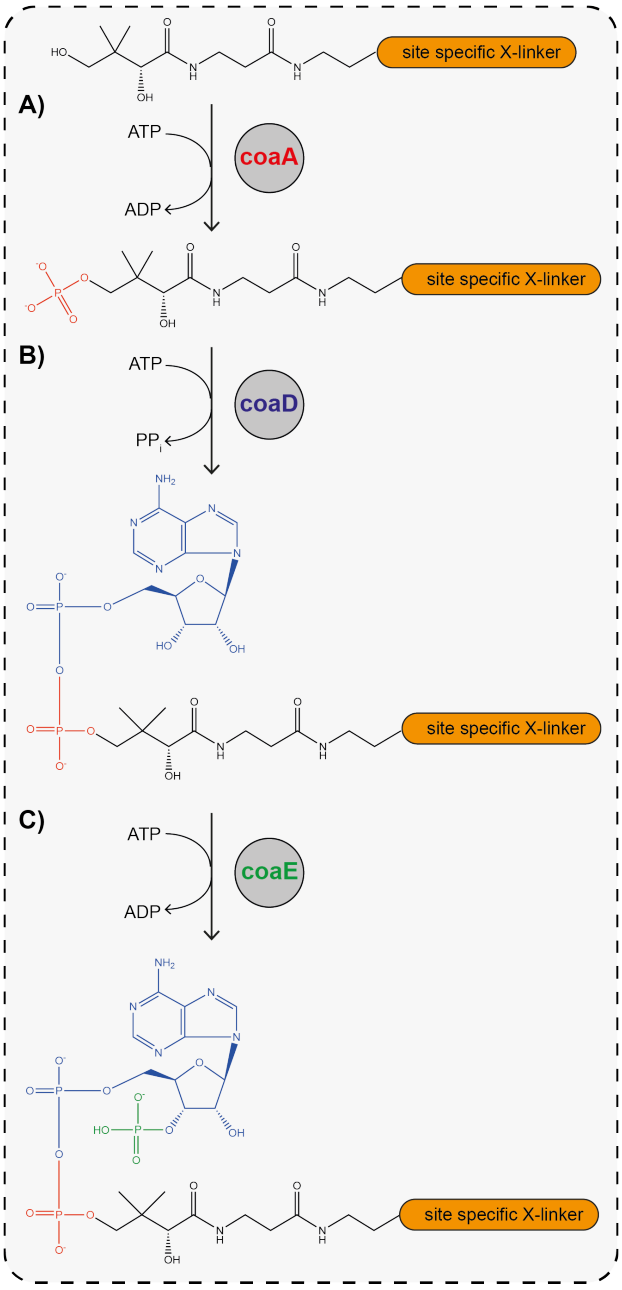

Figure 0.8: Enzymatic synthesis of crosslinker-CoA analogs. *The pantetheineamide analogue is processed in a stepwise enzymatical reaction. A) The pantothenate kinase CoaD catalyzes the transfer of a phosphate group from ATP to the pantetheineamide analogue, forming a phosphopantetheine amide analogue. B) The phosphopantetheine adenyltransferase CoaD catalyzes the transfer of adenosine monophosphate from ATP to the phosphate group of the phosphopantetheine amide analogue, resulting in a 3'-dephospho-CoA analogue. C) In a third reaction the dephospho-CoA kinase phosphorylates the 3'-dephospho-CoA analogue with the phosphate group deriving from ATP. The end-product of these three consecutive reactions is a coenzyme-A analogue. Depending on the pantetheine amide precursor, different analogues can be produced with this enzymatic assay.*

The resulting crypto-CoAs can be used to modify the inactive apo-ACP domain in an enzymatic phosphopantetheinylation reactions (*Figure 0.9, left*). The product of this reaction is a modified crypto-ACP that harbors a reactive group on its PPant arm (*Figure 0.9, right*) (La Clair et al., 2004; Mandel et al., 2004). Based on this concept Burkart and co-workers managed to crosslink the bacterial AcpP to different bacterial type II FAS enzymes. They further managed to solve the structures of these crosslinked complexes by X-ray crystallography.

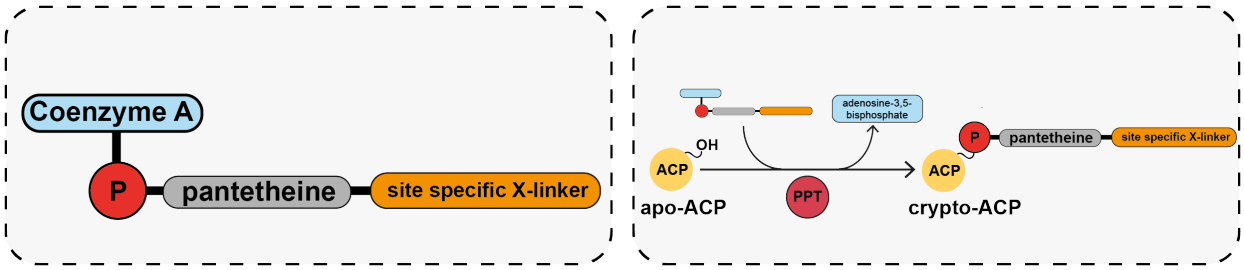

Figure 0.9: Enzymatic modification of apo-ACP with reactive crypto-CoA. *The chemo-enzymatic synthesized crosslinker-CoA molecule (left) can be used as a substrate for the PPTase catalyzed attachment to apo-ACP. This results in a crypto-ACP domain (right). The crypto-ACP can then further specifically crosslink to its target proteins of the FAS system.*

Inspired by the reaction of cerulenin with the keto synthase active site, different cysteine-reactive crosslinkers were developed (e.g., *Figure 0.10*). All these compounds rely on the covalent linkage to the sulfur atom of the active site cysteine. The harbor an electrophilic leaving group which allows a nucleophilic attack of the active site sulfur atom. The substitution of the leaving group results in the formation of a covalent linkage. (Worthington et al., 2006). α-bromopantetheineamide-based analogs (*Figure 0.10, i*) allow a modification of the crosslinker with hydro-carbon chains of alternating length. After the covalent linkage to a cysteine residue, the attached acyl-chain resembles the structure of a bound fatty-acyl chain. With help of these crosslinker, the E. coli AcpP was successfully crosslinked to the keto synthase domains FabB and FabF. The use of alternating chain lengths further allowed to draw an image of the complex architecture in presence of different substrate intermediates (Milligan et al., 2019a; Mindrebo et al., 2020b).

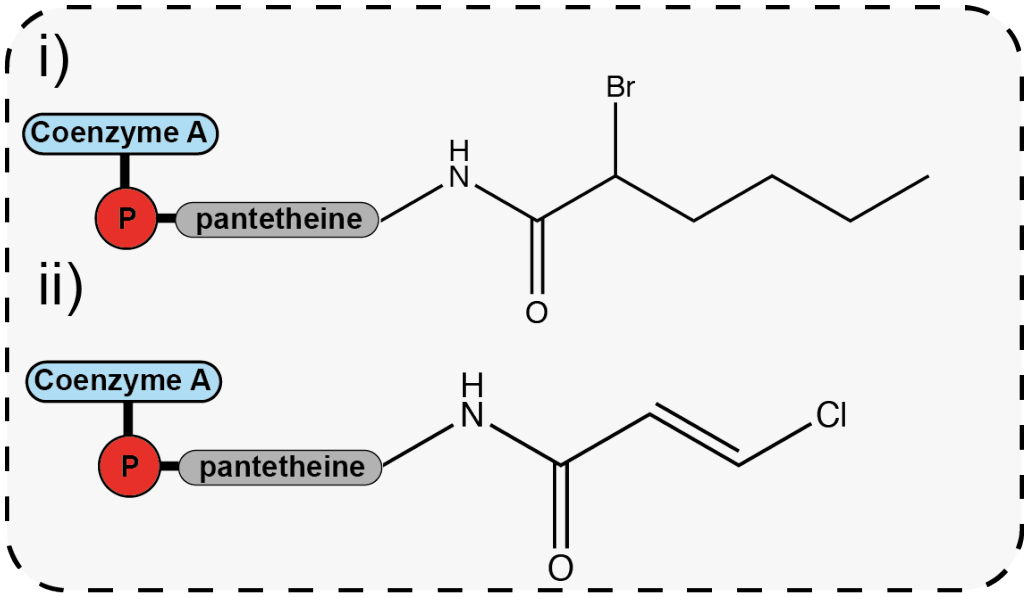

Figure 0.10: KS-specific crosslinker. *The two crosslinker-CoAs i) and ii) are both cysteine-reactive crosslinkers which allow the specific covalent binding to the KS cysteine active site residue. The active site cysteine residue of the keto synthase domain undergoes nucleophilic attack to substitute an electrophilic leaving group of the crosslinker. After the successful crosslinking reaction, the crosslinker i) corresponds to a C6-substrate intermediate bound to the KS domain.*

The second group of mechanism-based reactive pantetheineamide analogs is based on 3-decynoyl-N-acetylcysteamine (*Figure* 0.11). This histidine-specific molecule allowed the crosslinking of AcpP to the bacterial dehydratase domain FabA. Successful crystallization of the AcpP-FabA complex allowed to solve its structure by X-ray crystallography. (Helmkamp et al., 1968; Nguyen et al., 2014c).

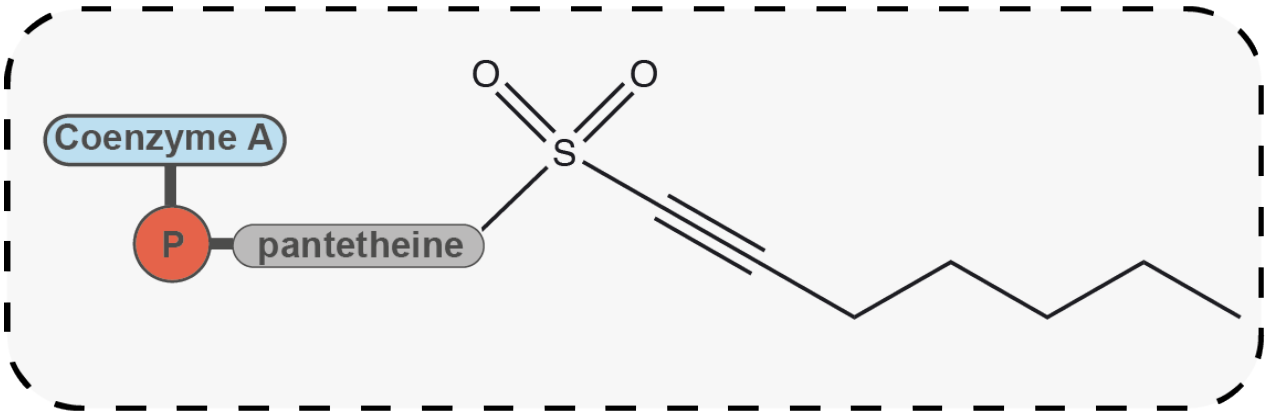

Figure 0.11: DH-specific crosslinker. *The DH specific crosslinker-CoA is based on a 3-decynoyl-N-acetylcysteamine reactive group which allows a histidine specific covalent linkage to the dehydratase active site histidine residue.*

Based on triclosan, a non-covalent inhibitor of the bacterial enoyl reductase (FabI), a pantetheineamide-triclosan precursor was synthesized (*Figure 0.12*). Using biochemical assays, it was shown that, a stable complex of AcpP-FabI is formed and thus could further be used for protein crystallographic investigations (Tallorin et al., 2016a). Since the inhibition of the enoyl reductase by triclosan is not of covalent nature, the complex formation of AcpP and FabI is most likely not as stable as for the probes that were mentioned above (Heath et al., 1999).

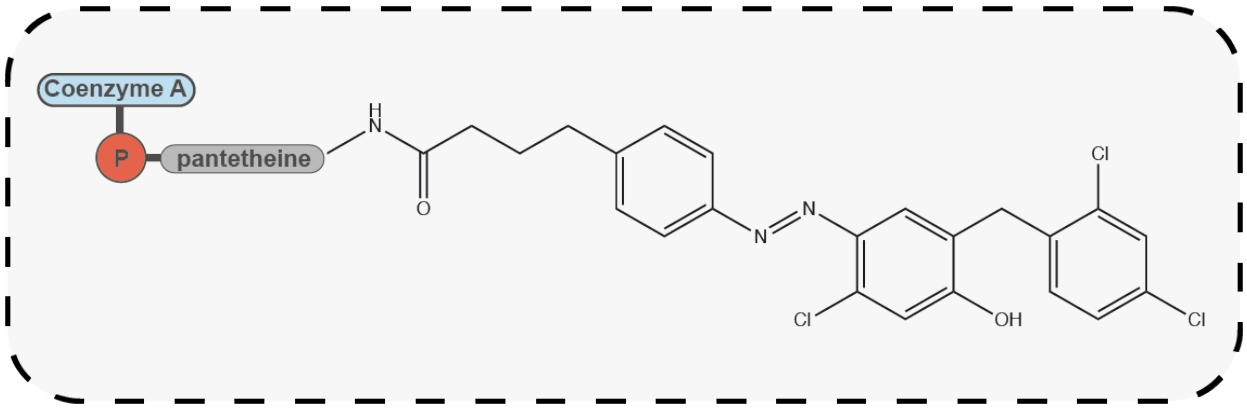

Figure 0.12: ER-specific crosslinker. *The ER-specific crosslinker-CoA allows a specific binding to the bacterial enoyl reductase domain. Other than the above described crosslinker-CoAs, the triclosan based binding domain does not undergo a covalent linkage to its target domain. The binding is specific to bacterial FabI, whereas the yeast enoyl reductase domain does not bind to the triclosan molecule.*

2 Aim of the Thesis

The fatty acid metabolism is a central process in all forms of life. For the chemo-enzymatic synthesis of fatty acids, two structurally different fatty acid synthase (FAS) systems have evolved separately from each other. While the bacterial type II system relies on serval independent domains, the type I system from eukaryotes and CMN-bacteria consists of a single macromolecular complex. Within this complex, all enzymatic domains that are required for the *de novo* synthesis of a fully saturated fatty-acyl chain are present. Despite several decades of research, amazingly little is known about the detailed catalytic mechanism of these enzymes as well as their regulation. Previous work has revealed that the fatty acid synthesis in both systems requires an acyl carrier protein (ACP). This ACP domain mediates the transport of the growing acyl-chain substrate to different enzyme active sites. Since the growing fatty-acyl chain is covalently bound to ACP, the different ACP-enzyme interactions are of transient nature. Only the weak and temporary interaction allows a binding to all catalytic domains. During the chain elongation and release process, the ACP domain must interact with six different enzymatic domains. The dynamic of these interactions makes them infeasible for structure determination methods. X-ray crystallography and Cryo-EM rely on the imaging of static interactions or conformations. Dynamic processes like the substrate shuttling of the yeast ACP are of transient nature and therefore cannot be visualized in higher detail.

To overcome these problems, we wanted to find a tool that allows the arresting of these dynamic movements at specific time points. With mechanism-based reactive substrates that were synthesized by a collaborating company (NovAliX, Illkirch-Graffenstaden, France) we aimed to establish a protocol that allows capturing of specific ACP-enzyme interactions within the yeast type I FAS system. The biochemical principle of this methods was formerly developed and successfully used for the visualization of interactions between the *E. coli* AcpP and other type II specific domains. A successful use of such mechanism-based crosslinkers within the macromolecular yeast FAS could enable the transfer to many other dynamic systems. Like the substrate shuttling of the yeast ACP, many other protein complexes are known to rely on similar processes. The possibility to control and trap these transient interactions in a static state would allow the visualization of manifold so-far unknown catalytic mechanisms.

3 Material & Methods

3.1 Chemicals

Chemicals	Producer
1,4-Dithiothreitol (DTT)	Carl Roth
2-(N-morpholino)ethanesulfonic acid (MES)	Sigma-Aldrich
Acetic Acid	Merck
Amido Black 10B	SERVA Electrophoresis
Ammonium sulfate	Merck
Benzamidine hydrochloride hydrate	Sigma-Aldrich
Betaine	Merck
Bis(2-hydroxyethyl)aminotris(hydroxymethyl)methane (BisTris)	Sigma-Aldrich
Bradford Quick Start™ 1x Dye Reagent	BioRad
Coomassie Brilliant Blue R-250	BioRad
D-Glucose	Merck
Dimethyl sulfoxide (DMSO)	AppliChem
Ethanol	Merck
Ethylene glycol	Sigma-Aldrich
Ethylenediaminetetraacetic acid (EDTA)	Merck
Glycerol	Merck
Hydrochloric acid (HCl)	Merck
Isopropanol	Merck
Isopropyl β-D-1-thiogalactopyranoside (IPTG)	Sigma-Aldrich
Lauryl maltose neopentyl glycol (LMNG)	Anatrace
Magnesium acetate ($Mg(OAc)_2$)	Merck
Magnesium chloride ($MgCl_2$)	Merck
Malonyl-CoA	Sigma-Aldrich
Acyl-CoAs	Avanti
Nicotinamide adenine dinucleotide phosphate (NADPH)	Carl Roth
Octyl glucose neopentyl glycol (OGNG)	Anatrace
pantetheineamide crosslinker variants	NovAliX (France)
PEG 3350	Sigma-Aldrich
Phenylmethane sulfonyl fluoride (PMSF)	Sigma-Aldrich
Polyethylene glycol (PEG) 400	Sigma-Aldrich
PEG 3350	Sigma-Aldrich
Potassium chloride (KCl)	Merck
Potassium hydroxide (KOH)	Merck
Potassium acetate (KOAc)	Sigma-Aldrich
Propanol	Merck
Rotiphorese® 10x SDS-PAGE Buffer	Carl Roth
Sodium chloride (NaCl)	Merck
Sodium malonate	Sigma-Aldrich
Sucrose	Merck
Terrific broth (TB) growth medium	Melford Biolabratory
Tri-fluoro acetic acid (TFA)	VWR
Yeast peptone (YP) medium	FORMEDIUM
β-Mercaptoethanol (β-ME)	Sigma-Aldrich

Table 3.1: Chemical compounds

3.2 DNA-Primers

Name	Sequence
FAS2_PPTase_del_fwd	5'ACTCTAAAAACATCCAAAGCAAGGACAGTTACATCAATGCTAACACCATTTGACTCGAGGCGCGCCACTTCTAAATAAGC 3'
FAS2_PPTase_del_rev	5'CAATAGATGGCAGTAATCGTTGAGACAACATAACTACCGGCCGTCCCTG GATATCATCGATGAATTCGAGCTCGTTT3'
ΔPPTase seq fwd	5' TTGGAAGAGGATGTTTACTTGG 3'
ΔPPTase seq rev	5' TATTCTGGGCCTCCATGTC 3'
γ-subunit_del_fwd	5'TTATAAAACATAAAGCAAATCAAAACATAATAACTACTACAAGTAACATACGACGGATCCCCGGGTTAAT-3'
γ-subunit_del_rev	5'ACAAAGAGTATGACGTGAAAATGATGCGCAGTAAAACTAAATCCCGTCTCGATATCATCGATGAATTCGAGCTCGTTT-3'
Check_Δγ-subunit_fwd	5' CACACCTACGAAAGTCCATTTTACTTCG 3'
Check_Δγ-subunit_rev	5' GGGTAGATAGAATAGACAAATGGAG 3'
Δsu_BJ2168_seq_fwd_01	5' GTCCATTTTACTTCGTAG 3'
Δsu_BJ2168_seq_fwd_02	5' ATCCGAACATAAACAAC 3'
Δsu_BJ2168_seq_rev_01	5' CTAGGGCTTTCGGAG 3'
Δsu_BJ2168_seq_rev_02	5' ATTACAAACAGGAATCG 3'

Table 3.2: DNA primers for molecular cloning

3.3 Enzymes

Enzyme	Producer
Bovine serum albumin (BSA)	Sigma-Aldrich
DpnI	New England BioLabs
Lysozyme	Sigma-Aldrich
Phusion® High-Fidelity DNA Polymerase	New England BioLabs
Q5 DNA-Polymerase	New England BioLabs
SUMO-protease	In-house preparation
T3 DNA Ligase	New England BioLabs
T4 Polynucleotide Kinase	New England BioLabs
TEV-protease	In-house preparation
Trypsin inhibitor protein	Sigma-Aldrich

Table 3.3: Enzymes for biochemical assay

3.4 Protein Overview

Protein	Abbreviation	Origin	Molecular weight [kDa]	Extinction coefficient Ɛ/1000 [1/M*cm]; reduced
wild-type yeast fatty acid synthase	wtFAS	*S. cerevisiae*	2,613	2440.9
ΔPPTase yeast fatty acid synthase	ΔPPTase-FAS	*S. cerevisiae*	2,526	2398.9
FAS from Δγ-subunit yeast strain	Δγ-FAS	*S. cerevisiae*	2,613	2440.9
Phosphopantethenyl transferase	yPPTase	*S. cerevisiae*	14.50	6.99
Adc17/Tma17/γ-subunit	Tma; γ-subunit	*S. cerevisiae*	16.77	5.96
γ-TesA	TmaTesA	*S. cerevisiae* + *E. Coli*	35.19	40.91
Bilirubin-inducible fluorescent protein	UnaG	*A. japonica*	15.58	18.45
γ-1xUnaG	Tma-1xUnaG	*S. cerevisiae* + *A. japonica*	31.24	25.90
γ-2xUnaG	Tma-2xUnaG	*S. cerevisiae* + *A. japonica*	47.82	45.84
Acyl-CoA thioesterase I	TesA	*E. coli*	23.62	40.45
Acyl Carrier Protein	AcpP	*E. coli*	8.64	1.49
Yeast Acyl Carrier Protein	yACP	*S. cerevisiae*	17.41	8.48
Pantothenate kinase	CoaA	*E. coli*	36.36	45.38
Phosphopantetheine adenylyl transferase	CoaD	*E. coli*	17.84	8.48
Dephospho-CoA kinase	CoaE	*E. coli*	22.62	16.96
Phosphopantethenyl transferase	Sfp	*B. subtilis*	26.17	28.88
Holo-ACP-synthase	AcpS	*E. coli*	14.05	17.99

Table 3.4: Endogenous and recombinant enzymes used for experiments

3.5 Consumables

Material	Producer
4-15% Criterion TGX protein gel	BioRad
Cheesecloth	Local retailer
Cryschem sitting drop crystallization plate	Hampton Research
Miracloth	Merck Millipore
Nitrocellulose syringe filter (0.2 µm)	Sartorius Stedim
Frozen-EZ Yeast Transformation II Kit	Zymo Research
PTFE membrane filter (0.2 & 0.8 µm)	Sartorius Stedim
Centrifugal concentrators (different MWCOs)	Amicon
Dialysis tubes (different MWCOs)	Merck

Table 3.5: Consumables

3.6 Machines & Equipment

Machine/Equipment	Producer
Balances	Sartorius Stedim
ZM 200 centrifugal mill	Retsch
Heraeus Multifuge X1	Thermo Fisher Scientific
Heraeus Pico Centrifuge	Thermo Fisher Scientific
Incubation shaker Multitron Pro	Infors HT
Orbital shaker RS020	Phoenix Instruments
Photometer Lambda BioX	PerkinElmer
Emulsiflex C3	Avestin Europe GmbH
Scorpion pipetting robot	ARI Instruments
Gradient Master 108	Biocomp Instruments
Ultracentrifuge WX Ultra 80/90	Thermo Fisher Scientific
Thermo Scientific Surespin 630 rotor	Thermo Fisher Scientific
SW 40 Ti swinging bucket rotor	Beckman Coulter
TH660 swinging bucket rotor	Beckman Coulter
Fiberlite F15-8 x 50cy fixed angle rotor	Thermo Fisher Scientific
A23 6x100 fixed angle rotor	Thermo Fisher Scientific
Criterion Vertical Electrophoresis Cell	BioRad
Mini-PPROTEAN Tetra Vertical Electrophoresis Cell	BioRad
CIMultus™ SO3/DEAE ion exchange columns	BIA Seperations
ÄKTA protein purification systems	Cytiva

Table 3.6: Machines and Equipment

3.7 Buffers

Buffer	Compounds
1x SB-acetate pH 6.5	50 mM BisTris pH 6.5 (acetic acid) 50 mM potassium acetate 10 mM magnesium acetate
1x SB	50 mM BisTris pH 6.5 (HCl) 50 mM KCl 10 mM $MgCl_2$
Resuspension buffer	1x SB-acetate pH 6.5 2% sucrose (w/v) 0.01 % LMNG (w/v) 5 mM TCEP
Crystallization buffer	1x SB-acetate pH 6.5 2% sucrose (w/v) 0.01 % LMNG 5 mM TCEP
stabilization buffer	0.1 M Na-HEPES pH 7.0 0.3 M Na-malonate pH 7.0 7.5%, 15%, 20% ethylene glycol (v/v) 11%, 13%, 15%, 20% PEG 3350 (w/v)
Affinity buffer A	1x SB-acetate pH 6.5 5% sucrose (w/v) 1 mM TCEP
Affinity buffer B	1x SB-acetate pH 6.5 5% sucrose (w/v) 1 mM TCEP 1 M KCl
1x PBS buffer	137 mM NaCl 2.7 mM KCl 10 mM Na_2HPO_4 1.8 mM KH_2PO_4 pH adjusted to pH 7.4 with NaOH/HCl
1x TBE	0.13 M Tris pH 7.6

	45 mM boric acid 2.5 mM EDTA
1x TAE	0.4 M Tris acetate pH 8.3 0.01 M EDTA
1x Binding assay buffer	50 mM BisTris pH 6.5 50 mM potassium acetate 0.5 mM magnesium acetate
5x ISO buffer	0.5 M Tris-HCl pH 7.5 50 mM $MgCl_2$ 1 mM dATP 1 mM dCTP 1 mM dGTP 1 mM dTTP 50 mM DTT 0.25 % (w/v) PEG 8000 5 mM NAD
Gibson master mix	320 µl 5x ISO-Buffer 6.4 U T5 exonuclease (NEB) 40 U Phusion polymerase (NEB) 6400 U Taq ligase (NEB) ddH_2O to 1200 µl

Table 3.7: Different working buffers

3.8 Deletion of the YDL110C gene in BJ2168 yeast cells

For deletion of the YDL110C gene in a BJ2168 (MATa prc1-407 prb1-1122 pep4-3 leu2 trp1 ura3-52 gal2) *S. cerevisiae* strain, the YDL110C gene was replaced by a KanMX resistance cassette via homologous recombination. The resistance cassette was amplified from the pTF267 plasmid (#44093, Addgene) with 5' and 3' homologous overlapping regions to the BJ2168 YDL110C gene. For amplification of the KanMX cassette and insertion of the homologous overlaps, the primer set γ-subunit_del_fwd and γ-subunit_del_rev was used. The PCR product was purified using a commercial PCR purification kit and used as a DNA template for homologous recombination in competent BJ2168 *S. cerevisiae* cells. For transformation, a total amount of 1 µg DNA was used in 50 µl competent cells. After transformation, the cells were grown for 1h in sterile YPD medium and finally grown on selective YPD-agar plates with 200 µg/ml of the antibiotic G418. After incubation for 48h at 30 °C, growing colonies were streaked out on a YPD-agar + G418 replica plate and again grown for 48h at 30 °C. Single colonies were picked and used to inoculate 100 ml liquid YPD medium containing 200 µg/ml G418. The liquid cultures were grown for 36h at 30 °C and 200 rpm. From each liquid culture, 500 µl were 1:1 mixed with sterile glycerol stored at -80°C. To verify the deletion of the Tma17 sequence and the correct insertion of the KanMX resistance cassette, genomic DNA (gDNA) was extracted from each liquid yeast culture using a commercially available gDNA extraction kit. With a primer set binding 5' and 3' of the tma17 coding sequence, the gDNA sequence was amplified using the both primers check_Δγ-subunit_fwd and check_Δγ-subunit_rev. The resulting PCR product was purified and send for sequencing using the four sequencing primers Δsu_BJ2168_seq_fwd, Δsu_BJ2168_seq_fwd_02, Δsu_BJ2168_seq_rev_01 and Δsu_BJ2168_seq_rev_02. The

sequencing showed successful insertion of the KanMX resistance cassette as well as the deletion of the YDL110C ORF for all tested cultures. A positive clone was picked and used to inoculate a 100 ml liquid culture (YPD-medium, 200 µg/ml G418) over 48 h at 30 °C. From the grown culture 500 µl were gently mixed with 500 µl of 40 % sterile glycerol (v/v) and aliquots were slowly frozen at -80 °C.

3.9 Creating an endogenous PPTase deficient yeast strain

For deletion of the c-terminal PPTase coding sequence within the FAS2 gene of the BJ2168 *S. cerevisiae* strain, a KanMX resistance cassette was amplified from the pTF267 plasmid (#44093, Addgene) with additional 5' and 3' homologous overlapping regions before (AA 1747) and after (AA 1887) the PPTase sequence using the primers FAS2_PPTase_del_fwd and FAS2_PPTase_del_rev. The resulting PCR product of approx. 1700 bp was gel-purified and used as template for homologous recombination in competent *S. cerevisiae* cells with a standard protocol. Since the PPTase domain of FAS2 is essential, the cells were rescued by addition of 50 µg/ml myristic, palmitic and stearic acid into the YPD-medium. For selection of ΔPPTase FAS2 clones, the transformed cells were streaked out on a YPD-agar plate with additional fatty acids and G418 antibiotic as resistance marker. The cells were grown for 48h at 30 °C. Grown single colonies were streaked out on a replica plate and grown again for 48h at 30°C on a selection plate. To verify the successful deletion of the resulting yeast colonies, colony PCRs were performed using the two primers ΔPPTase_seq_fwd and ΔPPtase_seq_rev. The resulting PCR product was purified and sent for sequencing, using the same primers as sequencing primers. Sequencing verified the deletion of the PPTase coding sequence within the FAS2 gene and the insertion of the 3' G418 resistance cassette. The positive yeast cells were transferred to 200 ml YPD medium + additional fatty acids and G418 antibiotics, grown for 24 h at 30 °C and were used for preparation of glycerol stocks. For the final glycerol stocks, 500 µl of yeast cell culture was 1:1 mixed with 40 % sterile glycerol (v/v) and stored at -80°C.

3.10 Cloning of recombinant bacterial expression vectors

For cloning of different bacterial expression vectors, the respective genes were amplified from commercially synthesized (Thermo Fisher) *E. coli* codon optimized plasmids using primers with specific restriction sites or homologous overhangs for a Gibson assembly reaction (see *Table 3.2*)

In case of standard enzyme restriction cloning, the linear PCR products were gel-purified, digested with respective restriction enzymes and introduced into a specific pre-digested expression vector. After a ligation/Gibson reaction, the plasmid was transformed into competent DH5α *E. coli* cells. The transformed cells were rescued for 1h (37 °C, 1000 rpm mixing) in liquid LB-medium and then streaked out on LB-agar plates with selective antibiotics and 1% D-glucose (w/v). Plates were grown for 16 h at 37 °C and single colonies were picked to inoculate 100 ml

liquid LB-medium cultures with selective antibiotics. The liquid cultures were grown (16 h, 37 °C, 200 rpm) harvested by centrifugation (5000 g, 15 min, 4 °C) and used for plasmid preparation using commercial kits (MN). The purified plasmids were sent for DNA sequencing (Seqlab). Positive clones were stored at -20 °C.

For Gibson assembly reactions, the expression vector was linearized by a standard PCR reaction with a primer set with 3' homologous overhangs to the sequence of the protein of interest (POI). The sequences of the POI were amplified with a primer set having 3' overhangs to the linearized expression vector or in case of insertion of several POI sequences, to the adjacent POI sequence. PCR product lengths of the expression vector as well as the POI sequences were loaded on a 1 % (w/v) agarose gel in 1x TBE buffer. For gel-purification, a commercial kit (MN) was used, and the final PCR product was stored at -20 °C until further usage. For Gibson assembly reaction, linearized vector and the POI inserts were mixed in a 1:2 to 1:5 molar ratio in a final volume of 5 µl with a total DNA amount of 200 ng. The mixed DNA was added to 15 µl of Gibson master mix and incubated at 50 °C for 60 min. For transformation into competent DH5α *E. coli* cells, 0.5 – 3 µl of the reaction product was used. The transformed cells were rescued for 1h (37 °C, 1000 rpm mixing) in liquid LB-medium and then streaked out on LB-agar plates with selective antibiotics and 1% D-glucose (w/v). Plates were grown for 16 h at 37 °C and single colonies were picked to inoculate 100 ml liquid LB-medium cultures with selective antibiotics. The liquid cultures were grown (16 h, 37 °C, 200 rpm) harvested by centrifugation (5000 g, 15 min, 4 °C) and used for plasmid preparation using commercial kits (MN). The purified plasmids were sent for DNA sequencing (Seqlab). Positive clones were stored at -20 °C.

3.11 Yeast cell cultures

For all experiments and cell cultures using yeast cells either the wild type *Saccharomyces cerevisiae* BJ2168 strain (MATa prc1-407 prb1-1122 pep4-3 leu2 trp1 ura3-52 gal2), a ΔYDL110C BJ2168 strain (MATa prc1-407 prb1-1122 pep4-3 leu2 trp1 ura3-52 gal2 YDL110C::KanMX) or a ΔPPTase-FAS2 BJ2168 strain (MATa prc1-407 prb1-1122 pep4-3 leu2 trp1 ura3-52 gal2 FAS2::FAS2Δ1750-1857_kanMX) were used. Cultures of the ΔYDL110C and FAS2Δ1750-1857_kanMX strains were grown with additional selective G418 antibiotic. The ΔPPTase-FAS required the addition of 50 µg/ml myristic, palmitic and stearic acid to the YPD-medium prior to autoclaving. To keep the external fatty acids in solution 1% (v/v) TWEEN20 was added to the warm medium after autoclavation.

To prepare pre-cultures for bio reactor fermentation, cells from glycerol stock were streaked out on YPD-agarose plates and incubated for 48h at 30°C. A single colony was picked and used to inoculate 250 ml YPD medium (24h, 200rpm, 30°C) until an OD_{600} of 2-3 was reached as a pre-culture. The pre-culture was used to inoculate 10 x 500 ml YPD at OD_{600}. Cultures were grown (24h, 200 rpm, 30°C) and either used as pre-culture for a 250l fermenter (Infors 250) or spun

down (10 min, 5.000g 4°C). Pelleted cells were washed with cold ddH_2O, spun (10 min, 5.000 g, 4°C) and finally resuspended with 2 ml 2x SB with 20% sucrose (w/v) per gram of cell pellet. The resuspended cells were frozen as beads by dropping the suspension drop for drop into liquid nitrogen and stored at -80°C.

3.12 Bacterial cell cultures

Transformation into competent *E. coli* expression strains (*Table 3.8*) was performed using a standard heat-shock protocol and plated out on LB-agar with the appropriate antibiotics and incubated (24h, 37 °C). 100 ml pre-cultures in LB medium were inoculated with single colonies containing 1% glucose (w/v) and antibiotics and incubated (16 h, 180 rpm, 37 °C). For expression cultures 500 ml of TB medium with 1% glucose (w/v) and antibiotics was inoculated using the pre-culture to an OD_{600} of 0.05. Cultures were grown (37 °C, 180 rpm) until an OD_{600} of 0.6-0.8 was reached. Then the temperature was lowered to 18 °C and after 1 h incubation cultures were induced by addition of 1% (w/v) IPTG and 2% (w/v) arabinose if required. Overexpression was performed for 16 h at 18°C and 1800rpm shaking. Cells were harvested by centrifugation (5,000 g, 5 min, 4 °C) resuspended and washed with ice-cold 1x PBS-buffer (137 mM NaCl, 2.7 mM KCl, 10 mM Na_2HPO_4, 1.8 mM KH_2PO_4; pH 7.4) and again spun (5000 g, 5 min, 4 °C). The final pellet was flash frozen in liquid nitrogen and stored at -80 °C.

protein	expression vector	resistance	expression strain	affinity tag
yACP	pET21c	ampicillin	BL21 (DE3) star	His_6
yACP S180H	pET21c	ampicillin	BL21 (DE3) star	His_6
E.c. AcpP	pET29a	kanamycin	BL21 (DE3) star	His_6
H.s. PPTase	pRSETA	ampicillin	BL21 (DE3)	His_6
AcpS	pET28b	kanamycin	BL21 (DE3)	His_6
1x-UnaG	pRSETA	ampicillin	BL21 (DE3)	His_6
2x-UnaG	pRSETA	ampicillin	BL21 (DE3)	His_6
Tma	pET151/D-TOPO	ampicillin	BL21 (DE3) star	His_6
TmaTesA	pET151/D-TOPO	ampicillin	BL21-AI	His_6
Tma-1xUnaG	pET151/D-TOPO	ampicillin	BL21 (DE3) star	His_6
Tma-2xUnaG	pET151/D-TOPO	ampicillin	BL21 (DE3) star	His_6
Sfp	pET29b	kanamycin	BL21 (DE3)	His_6
CoaA	pET28a	kanamycin	BL21 (DE3)	His_6
CoaD	pET28a	kanamycin	BL21 (DE3)	His_6
CoaE	pET28a	kanamycin	BL21 (DE3)	His_6

Table 3.8: Constructs for expression of recombinant proteins

3.13 Purification of recombinant proteins

For purification of recombinant protein, overexpressed cells were resuspended in 5 ml resuspension buffer per gram of cells. The resuspension was incubated (30 min, 4 °C, mixing) after adding 2 U/ml DNAse (NEB) and 0.33 mg/ml lysozyme. Cells were lysed by two rounds of

passing through an Emulsiflex C3 (Avestin) at 15,000 PSI, the lysate was centrifuged (50,000 g, 30 min, 4°C) filtered through a cellulose-acetate syringe filter (Startorius Stedim) and loaded on a 10 ml Ni-NTA column pre-equilibrated in 20 CV of resuspension buffer. After binding of the protein of interest, the column was washed with 10 CV of washing buffer. For elution, 1 CV of elution buffer was applied and the flow-through was collected in 1 ml fractions. The eluting fractions were analyzed via SDS-PAGE and alle fractions containing the desired protein were pooled.

For specific cleavage of the appropriate affinity tag, the pooled protein solution was digested by addition of TEV-protease or SUMO-protease in an enzyme-to-protein ration of 1:50, respectively. The digestion reaction was performed overnight (16 h, 4 °C, gently mixing) in a dialysis tube (6,000-8,000 MWCO) against 5 l of dialysis buffer. To remove the affinity tag as well as undigested protein, the dialyzed protein solution was loaded on a 10 ml Ni-NTA column equilibrated in 10 CV dialysis buffer. The flow-through was collected and analyzed via SDS-PAGE.

If required, additional chromatographic purification steps (size exclusion chromatography or ion exchange chromatography) were made to achieve the highest possible purity. For concentration of the final protein, centrifugal filters of appropriate pore size were used, and the protein concentration was determined spectroscopically using the specific extinction coefficient as well as the molecular weight (Table 3.4). The final protein solutions were aliquoted, frozen in liquid nitrogen and stored at -80 °C.

3.14 Chromatography-free Δγ-FAS purification

The endogenous FAS from *S. cerevisiae* wild-type strain as well as all mutant yeast strains were purified using the same purification protocols.

Yeast cells were lysed by grinding the frozen beads with a centrifugal mill (Retsch ZM200). The resulting cell powder was thawed in a water bath (15 min, 37°C, mixing). Per gram of lysed cells 2 ml of SB-purification buffer supplemented with 20% sucrose (w/v) was added and incubated (30 min, 25 °C, mixing). The lysate was cleared by centrifugation (30,000 g, 30 min, 4°C) and the supernatant was filtered through three layers of Miracloth and cheesecloth. In a next step 0.02% OGNG (w/v) was added to the S30 lysate and incubated (1 h, 25 °C, mixing) followed by a further centrifugation (1 h, 100,000 g, 4 °C) and filtration step through three layers of Miracloth and cheesecloth. The S100 lysate was subjected to polyethylene glycol (PEG) precipitation using an 80% PEG 400 (v/v) stock in 1x SB-acetate. In a first precipitation step, proteins were precipitated with 20% PEG 400 (v/v). After incubation (30 min, 18 °C, mixing) the precipitated solution was spun (30,000 g, 30 min, 4°C), the pellet discarded, and the supernatant further precipitated by the addition of PEG 400 to a final concentration of 30% (v/v). The solution was again incubated (30 min, 18 °C, mixing) and spun (30 min, 30,000 g, 4°C). The resulting

pellet was kept and resuspended (18 °C, gentle shaking) in resuspension buffer (1x SB-acetate, 2% sucrose (w/v), 0.01 % LMNG, 5 mM TCEP). For further purification the resuspended pellet was loaded on linear sucrose gradients of Surespin 630 tubes (10-45% sucrose (w/v), 1x SB-acetate, 2.5 mM TCEP) and ultra-centrifuged (16 h, 132,000 g, 4°C). Per tube approximately 45 mg of protein were loaded. Gradients were harvested in 1 ml fractions from top to bottom and analyzed by SDS-PAGE. The FAS containing fractions identified by SDS-PAGE were pooled and precipitated by addition of 80% PEG 400 in 1x SB-acetate to a final concentration of 40% PEG 400 (v/v). After incubation (1h, 18°C, mixing) the solution was spun (1h, 50,000 g, 4°C) and the resulting pellet was resuspended (18°C, gentle shaking) in resuspension buffer. The protein was loaded on linear SW40 sucrose gradients (10-45% sucrose (w/v), 1x SB-acetate, 2.5 mM TCEP). Per tube approximately 7 mg of protein were loaded. By ultra-centrifugation (16h, 79.000 g, 4°C) the protein was further purified. The gradients were harvested from top to bottom in 400 µl fractions and analyzed by SDS-PAGE. FAS containing fractions identified by SDS-PAGE were pooled and precipitated by addition of 80% PEG 400 to a final concentration of 40% PEG 400 (v/v) and spun (1 h, 50,000 g, 4 °C). Depending on the purity and purpose of further usage, the pellet was resuspended in crystallization buffer (1x SB-acetate, 10 % sucrose (w/v), 0.01 % LMNG (w/v), 5 mM TCEP) or normal resuspension buffer (see above). In case additional purification was necessary, the protein solution was again loaded on linear SW40 sucrose gradients (10-45% sucrose (w/v), 2.5 mM TCEP, 1x SB-acetate), ultra-centrifuged (16 h, 160,000 g, 4 °C) and analyzed via SDS-PAGE. The FAS containing fractions identified by SDS-PAGE were pooled, precipitated with 40% PEG 400 (v/v) and centrifuged (1h, 50,000 g, 4°C) and resuspended in crystallization buffer. The protein concentration was photometrically determined and stored at 4°C or flash frozen in liquid nitrogen.

3.15 Chromatography-free ΔPPTase-FAS purification

For the chromatography-free purification of the ΔPPTase-FAS protein, the protocol (*see 3.14*) was modified by the addition of nucleic acid precipitation using 2% (w/v) streptomycin sulfate after the first S30 step. After addition of streptomycin, the solution was incubated (30 min, 25 °C, mixing) and clarified (30 min, 30.000g, 4 °C). This resulted in the successful removal of unspecific nucleic acid binding proteins which allowed us to reduce the purification protocol by one density gradient step (see *3.14*). By dispensing this third density gradient step we were able to shorten the protocol by a whole working day.

3.16 Salt dependent γ-subunit dissociation

To investigate the salt-dependent dissociation of γ-subunit from wtFAS, freshly purified wtFAS protein was loaded on sucrose gradients of different ionic strength (10-45 % sucrose, 1x SB-acetate, 1 mM TCEP, 50/150/250 mM KCl). Per gradient a total amount of 0.2 nmol wtFAS was

loaded and the gradients were ultra-centrifuged (120,000 g, 16 h, 4 °C). The gradients were harvested from top to bottom in 200 µl fractions and all fractions were analyzed by SDS-PAGE. As a control reaction we used freshly purified Δγ-FAS without γ-subunit using the same protocol.

3.17 γ-subunit binding affinity to Δγ-FAS

To determine the binding affinity of the γ-subunit to FAS, the recombinant γ-subunit was labelled with a fluorescent NHS-rhodamine dye. For labelling, 1 ml of a 1 mM γ-subunit solution in γ dialysis buffer was incubated (1 h, 25 °C, protected from light) with a tenfold molar excess of NHS-rhodamine. To remove unbound NHS-rhodamine dye, the reaction was loaded on centrifugal desalting columns (Thermo Fisher). The labelled γ-subunit was added in different final concentrations (0 µM – 30 µM) to 1 µM Δγ-FAS reactions in a final volume of 40 µl binding assay buffer (50 mM BisTris pH 6.5, 50 mM potassium acetate, 0.5 mM magnesium acetate). All reactions were incubated (30 min, 30 °C, protected from light) and 10 µl of each reaction was loaded onto a 1.5 % (w/v) agarose gel (0.5x TBE, 2 mM $MgCl_2$). The gel was run (2 h, 75 mA, 4 °C, protected from light). For detection of the fluorescent signal from the NHS-rhodamine labelled γ-subunit, the gel was imaged with an Amersham Imager 600 (GE-Healthcare). For quantification of the fluorescent signal from the digital images, ImageJ was used. The dissociation constant was calculated with the Hill equation, based on the fluorescent signal resulting from the Δγ-FAS bands with bound fluorescent NHS-γ-subunit. All reactions were performed in triplicates and used for the calculation of the standard deviation for each NHS-γ-subunit concentration. As a control reaction, we used commercially available trypsin inhibitor (Sigma-Aldrich) which was also fluorescently labelled with NHS-rhodamine and used in the same molar ratios as the NHS-γ-subunit.

To investigate the binding behavior of the two recombinant γ-subunit truncation variants Δ1-25 and Δ117-150, we used the same experimental procedures as described above. Binding reactions with labelled γ-subunits were also loaded onto agarose gels and the fluorescent signal was computationally quantified with ImageJ.

3.18 γ-subunit mediated binding to Δγ-FAS

For binding studies of the designed protein constructs γ-1xUnaG, γ-2xUnaG and γ-TesA to Δγ-FAS, the three recombinant proteins were added in a 50x molar excess to 50 pmol of freshly purified Δγ-FAS in a final volume of 50 µl resuspension buffer. After incubation (30 min, 30 °C), the reactions were loaded on linear sucrose gradients (TH660, 10-45% sucrose (w/v), 1x SB-acetate, 1 mM TCEP) and ultra-centrifuged (16 h, 120,000 g, 4 °C). The gradients were harvested from top to bottom in 21 x 200 µl fractions and analyzed via SDS-PAGE. To investigate whether the protein constructs were binding to the Δγ-FAS, the SDS-gels were checked for co-sedimentation of the corresponding constructs into the 40 S region of the gradient. As control

reactions, gradients with either only Δγ-FAS or one of the three protein constructs alone were run to verify, that the co-sedimentation in the 40 S region is mediated by FAS binding.

3.19 FAS steady-state kinetic measurements

For steady-state kinetic measurements of the Δγ-FAS in the presence and absence of the γ-subunit, a spectrophotometric assay monitoring the NADPH consumption was established. All measurements were made using a V750 UV-vis spectrophotometer (Jasco Instruments) at 340 nm and 30 °C. The substrate concentration dependance of FAS activity was monitored for all three substrates (NADPH, acetyl-CoA, and malonyl-CoA). All measurements were made at a constant Δγ-FAS concentration of 12.7 nM in 200 µl. Due to impurities of the commercially available substrates acetyl- and malonyl-CoA were additionally purified by reversed phase HPLC (ÄKTA Basic 900, GE-Healthcare) using a preparative C18 column (Macherey-Nagel Nucleodur 100-5-C18, 250 mm x 21 mm, 5 µm) with a flow rate of 10 ml/min. The UV-absorption was continuously monitored at 215 nm, 260 nm and 280 nm and elution was performed using a linear gradient from 100% A (ddH_2O, 0.1% (v/v) TFA) to 100% B (79.9 % acetonitrile, 20% ddH_2O, 0.1% (v/v) TFA). The substrate containing peak fractions were collected and lyophilized. For further usage, the lyophilized substrates were dissolved in ddH_2O, and the exact concentrations were spectrophotometrically determined using the specific molar extinction coefficients (acetyl-CoA: ε_{260} = 15,400 1/M*cm; malonyl-CoA: ε_{260} = 15,400 1/M*cm; NADPH: ε_{340} = 6220 1/M*cm). For acetyl-CoA concentration dependent activity measurements, malonyl-CoA (120 µM) and NADPH (320 µM) concentrations were constant, while the acetyl-CoA concentration was titrated from 0 µM to 240 µM. For malonyl-CoA concentration dependent activity, NADPH (320 µM) and acetyl-CoA (180 µM) were constant, and malonyl-CoA was titrated from 0 µM to 240 µM. For NADPH concentration dependent activity measurements, acetyl-CoA (180 µM) and malonyl-CoA (120 µM) were constant, and NADPH was titrated from 0 µM to 320 µM. All reactions were performed in a total reaction volume of 200 µl kinetic assay buffer (50 mM BisTris pH 6.5, 50 mM potassium acetate, 0.5 mM magnesium acetate, 10% (w/v) sucrose). Prior to the kinetic measurement, a 0.254 µM Δγ-FAS solution in kinetic assay buffer without sucrose was pre-incubated with or without additional γ -subunit (500x molar excess) for 30 min at 30 °C. The final assays contained 12.7 nM Δγ-FAS, 0.2 mg/ml trypsin inhibitor protein (non-crowding condition), 20 mg/ml trypsin inhibitor protein (crowding conditions), 6.35 µM γ-subunit (in Δγ-FAS_{rec} conditions) and the corresponding substrate concentrations. Each reaction was prepared and incubated (1 min, 30 °C), transferred to a Quartz cuvette (Hellma Analytics) and the reaction was started by addition of malonyl-CoA. Each reaction was measured in triplicates for calculation of the standard deviation. In case of the acetyl-CoA and malonyl-CoA concentration dependent, the initial steady-state rates were analyzed by linear regression of the absorbance change at 340 nm within the

first five seconds after mixing (see 3.20). For NADPH, equation III was used to distinguish for time-dependent change of the slope between higher and lower activities (see 3.20).

3.20 Equations for steady-state kinetic evaluation

The use of the following equations for evaluation of the steady-state enzyme kinetic measurements were suggest by Dr. Viktor Sautner and Prof. Dr. Kai Tittmann.

$$\text{I.} \quad v(s) = \frac{V_{max} * [S]^n}{K_{0.5}^n + [S]^n}$$

$$\text{II.} \quad v(s) = \frac{V_{max} * [S]^n * (K_i)}{K_{0.5}^n * (K_i) + [S]^n * (K_i + [S])}$$

$$\text{III.} \quad v(s) = \frac{V_{max} * [S]^n * (K_i + \alpha * [S])}{K_{0.5}^n * K_i + [S]^n * (K_i + [S])}$$

To measure the ΔPPTase-FAS activity after activation with yPPTase and CoA, the same NADPH dependent activity assay was used. Activity reactions were measured at a final FAS concentration of 19.23 nM with substrate concentrations of 200 µM (NADPH), 100 µM (acetyl-CoA) and 60 µM (malonyl-CoA) in 100 µl reaction volume. The reactions were started by addition of malonyl-CoA and the absorbance at λ_{340nm} was monitored at 25 °C for 1 min. For activity determination and comparison amongst different reactions, the activity (ΔAbs/min) was calculated for the time range from 0s to 10s.

3.21 GC-MS product analysis

For product analyses of different FAS enzyme assays, end-point reactions were prepared and analyzed via GC-MS. 253.8 nM of freshly purified FAS was mixed with a 500x molar excess of γ-subunit or TesA-constructs, respectively. All reactions were incubated for 30 min at 25°C to ensure a binding of the added proteins to the FAS protein. To start the enzymatic reactions, the protein solution was 1:20 diluted with 1x SB-acetate buffer and final substrate concentrations of 100 µM (acetyl-CoA), 60 µM (malonyl-CoA) and 320 µM (NADPH). Reactions were incubated for 30 min at 30 °C until no further enzymatic activity was measurable due to NADPH consumption. The final reaction assays were frozen in liquid nitrogen and kept at -80 °C. GC-MS analyses of the reactions were made by PD Dr. Meina Neumann-Schaal and her team at the DSMZ Braunschweig. CoA thioesters were analyzed by HPLC-MS using an Agilent 6545 QTOF system equipped with an ESI source coupled to a 1290 series HPLC system. One µl of the enzyme assay

was directly injected onto a Gemini C18 column (3 µm, 110 Å, 150 x 2 mm). The solvent used were 50 mM ammonium formate, pH 8.1 (A) and acetonitrile (B) at 35°C with the following gradient: 95% A for 1 min, gradient to 30% B in 18 min, gradient to 95% B in 17 min and gradient to 100% B in 4 min. The QTOF was run at following settings: positive mode, gas temperature 200°C, Sheath gas temperature 325°C, Fragmentor 180 V, Skimmer 45 V, Capillary voltage 4500 V. Data were evaluated using the MassHunter Qualitative Navigator software by extracting ion chromatograms for the $[M+H]^{+}$ and the $[M+2H]^{++}$ m/z of the respective CoA thioesters. The retention time was confirmed using authentic standards.

3.22 Activation of ΔPPTase-FAS with CoA

For activation of the ΔPPTase-FAS, 0.38 µM FAS was mixed with a 60x molar excess (23 µM) of trimeric enzymatically active yPPTase (Johansson et al., 2009b) activation buffer (1x SB-acetate pH 6.0, 1 mM CoA, 1 mM TCEP, 1.0 µM PDCL3). The PDCL3 protein which was used as a crowding agent was provided by my colleague Dr. Elham Paknia. After 30 min at 25 °C, the activation reaction was diluted with an equal volume of activation buffer. The reaction was then transferred to a dialysis tube (3.000 MWCO, Merck) and dialyzed (18 °C, 16h) against 500 ml activation dialysis buffer (1x SB-acetate, 10 µM CoA, 1 mM TCEP). The dialyzed protein solution was used to test the enzymatic activity using the standard FAS NADPH activity assay (see 3.19). To test the ΔPPTase-FAS activation by other PPTases, the same protocol, using a 60x molar excess over ΔPPTase-FAS was used. Activities were measured with the NADPH activity assay described above. For statistics, all activities were measured in triplicates. The different activities were plotted with standard deviation and visualized for comparison in a histogram.

3.23 Chemo-enzymatic synthesis of CoA from D-pantethine

150 mM D-pantethine was dissolved in 1xSB-acetate and reduced by addition of 150 mM TCEP. The solution was incubated for 10 min at 25 °C. For further experiments, after the reduction by TCEP, a 300 mM concentration of D-pantetheine was assumed. For the synthesis of CoA starting from D-pantethein an enzymatic synthesis reaction using *E. coli* CoaA, CoaD and CoaE was made. 1x SB-acetate pH 7.0, 24 mM ATP, 30 mM $MgCl_2$, 5 µM CoaA, 5 µM CoaD, 5 µM CoaE, 10 % DMSO (v/v) and three different concentrations (10 mM, 50 mM, 100 mM) of freshly reduced D-pantetheine were mixed in a final volume of 200 µl and incubated for 24h at 37 °C. The DMSO was added to ensure a comparability with the chemo-enzymatic crypto-CoA reactions which were performed with a total amount of 10% DMSO (v/v). After incubation, the reactions were cleared by centrifugation (17.000 g, 10 min, 4 °C) and the supernatant was stored at – 80°C.

For activation of ΔPPTase FAS using the synthesized CoA the standard activation protocol was used. The final CoA concentration was assumed to correspond to the input D-pantetheine concentration.

3.24 Synthesis of pantetheinamide crosslinker CoAs

For enzymatic synthesis of mechanism-based reactive crosslinker the modified pantetheineamide precursor molecules were processed to crosslinker CoAs (crypto-CoA) using the *E. coli* enzymes CoaA, CoaD and CoaE. A synthesis reaction was performed in a total volume of 10 ml, containing 1x SB-acetate pH 6.5, 24 mM ATP, 30 mM $MgCl_2$, 5 µM CoaA, 5 µM CoaD, 5 µM CoaE, 10 mM pantetheinamide crosslinker, 1 mM TCEP. The reaction was incubated for 16h at 37 °C, cleared by centrifugation (20.000 g, 4 °C, 15 min) and stored at -80°C.

3.25 In vitro activation of recombinant *S. cerevisiae* apo-ACP

To test whether the yPPTase is active in phosphopantetheinylation of yeast apo-ACP, apo-ACP was modified with CoA and C_{17}-CoA. As negative control, a S180A-ACP mutant was used. Phosphopantetheinylation reactions were made in one-pot assays containing 20 mM BisTris pH 7.5, 10 mM NaCl, 100 mM KCl, 5 mM $MgCl_2$, 10 mM $CaCl_2$, 1 mM TCEP, 15% glycerol (v/v), 0.2 mM CoA/C_{17}-CoA, 46 µM apo-ACP/S180A-ACP, 5 µM yPPTase as it was formerly described by Burkart and co-workers (Worthington and Burkart, 2006). The reactions were incubated o/n at 18 °C and analyzed via SDS-PAGE on an Any-kD gel (BioRad).

3.26 Loading of apo-AcpP with pantetheinamide crosslinkers

To test whether the different pantetheine crosslinkers can be further processed to crosslinker-CoA by the *E. coli* enzymes CoaA, CoaD and CoaE and then further used as substrate for *B. subtilis* Sfp-induced loading on *E. coli* apo-AcpP, a one-pot reaction was performed. 200 µl reactions containing 50 mM potassium phosphate pH 7.0, 8 mM ATP, 10 mM MgCl2, 1.0 µM CoaA, 1 µM CoaD, 1 µM CoaE, 1.5 µM Sfp, 100 µM apo-AcpP, 200 µM pantetheineamide crosslinker and 5% DMSO (v/v) were incubated o/n at 37 °C. For site crosslinking, 70 µM of FabA, FabB and FabI were added to their corresponding crypto-CoA solution. The crosslinking reactions were incubated o/n at 25 °C and analyzed via SDS-PAGE.

3.27 Loading of ΔPPTase FAS with crypto-CoAs

For loading of the ΔPPTase FAS with mechanism specific reactive substrates from crypto-CoAs, the same ΔPPTase-FAS activation protocol was used (see *3.22*). From the chemo-enzymatic synthesized crypto-CoAs we used final concentrations of 1 mM for the activation reaction and 10 µM in the activation dialysis buffer.

3.28 Structure determination

Structures of the different FAS complexes were determined by cryo-EM and protein X-ray crystallographic techniques. For model building and structure representation Coot and ChimeraX were used (Emsley and Cowtan, 2004; Pettersen et al., 2004, 2021)

3.29 Cryo-EM sample preparation

For cryo-EM data collection, EM grids of all FAS constructs were prepared with a final protein concentration of 0.5 mg/ml. For grid preparation, the protein was bound to a floating continuous carbon film (2 min at 4°C) and then attached to a Quantifoil grid (3.5/1) (Quantifoil, Jena/Germany). For plunge freezing in liquid ethane a Vitrobot Mark IV (Thermo Fisher, Germany) was used (8s blotting at 4 °C and 100% relative humidity).

3.30 Crystallization and stabilization of Δγ-FAS/ Δγ-FAS + γ-subunit

The Δγ-FAS was crystallized at a concentration of 7 mg/ml. A volume of 1 µl from the protein solution was mixed with 1 µl of reservoir solution (0.1 M Na-HEPES pH 7.0, 0.2M-0.3M Na-malonate pH 7.0, 11%-13% (w/v) PEG 3350). The crystals grew in both, sitting and hanging drop plates over 4-5 days at 18 °C. For stabilization and cryo-cooling of crystals, the plates were cooled down over 24 h in a linear temperature gradient from 18 °C to 4 °C. Crystals were stabilized and cryo-protected by stepwise buffer exchange with stabilization buffers (*Table 3.7*) of increasing ethylene glycol (7.5% to 20%) and PEG 3350 (11% to 20%) concentrations.

For the crystallization of Δγ-FAS$_{rec}$, the Δγ-FAS was crystallized at a FAS concentration of 7 mg/ml with additional γ-subunit$_{rec}$ in 50x molar excess. Using the same crystallization conditions and sitting drop vapor diffusion.

3.31 Crystallization and stabilization of ΔPPTase-FAS

For crystallization of the *in vitro* modified ΔPPTase-FAS, crystals were grown in conditions of 0.1 M Na-HEPES pH 7.0, 11%-15% PEG 3350 (w/v), 0.1M-0.5M Na-malonate pH 7.0. The protein concentration was varied between 3.5 mg/ml and 6.0 mg/ml, the reservoir volume of both, hanging and sitting drop plates was 500 µl and 1 µl of protein solution was 1:1 mixed with the reservoir

solution. The crystals grew over 5 to 7 days at 18 °C. For cryo-cooling and stabilization, the crystal plates were cooled down over 24 h in a linear temperature gradient from 18 °C to 4 °C. Crystals were stabilized and cryo-protected by stepwise buffer exchange with stabilization buffers (*Table 3.7*) of increasing ethylene glycol (7.5% to 20%) and PEG 3350 (11% to 20%) concentrations.

3.32 Cryo-EM data collection and image processing

The Cryo-EM data collection and image processing steps were performed by Kashish Singh. For data acquisition a Titan Krios (Thermo Fisher) at 300 kV with a Falcon 3 or K2 summit (Gatan Inc.) electron detector was used in counting mode. The collected movies were motion and dose corrected with Motioncor2 (Zheng et al., 2017) and split in patches of 5x5. After frame alignment CTF estimation was performed using GCTF (Zhang, 2016) and single particles were automatically selected using Gautomatch (Zhang Software, MRC Laboratory). Further image processing was performed with Relion 3.0 (Scheres, 2012; Zivanov et al., 2018). To remove bad images the extracted single particles were selected by three subsequent rounds of reference free 2D classification. For 3D reconstruction, the final particles were refined with a refinement mask around the hexameric central wheel with an applied D3 symmetry. As starting model the published FAS structure EMDB: 1623 (Gipson et al., 2010a) was filtered to a resolution of 30 Å and used as reference for all 3D refinement and classification methods. The particles resulting from the 3D refinement were extracted, separated and 3D classified w/o alignment and by using a mask of the FAS domes. The particles of the highest resolved 3D classes were selected and used for a further round of 3D classification and refinement. The particles of the 3D class with high resolution information over the entire 3D model were extracted and used for CTF refinement with following 3D refinement. The final 3D refinement step was then performed with three different symmetry options (C1, C3 and D3).

3.33 X-ray diffraction data collection

After stepwise buffer exchange to the respective stabilization buffer conditions the protein crystals were harvested in Spine Litholoops (Jena BioSciences, Jena/Germany) and flash frozen in liquid nitrogen. For data collection of the $\Delta\gamma$-FAS and the $\Delta\gamma$-FAS_{rec}, the EMBL beamline P14 at PETRA III storage ring (DESY, Hamburg/Germany) with an EIGER 16M detector (Dectris, Baden/Switzerland) was used. For scaling and integration of the recorded x-ray diffraction data sets the XDS package was used (Kabsch, 2010).

For data collection of the ΔPPTase-FAS, the EMBL beamline P14 at PETRA III was used with an EIGER2 CdTe 16M detector (Dectris, Baden/Switzerland).

3.34 X-ray structure determination

The structure determination experiments for the Δγ-FAS and Δγ-FAS$_{rec}$ were performed by my colleague Kashish Singh as following.

The initial phases of the Δγ-FAS were determined with molecular replacement by us of the formerly published FAS structure PDB: 2UV8 (Leibundgut et al., 2007) with the program MOLREP (Vagin and Teplyakov, 2010). After manual model building in Coot (Emsley and Cowtan, 2004) and refinement using Refmac5 (Murshudov et al., 2011) the final structure was TLS-refined. The final structure showed a stereochemistry of 19.7% / 21.8% (R_{work}/R_{free}) (*Figure 8.2*).

For the Δγ-FAS$_{rec}$ complex initial phases were determined with MOLREP by molecular replacement using the structure of the Δγ-FAS. For further refinement processes, the structure resulting from the cryo-EM dataset of the Δγ-FAS$_{rec}$ complex was used. To prevent any bias from the Δγ-FAS$_{rec}$ EM model to the refinement of the crystal structure, the ACP and γ-subunit domains were deleted from the EM structure. Due to the resolution of 4.9 Å an Cα-trace model was built for the Δγ-FAS$_{rec}$ complex. The final structure turned out to show a stereochemistry of 25.1% / 31.0% (R_{work}/R_{free}) (*Figure 8.2*).

The initial phases of the PPTase-FAS complex were determined with MOLREP by molecular replacement using the structure of the Δγ-FAS. For further model refinement processes with REFMAC5 the PPTase domain of the Δγ-FAS model was removed. After several rounds of manual model building in Coot the covalent bound pantetheine amide crosslinker was built with JLigand (Lebedev et al., 2012) and introduced into the ΔPPTase-FAS structure. The final structure was TLS refined until a stereochemistry of 18.8% / 21.1% (R_{work}/R_{free}) (*Figure 8.2*). The high resolution of 2.9 Å allowed a model building of almost all amino acid side chains.

3.35 Cryo-EM model building

The cryo-EM model building was mad by Kashish Sing as following. The cryo-EM model of both the Δγ-FAS and Δγ-FAS$_{rec}$ was built by refinement of the crystallographic Δγ-FAS model into the EM density using USCF Chimera (Pettersen et al., 2004). After several more rounds of manual model building using Coot, the final model was refined using Refmac5. The model of the γ-subunit was built in Coot using the amino acid sequence and high-resolution information of visible amino acid side chains.

4 Results

Within the following part I will present the most recent findings that were made within the last four years during the work on my doctoral thesis. Since the research of large protein complexes involves many different methods and techniques it would have not been possible to address all upcoming questions without the close collaboration of different people. Therefore, I would like to thank Dr. Andreas Linden (Bioanalytical Mass Spectrometry, MPI-BPC/UMG Göttingen) for his work on the mass spectrometric experiments, Dr. Viktor Sautner (Department of Molecular Enzymology, Georg-August-University Göttingen) for his help with the establishing of enzyme kinetic measurements, PD Dr. Meina Neumann-Schaal (DSMZ – Leibniz Institute, Braunschweig) for product analysis using GC-MS. The different pantetheineamide precursor molecules which are used for several experiments were provided by our industry collaborator NovAliX (Illkirch-Graffenstaden, France). I would also like to thank my colleague Dr. Elham Paknia for providing PDCL3 protein, which was used a crowding agent for different enzymatic assays. Furthermore, I would like to mention that certain experiments which are presented in the first half of the thesis were carried out and evaluated by my former colleague Dr. Kashish Singh (Department of Structural Dynamics, MPI-BPC). The establishing of a chromatography-free purification, parts of protein binding experiments as well as structural investigations of the FAS complex ± γ-subunit by Cryo-EM and X-ray crystallography were performed by him. To draw a coherent picture of the progress and findings within this collaborative and exciting research project I decided to also include all these experiments and put them into context with all the experiments and findings I made during the last four years.

4.1 Chromatography-free FAS purification

Former studies of macromolecular protein complex purifications showed that chromatographic steps can have a detrimental impact on the biochemical and structural integrity of complexes (Haselbach et al., 2018; Schrader et al., 2016). While early protocols for the purification of the type I FAS from yeast were based on partially non-chromatographic purification techniques, researchers recently changed towards chromatographic steps based on affinity-tags or size exclusion (Johansson et al., 2008; Karam and Arslanian, 1984; Leibundgut et al., 2007; Lomakin et al., 2007; Lynen et al., 1980). To prevent possible negative effects of a chromatographic steps to the wild-type FAS (wtFAS) complex, my colleague Kashish Singh successfully established a chromatography-free purification protocol. This protocol involves polyethylene glycol (PEG) based protein precipitation in combination with sucrose density gradients. Other than former chromatography-free purification techniques, the use of PEG instead of ammonium sulphate allowed us to keep a constant and relatively low ionic strength (< 100 mM salt) over all purification steps. (Chun et al., 1967; Lomakin et al., 2007; Lynen et al., 1980; Polson et al., 1964)

For purification of the wtFAS, frozen yeast cells were lysed with a centrifugal mill. The proteins of the cell lysate were stepwise precipitated using increasing PEG concentrations. By application of centrifugal steps, the precipitated proteins were removed. The FAS containing protein pellet was kept and applied to linear sucrose density gradients. Over three sequential ultra-centrifugation steps in combination with wtFAS specific fraction collection and PEG-based protein precipitation we managed to purify the wtFAS protein to a high degree of purity, according to SDS-PAGE analysis. Starting from 230 g of dry-weight yeast cells, the protocol allowed us to purify 10-15 mg of pure wtFAS (*Figure 4.1*).

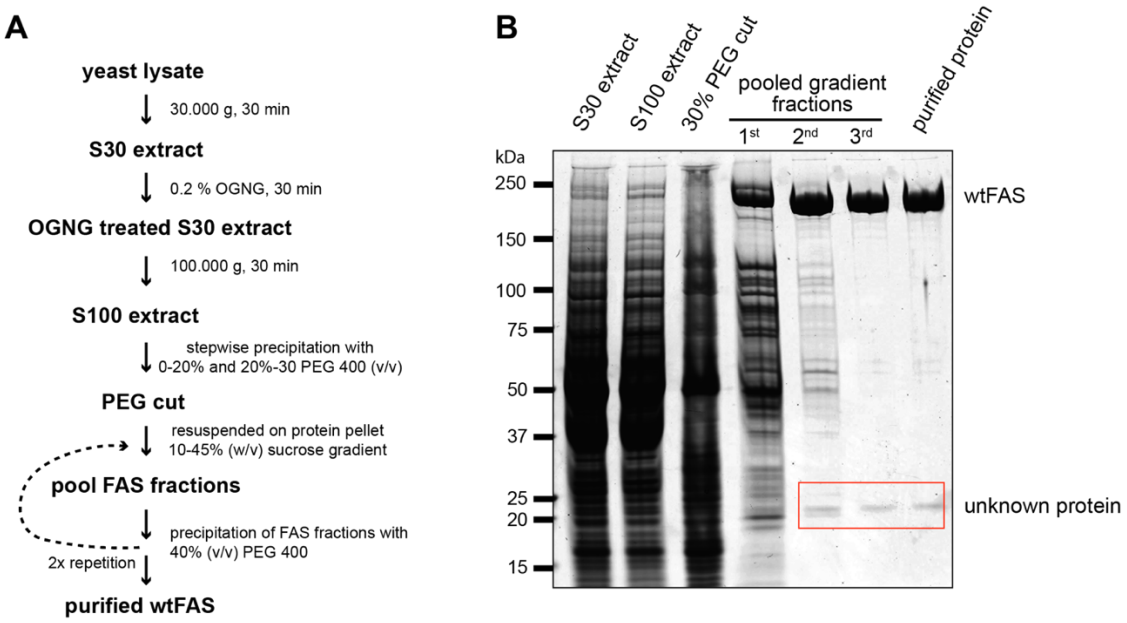

Figure 4.1: Schematic representation of the chromatography-free wtFAS purification. A) *Schematic overview of the FAS purification protocol using three sequential sucrose density gradients and various PEG-based protein precipitation steps.* ***B)*** *SDS-PAGE analysis of different S. cerevisiae wtFAS purification steps. After two first centrifugal cleaning steps to remove cell debris from the lysate (S30 extract, S100 extract), proteins were precipitated with 30% (v/v) PEG 400 (30% PEG cut). The resulting protein pellet containing the wtFAS was resuspended and loaded on linear 10%-45% sucrose density gradients followed by ultra-centrifugation. Over three sequential sucrose gradients the FAS containing fractions were pooled (1^{st}-3^{rd}). The final wtFAS was relatively pure and showed only one additional band of an unknown protein with an apparent size of approximately 20 kDa.*

4.2 Discovery of an additional FAS-binding protein

Although, former structural and biochemical studies showed that the yeast wtFAS is a heterododecameric complex of six α-chains (206.9 kDa) and six β-chains (228.7 kDa), SDS-PAGE analysis of pure wtFAS revealed a third protein band (*Figure 4.1 B and Figure 4.2*). Since this additional protein was co-purified over three sequential sucrose gradients, we considered that this band with an apparent size of 20 kDa could belong to a protein which is somehow associated to the FAS complex.

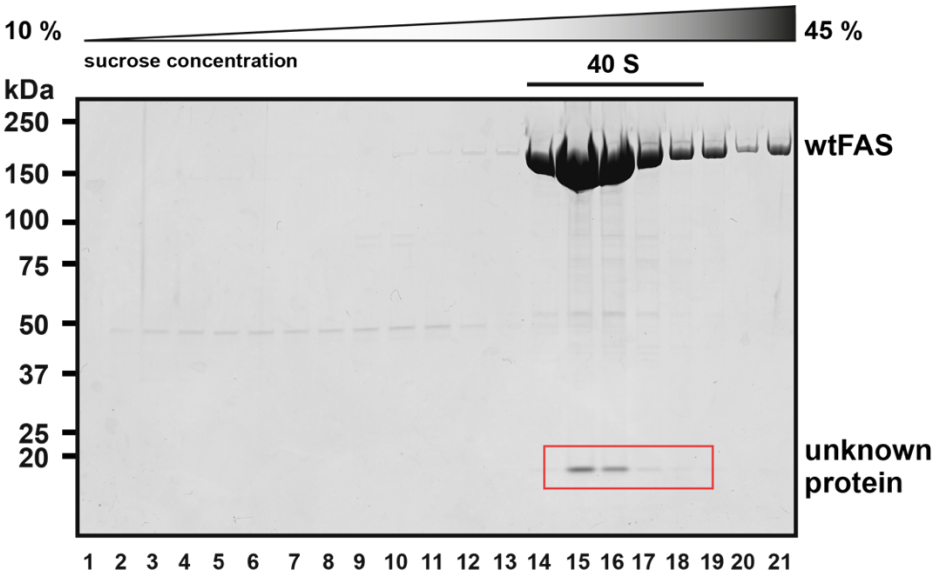

Figure 4.2: A unknown protein co-purifies with the yeast wtFAS. *SDS-PAGE analysis of fractions from the 3rd sucrose density gradient of a wtFAS purification. Together with the wtFAS an unknown protein of approx. 20 kDa is co-sedimenting into the 40S region of the linear 10-45% sucrose gradient.*

For identification of the additional protein band, we collaborated with Dr. Andreas Linden. A tryptic digest of the 20 kDa band, followed by tandem mass-spectrometry identified the unknown protein as the product of the *S. cerevisiae* YDL110C locus. Literature studies showed that the protein product of the YDLL110C locus was already formerly described in different studies. First, the protein was designated as a translation-machinery-associated protein 17 (Tma17p) according to findings that it is co-sedimenting with ribosomes (Fleischer et al., 2006). Later characterizations showed that Tma17p might not be ribosome associated but rather is a stress-induced ATPase dedicated chaperone involved into the assembly of the 26S proteasome (Adc17) (Hanssum et al., 2014; Rousseau and Bertolotti, 2016). According to the different descriptions I will designate the unknown protein for now as Tma17p/Adc17. Protein BLAST (BLASTp) analysis against the UniprotKB proteome database showed a conservation of the Tma17p/Adc17 sequence in the order of *Saccharomycetales* within the kingdom of *fungi* (Altschul et al., 1990; UniProt Consortium, 2015). To validate, whether parts of the Tma17p/Adc17 sequences are conserved, additional protein multiple sequence alignments (MSA) were made using the UniprotKB proteome. The MSA revealed a high conservation of two Tma17p/Adc17 regions within different members of the *Saccharomycetales (Figure 4.3, histogram highlighted in purple).*

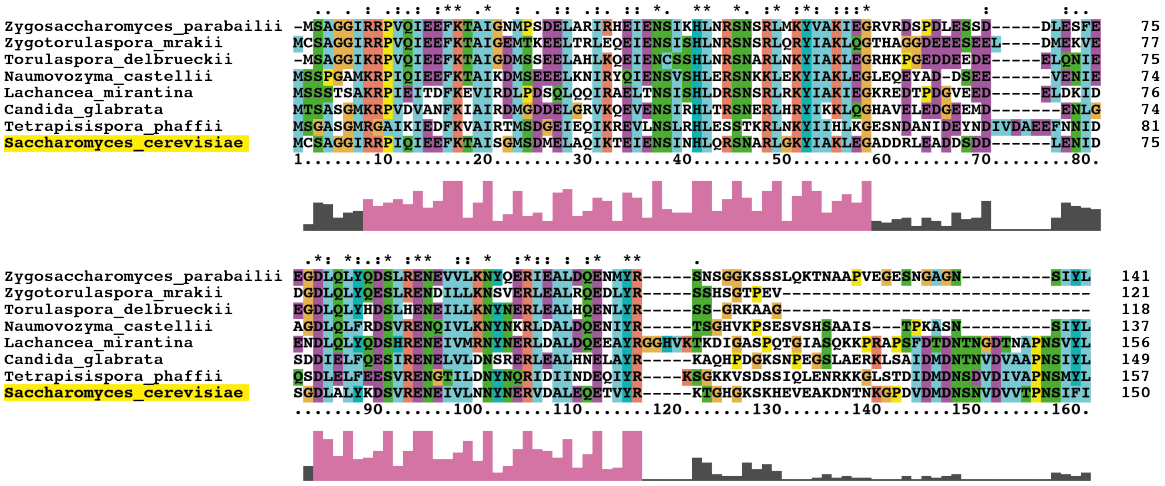

Figure 4.3: Results of Tma17p/Adc17 multiple sequence alignment. *The MSA of Tma17p/Adc17 protein sequences from seven members of the Saccharomycetales shows a high conservation of two regions (purple). The sequence of the S. cerevisiae (yellow) Tma17p/Adc17 was used as query sequence for the MSA analysis.*

4.3 Specificity of Tma17p/Adc17 to wtFAS

Since the endogenous yeast wtFAS was already purified by other groups using different protocols, we asked ourselves why Tma17p/Adc17 was overlooked as a FAS specific protein for several decades of research. By comparing former FAS purification protocols with ours, we noticed that other groups were either using chromatographic columns or chromatography-free protocols but employing ammonium sulfate precipitation instead of PEG precipitation. Other than PEG, the use of ammonium sulfate salt exposes the FAS to conditions corresponding to a high ionic strength. (Johansson et al., 2008; Lomakin et al., 2007; Lynen et al., 1980; Maier et al., 2008). To test, whether the ionic strength of the buffer conditions influences the binding of Tma17p/Adc17 to the wtFAS, we loaded freshly purified wtFAS protein (*Figure 4.2*) on density gradients with increasing ionic strengths (*Figure 4.4*). The different sucrose gradients were harvested manually and analyzed via SDS-PAGE. According to the SDS-PAGE analysis of the gradient fractions Tma17p/Adc17 showed a co-sedimentation wtFAS at an ionic strength corresponding to 50 mM KCl (*Figure 4.4, top).* At increasing ionic strength, a partial dissociation of Tma17p/Adc17 from wtFAS was induced (*Figure 4.4, mid*). At an ionic strength corresponding to 250 mM KCl Tma17p/Adc17 did not show any co-sedimentation with the wtFAS (*Figure 4.4, bottom*). Thus, we concluded that the binding of Tma17p/Adc17 to wtFAS is salt labile and may therefore have been overlooked by former groups using purification protocols at ionic strengths greater than 150 mM KCl.

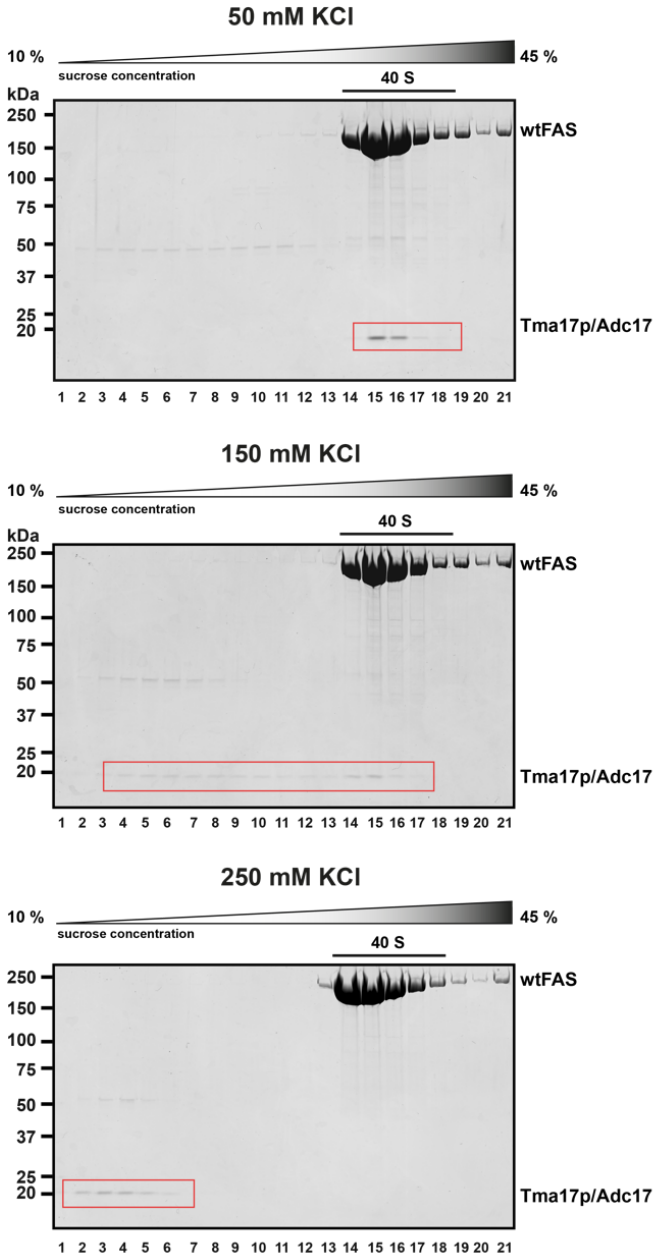

Figure 4.4: Salt dependent dissociation of Tma17p/Adc17 from wtFAS. *SDS-PAGE analysis of wtFAS sucrose density gradients with different ionic strength after ultra-centrifugation. At an ionic strength corresponding to 50 mM KCl (top) Tma17p/Adc17 shows a co-sedimentation with the wtFAS into the 40S region of the gradient (lanes 14-18). With increasing ionic strength corresponding to 150 mM KCl (mid) Tma17p/Adc17 starts to dissociate from wtFAS, which results in a spread over all fractions above the 40S region (lanes 4-17). At an ionic strength corresponding to 250 mM KCl Tma17p/Adc17 was only found in the top-layer fractions of the sucrose gradient (lanes 1-7).*

Based on the co-sedimentation of Tma17p/Adc17 with the endogenous wtFAS over three sequential sucrose gradients and its sequence conservation within *Saccharomycetaceae* we concluded that the Tma17p/Adc17 is a so far overlooked additional subunit of the heterododecameric $\alpha_6\beta_6$ yeast wtFAS complex. Following the already established nomenclature, we proposed to rename Tma17p/Adc17 to γ-subunit. Within this thesis, I will thus further use the designation of γ-subunit for the Tma17p/Adc17 protein.

4.4 Deletion of the YDL110C locus

After the discovery of the γ-subunit we asked ourselves what the role of this subunit within the wtFAS complex could be. Therefore, my colleague Kashish Singh created a mutant yeast strain with a deletion of the YDL110C locus, encoding the γ-subunit. The YDL110C locus was replaced by a G148 resistance cassette (BJ2168 MATa prc1-407 prb1-1122 pep4-3 leu2 trp1 ura3-52 gal2 YDCL110C::KanMX) via homologous recombination in chemically competent yeast cells. After successful replacement of the YDL110C gene with the resistance cassette the resulting deletion strain was named Δγ-BJ2168. The FAS protein purified from this strain is thus further designated as Δγ-FAS. Besides their G418 antibiotic resistance, the Δγ-BJ2168 cells did not show any differences in cell growth or temperature sensitivity to those of the wild-type BJ2168 cells (*Figure 4.5 A and B*).

With help of the Δγ-BJ2168 strain, we wanted to investigate the role of the γ-subunit within the FAS complex. We thus purified the Δγ-FAS with the same chromatography-free protocol. Throughout the whole purification process we did not see any changes in the sedimentation behavior of the Δγ-FAS. As expected, the final Δγ-FAS protein did also not show any additional band of the γ-subunit (*Figure 4.5 C*). Thus, we concluded that the Δγ-FAS must be fully assembled, and the γ-subunit does most likely not play any role in the FAS assembly process. To further investigate the role of the γ-subunit within the FAS complex, we performed additional biochemical experiments with a recombinant γ-subunit (γ-subunit$_{rec}$).

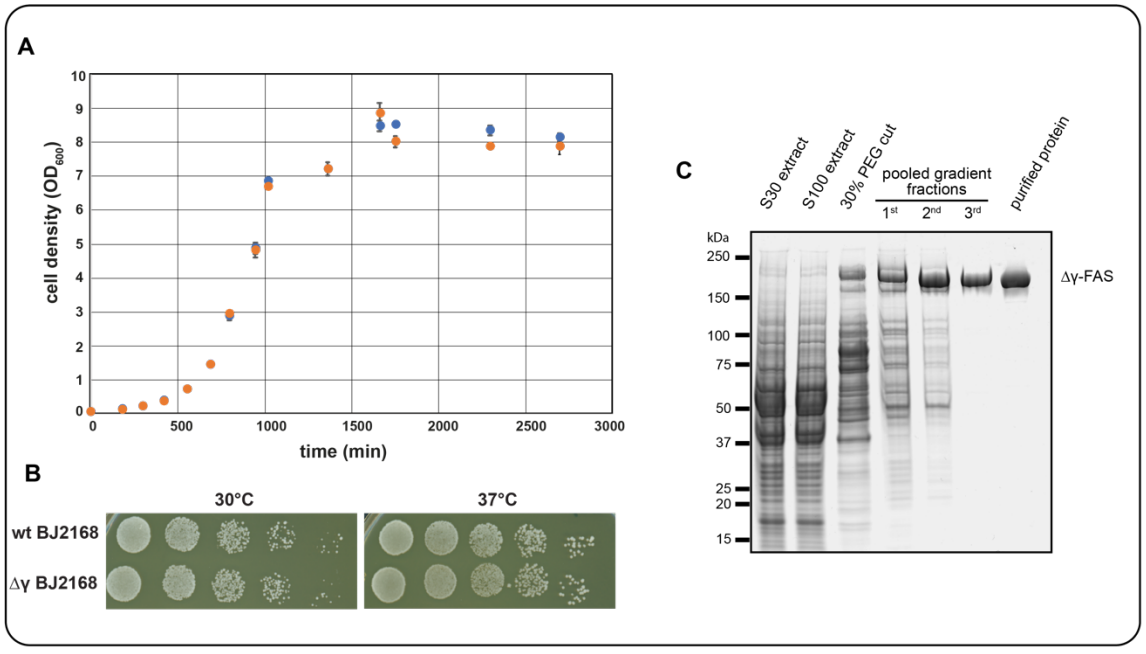

Figure 4.5: Deletion of the YDL110C locus has no impact on cellular growth and temperature sensitivity. A) *Growth curves of both, the wtBJ2168 (blue) and Δγ-BJ2168 (orange) yeast strains over 3000 min at 30 °C. Neither the doubling time nor the final cell density changed upon deletion of the YDL110C locus.* ***B)*** *The deletion of the YDC110L locus (Δγ-BJ2168) did not have any impact on the temperature sensitivity compared to the wtBJ2168 cells. Bot strains showed comparable growth at both tested temperatures (30 °C, left and 37 °C, right).* ***C)*** *SDS-PAGE analysis of chromatography-free Δγ-FAS purification from Δγ-BJ2168 lysate. Using the same purification protocol as described for wtFAS, the Δγ-FAS fractions did not show any additional band of γ-subunit at 20 kDa.*

4.5 Specificity of the recombinant γ-subunit

With help of a bacterial expression vector encoding a His_6-tagged γ-subunit sequence, we managed to purify 30 mg of recombinant γ-subunit (γ-$subunit_{rec}$) with a Ni-NTA-based affinity chromatographic protocol. According to SDS-PAGE analysis the TEV digested γ-$subunit_{rec}$ showed a high purity and was thus used for further experiments (*Figure 4.6*).

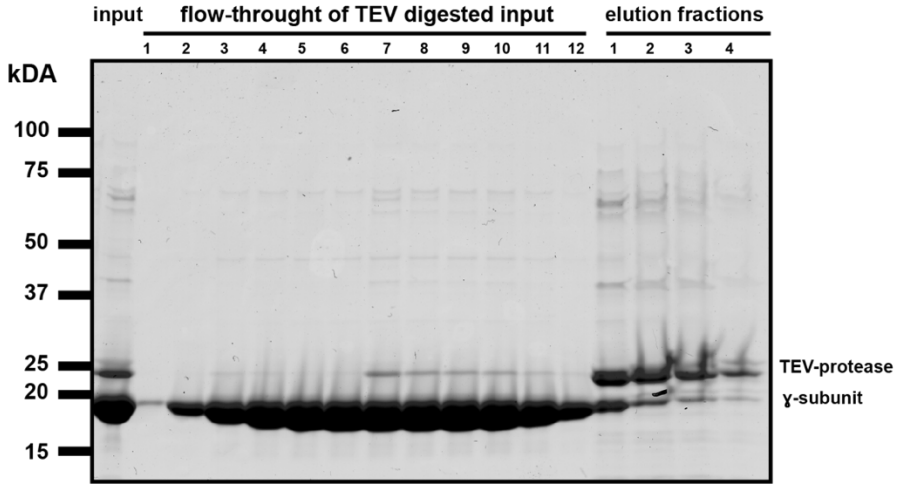

Figure 4.6: Purification of the recombinant γ-subunit. *SDS-PAGE analysis of different fractions from the γ-$subunit_{rec}$ purification. After TEV-digestion of the His_6-γ-$subunit_{rec}$, the protein was loaded onto a Ni-NTA column (input). The flow-through fractions (FT 1-12) contained γ-$subunit_{rec}$ with relatively low impurities. Within the elution fractions (lanes 1-4) the TEV-protease and undigested γ-$subunit_{rec}$ was eluted. The flow-through fractions containing digested γ-$subunit_{rec}$ were pooled and concentrated for further experiments.*

To investigate, whether γ-$subunit_{rec}$ binds to Δγ-FAS, we incubated 40 pmol of Δγ-FAS with a 50x molar excess of γ-$subunit_{rec}$. With linear sucrose gradients we tested whether the γ-$subunit_{rec}$ co-sediments with the Δγ-FAS into the 40S region. SDS-PAGE analysis of all gradient fractions indeed showed a co-sedimentation of γ-$subunit_{rec}$ with the Δγ-FAS (*Figure 4.7 A*). Therefore, we concluded that the addition γ-$subunit_{rec}$ to Δγ-FAS leads to the formation of a Δγ-FAS-γ-$subunit_{rec}$ complex (Δγ-FAS_{rec}). With further experiments we wanted to see whether the Δγ-FAS_{rec} shows the same salt-labile behavior as the wtFAS (Figure 4.7). To do so, we loaded Δγ-FAS_{rec} on three linear sucrose density gradients of increasing ionic strengths (*Figure 4.7*). After analysis of the gradient fractions by SDS-PAGE, we could show that γ-$subunit_{rec}$ only co-sediments with Δγ-FAS at an ionic strength corresponding to 50 mM KCl (*Figure 4.7 A*). The gradients at ionic strength corresponding to 150 mM KCl and 250 mM KCl showed a complete dissociation of γ-$subunit_{rec}$ from the Δγ-FAS complex (*Figure* 4.7 *B and C*).

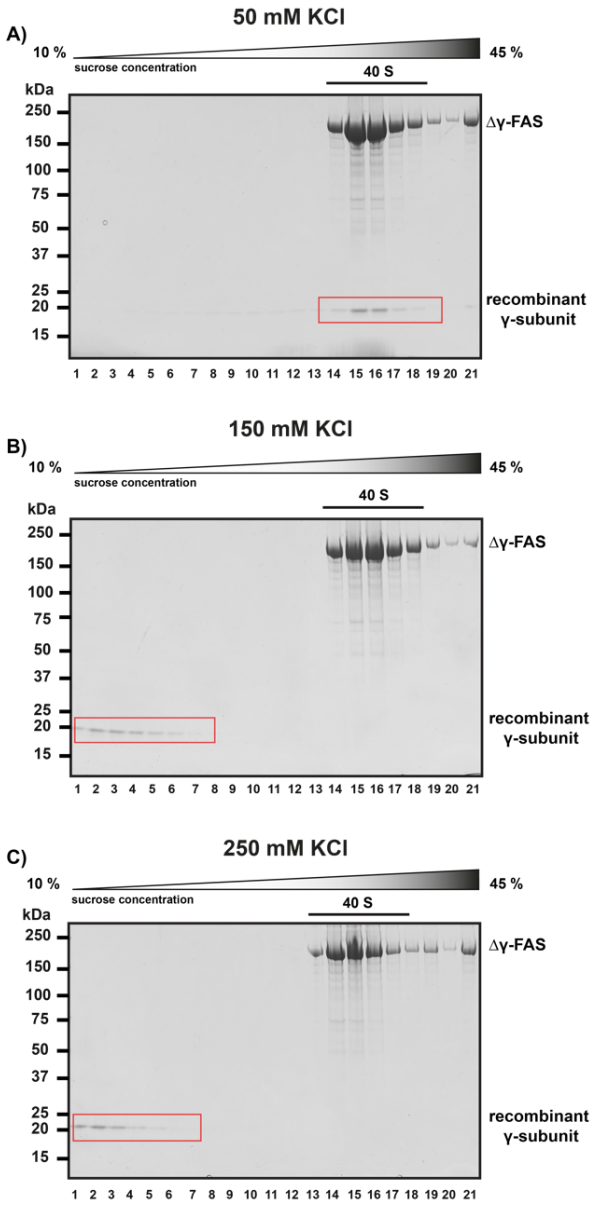

Figure 4.7: Salt dependent dissociation of recombinant γ-subunit from Δγ-FAS$_{rec}$. *SDS-PAGE analysis of Δγ-FAS$_{rec}$ sucrose density gradients with different ionic strength after ultra-centrifugation. At an ionic strength corresponding to 50 mM KCl (top) γ-subunit$_{rec}$ shows a co-sedimentation with the wtFAS into the 40S region of the gradient (lanes 14-19). With increasing ionic strength corresponding to 150 mM KCl (mid) and 250 mM KCl (bottom) γ-subunit$_{rec}$ dissociates completely from Δγ-FAS (lanes 1-7, respectively).*

Since the γ-subunit within the endogenous wtFAS complex showed lower sensitivity to salt compared to the reconstituted Δγ-FAS$_{rec}$ complex, we asked ourselves whether post-translational modifications of the γ-subunit could play a role in the stability of these complexes. To address this question, our collaborator Dr. Andreas Linden analyzed the endogenous γ-subunit as well as γ-subunit$_{rec}$ by tandem protein mass spectrometry. While for γ-subunit$_{rec}$ no post-translational modifications were found, we identified four phosphorylated serine residues in the endogenous γ-subunit. The phosphorylation sites, located at serine residues 24, 38, 68 and 78 showed a high localization probability (*Table 4.1*) Therefore it can be assumed that the endogenous γ-subunit is

indeed post-translationally modified. These modifications could explain the dissociation of γ-subunit$_{rec}$ at lower ionic strength than those of the endogenous γ-subunit.

Proteins	Protein position	Localization probability	Amino acid	Phosphorylation (STY) Probabilities
endogenous γ-subunit	68	1	S	LEADDS(1)DDLENIDSGDLALYK
	76	0,987092	S	LEADDS(1)DDLENIDS(0.987)GDLALY(0.013)K
	24	0,942765	S	T(0.001)AIS(0.056)GMS(0.943)DMELAQIK
	38	1	S	TEIENS(1)INHLQR
γ-subunit$_{rec}$	No phosphorylated sites were found on the recombinantly expressed γ-subunit			

Table 4.1: Protein mass spectrometry reveals four phosphorylation sites within the γ-subunit. *Mass spectrometric analysis of the endogenous γ-subunit revealed a post-translational phosphorylation at four serine residues (amino acid residues 24, 38, 68 and 76) with a high localization probability (> 0,94). For the recombinant γ-subunit no phosphorylated residues were found.*

So far, we have been able to show that γ-subunit binds and co-sediments with the FAS complex in a salt-labile manner. By addition of γ-subunit$_{rec}$ to Δγ-FAS we were also able to reconstitute the complex (Δγ-FAS$_{rec}$), which is stable until ionic strength corresponding to 50 mM KCl. For quantification of the Δγ-FAS$_{rec}$ binding thermodynamics my colleague Kashish Singh performed binding experiments with fluorescent labelled γ-subunit$_{rec}$. 1 µM of freshly purified Δγ-FAS was incubated with increasing amounts of γ-subunit$_{rec}$ (0 µM – 30 µM). All binding reactions were applied to native agarose gel electrophoresis. By computational quantification the fluorescence signal of labelled γ-subunit$_{rec}$ was determined using ImageJ (Schneider et al., 2012). Since the binding of γ-subunit$_{rec}$ to Δγ-FAS resulted in a co-migration with Δγ-FAS within the agarose gel, the fluorescence signal of the Δγ-FAS$_{rec}$ bands was used as readout for the binding of γ-subunit$_{rec}$. Evaluation of the γ-subunit$_{rec}$ concentration dependent fluorescence intensities using a sigmoidal binding model (Hill equation) revealed a positive cooperativity (Hill coefficient $n_H = 1.6 \pm 0.1$) and a dissociation constant of $K_{0.5} = 3.1 \pm 0.1$ µM for binding of γ-subunit$_{rec}$ to Δγ-FAS (*Figure 4.8 A*). As a control reaction, we used NHS-rhodamine labelled trypsin inhibitor, a protein of similar size and charge like the γ-subunit$_{rec}$. In contrast to γ-subunit$_{rec}$, the trypsin inhibitor did not co-migrate with the Δγ-FAS in the native agarose gels. Therefore, we concluded, that the binding of γ-subunit$_{rec}$ to Δγ-FAS is specific (*Figure 4.8 B and C*).

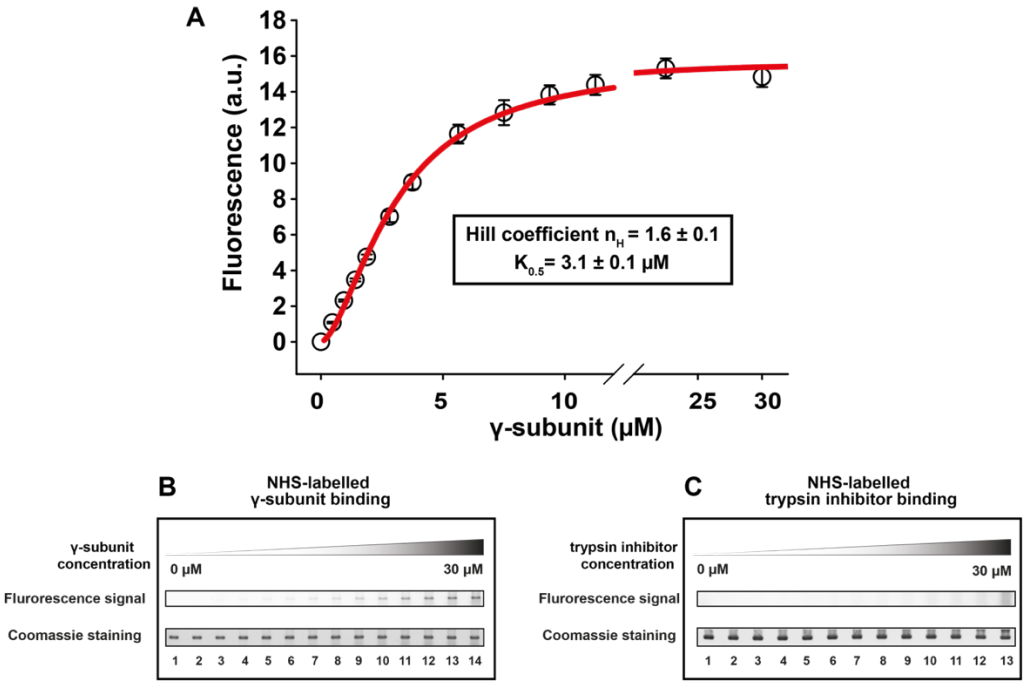

Figure 4.8: γ-subunit$_{rec}$ binding to Δγ-FAS is specific and reveals a positive cooperativity. A) *Quantitative analysis of the fluorescence signal from labelled γ-subunit$_{rec}$ revealed a positive binding cooperativity (n_H = 1.6 ± 0.1) and a dissociation constant of $K_{0.5}$ = 3.1 ± 0.1 µM when evaluated with the Hill equation. Single datapoints were measured in triplicates (n=3) and error bars indicate the standard deviation of each point.* ***B)*** *The middle panel shows the fluorescence signal from Δγ-FAS fractions at increasing concentration of NHS-rhodamine labelled γ-subunit$_{rec}$ (0 µM – 30 µM; top panel). The lower panel shows the same Δγ-FAS fractions of the agarose gel stained with Coomassie, indicating that Δγ-FAS migration did not change upon γ-subunit$_{rec}$ addition and comparable quantities were loaded.* ***C)*** *The middle panel shows the fluorescence signal from Δγ-FAS fractions at increasing concentration of NHS-rhodamine labelled trypsin inhibitor (0 µM – 30 µM; top panel). The lower panel shows the same Δγ-FAS fractions of the agarose gel stained with Coomassie, indicating that Δγ-FAS migration did not change upon trypsin inhibitor addition and comparable quantities of Δγ-FA were loaded.*

Knowing that the N- and C-terminal regions of the γ-subunit are conserved within *Saccharomycetaceae* (*Figure 4.3*), we wanted to know whether these conserved regions are somehow essential for the binding specificity of γ-subunit$_{rec}$ to Δγ-FAS.

Therefore, we cloned, expressed, and purified N-terminal ($\gamma^{\Delta 1\text{-}25}$) and a C-terminal ($\gamma^{\Delta 117\text{-}150}$) truncated variants of γ-subunit$_{rec}$. To determine the binding constant of the two variants to Δγ-FAS, both variants were also fluorescently labelled. The reconstitution of the $\gamma^{\Delta 1\text{-}25}$-Δγ-FAS and $\gamma^{\Delta 117\text{-}150}$-Δγ-FAS complexes was tested with the same method as described above. Evaluation of the two binding assays showed that neither $\gamma^{\Delta 1\text{-}25}$ nor the $\gamma^{\Delta 117\text{-}150}$ showed any co-migration with the Δγ-FAS on the native agarose gel (*Figure 4.9 A and B*). Since the fluorescence signal of the Δγ-FAS band for reactions with the two truncated variants was comparable to that of the trypsin inhibitor control (*Figure 4.8 C*), we concluded, that both variants were not able to bind to Δγ-FAS. We therefore surmised that the N- and C-termini are crucial to mediate a binding of γ-subunit$_{rec}$ to the Δγ-FAS complex.

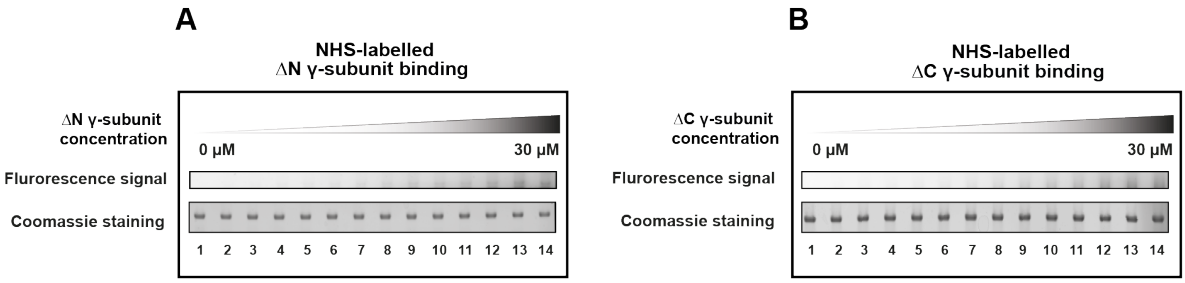

Figure 4.9: N- and C- termini of γ-subunit$_{rec}$ are essential for Δγ-FAS binding. A) *The middle panel shows the fluorescence signal from Δγ-FAS fractions at increasing concentration of NHS-rhodamine labelled $\gamma^{\Delta 1-25}$(ΔN γ-subunit) (0 µM – 30 µM; top panel). The lower panel shows the same Δγ-FAS fractions of the agarose gel stained with Coomassie, indicating that Δγ-FAS migration did not change upon $\gamma^{\Delta 1-25}$ addition, and comparable quantities were loaded.* ***B)*** *The middle panel shows the fluorescence signal from Δγ-FAS fractions at increasing concentration of NHS-rhodamine labelled $\gamma^{\Delta 117-150}$(ΔC γ-subunit) (0 µM – 30 µM; top panel). The lower panel shows the same Δγ-FAS fractions of the agarose gel stained with Coomassie, indicating that Δγ-FAS migration did not change upon $\gamma^{\Delta 117-150}$ addition and comparable quantities were loaded.*

4.6 Investigating the role of the γ-subunit

To investigate the role of the γ-subunit in association with the FAS complex we decided to use methods for protein structure determination and steady-state enzyme kinetic measurements. To achieve these extensive experiments my colleague Kashish Singh and me decided to split the experimental work. He used X-ray crystallography and Cryo-EM for protein structure determination experiments. Dr. Andreas Linden helped us with protein mass spectrometric measurements and with the help of Dr. Viktor Sautner I managed to establish a steady-state enzyme kinetic assay that allowed us the kinetic characterization of the Δγ-FAS and the Δγ-FAS$_{rec}$ complex.

4.7 Crosslinking Mass Spectrometry of the Δγ-FAS$_{rec}$ complex

The following crosslinking mass spectrometric (XL-MS) measurements were made in collaboration with Dr. Andreas Linden. To determine the spatial proximity and localize potential protein-protein interactions between γ-subunit$_{rec}$ and Δγ-FAS in the reconstituted Δγ-FAS$_{rec}$ complex three different crosslinkers were used. BS3, SDA and EDC-NHS with spacer arm length of 11.4 Å, 3.9 Å and 0 Å, respectively (*Figure 4.10, left*). The crosslinking sites of the different probes indicated a spatial proximity of the γ-subunit$_{rec}$ to the KS, KR, ER and MPT domain, respectively (*Figure 4.10, right*). N-terminal residues 51-72 of γ-subunit$_{rec}$ revealed a close interaction with residues from the MPT domain located at the α- and β-subunit (mainly SDA and EDC crosslinks). The C-terminal region of the γ-subunit$_{rec}$ showed mainly crosslinks with BS3 and the KS-domain. The interaction with BS3 indicates a larger distance for the protein-protein interaction (residues 111-124). Also, for the ER and DH domains, both located on the β-subunit several crosslinks with the middle and C-terminal part of the γ-subunit$_{rec}$ were found. These crosslinks were mostly formed by the SDA and EDC indicating a short distance between the γ-

subunit$_{rec}$ and those two domains. While we found only a single crosslink with the AT domain, no crosslinks with the ACP and PPT domain were detected. A comparison of all detected crosslinks with the published structures of the wtFAS complex (Leibundgut et al., 2007; Lomakin et al., 2007) revealed that only amino acid residues located at the inner cavity of the wtFAS formed crosslinks with the γ-subunit$_{rec}$ (data not shown). Thus, we concluded that the γ-subunit$_{rec}$ is most likely located inside FAS halve domes and somehow interacts with the KR, KS, ER, DH and MPT domains, respectively.

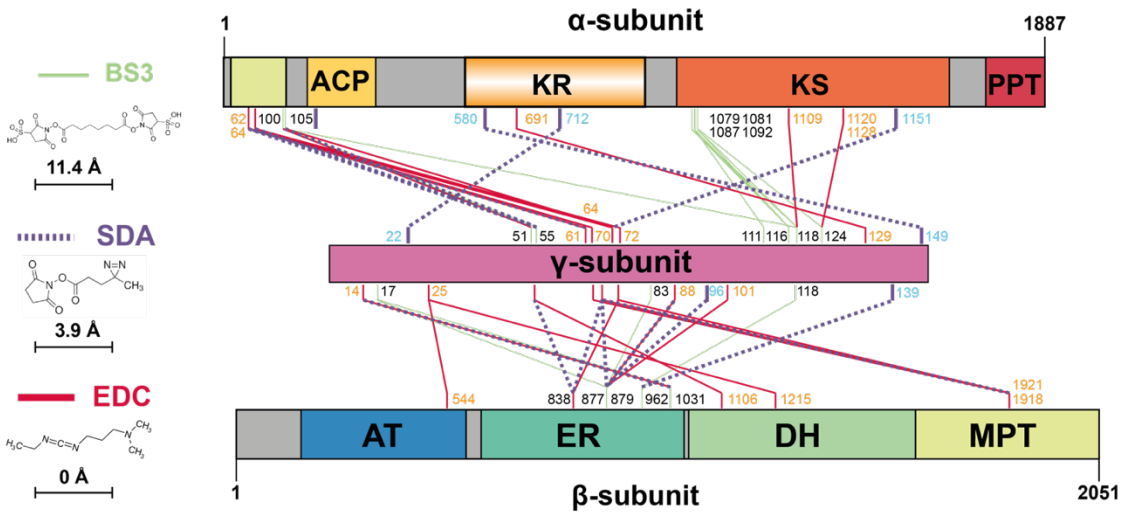

Figure 4.10: XL-MS analysis reveals γ-subunit$_{rec}$ interaction with different Δγ-FAS domains. *Illustration of crosslinks between γ-subunit$_{rec}$ and γ-FAS after crosslinking reaction* with the three different crosslinkers BS3, SDA and EDC having spacer arm length of 11.4, 3.9 and 0, respectively. While for the ACP and PPT domain no crosslink and for the AT domain only one crosslink was found, the other domains showed various crosslinks with all three crosslinkers used.

4.8 Structure determination of Δγ-FAS and Δγ-FAS$_{rec}$

Since the structure of the wild-type $\alpha_6\beta_6$ yeast FAS has already been solved by other groups using X-ray crystallography and Cryo-EM (Johansson et al., 2008, 2009a; Leibundgut et al., 2007; Lomakin et al., 2007), we wanted to verify whether the endogenous Δγ-FAS purified with our novel, chromatography-free purification method could also be used for structural studies via X-ray crystallography and Cryo-EM. Furthermore, we wanted to see whether it is possible the solve the structure of Δγ-FAS$_{rec}$ using any of those methods. In combination with the XL-MS results the structural information could help us to locate the γ-subunit binding and draw conclusion about its role.

4.9 X-ray structure of Δγ-FAS

For X-ray structure determination of Δγ-FAS we grew protein crystals using sitting-drop vapor diffusion. The crystals reached a maximum size of 150 µm in all dimensions and we obtained an X-ray crystallographic dataset with a resolution of 2.90 Å. The diffracting crystals of the Δγ-FAS complex belonged to the primitive monoclinic $P2_1$ space group with a single Δγ-FAS molecule in the asymmetric unit and revealed unit cell constants of a = 217.6Å, b = 347.6Å, c = 265.3 Å, β = 107.9°. The resolution of 2.9 Å allowed a reliable modelling of all enzymatic domains including most of the amino acid side chains (*Figure 4.11 A*). The ACP domain was found in proximity to the KS domain located at the central wheel (*Figure 4.11 B*). The electron density allowed us to build most of the ACP domain including the post-translational PPant modification at Ser^{180} (*Figure 4.11 C*).

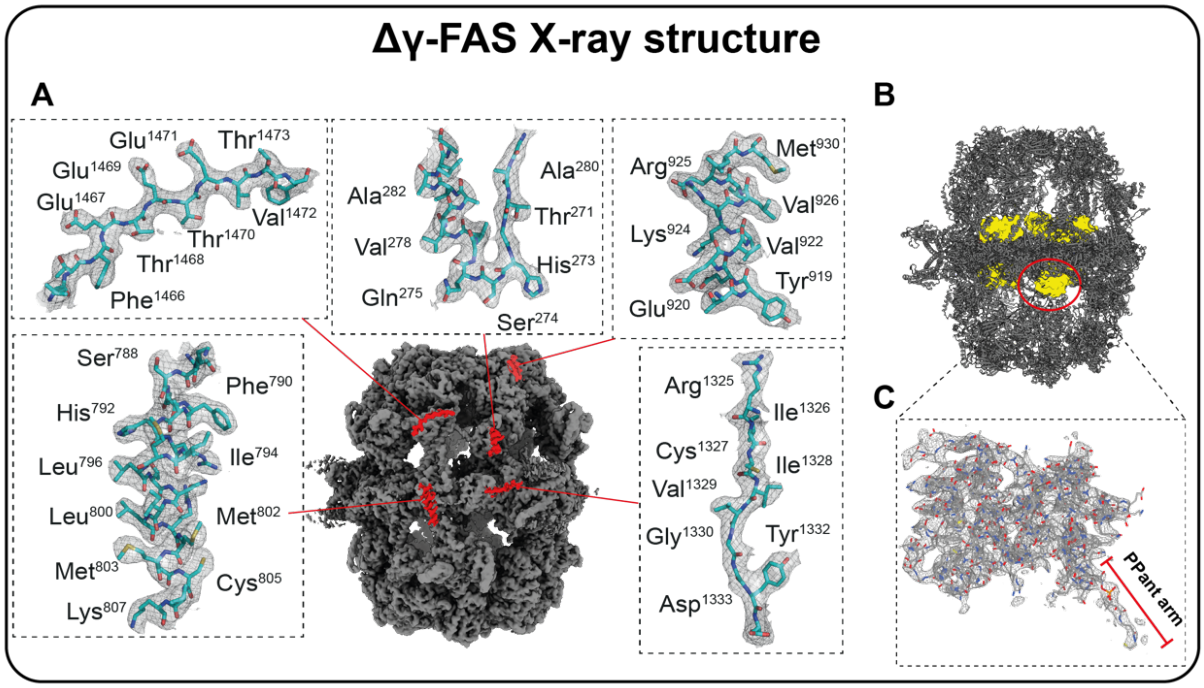

Figure 4.11: X-ray structure of the Δγ-FAS at 2.9 Å. A) *The electron density of the whole Δγ-FAS molecule as surface structure (bottom mid). Representative for the quality of the electron density over the whole molecule, different areas are magnified (boxes 1-5 around the FAS molecule, highlighted in red). The high quality of the electron density contoured at 1.5 σ allowed the reliable modelling of most amino acid side chains over the whole molecule.* ***B)*** *The ACP domain (yellow) was found to be located at the central wheel.* ***C)*** *The electron density map contoured at 1.5 σ allowed the modelling of most parts from the ACP domain. We also found a continuous electron density at the Ser^{180} residue of the ACP which allowed the modelling of the whole PPant arm residue (red bar).*

4.10 Cryo-EM structure of Δγ-FAS

For cryo-EM investigation a large dataset of Δγ-FAS particles was recorded. Image processing of extracted single particles under application of a D3 symmetry allowed us the reconstruction of a model with the estimated resolution of 2.9 Å using the 0.143 Fourier shell correlation (FSC) criterion. The use of a C3 symmetry and a C1 asymmetric reconstitution resulted in final resolutions of 3.0 Å and 3.3 Å, respectively. The resolution of 2.9 Å allowed us to build a reliable model of all Δγ-FAS domains including most of the amino acid side chains (*Figure 4.12 A*). Other than the X-ray structure with comparable nominal resolution, the density did not allow to build the PPant arm of the ACP domain which was also found to be located at the central wheel in proximity to the KS domain (*Figure 4.12 B and C*). Processing of the Cryo-EM dataset revealed the sorting of 8% of the single particles into a distinct subgroup. The reconstruction of these particles resulted in a model that showed fundamental structural differences. The ACP domain was found to be located opposite of the centra wheel, right under the tope of both halve domes of the cavity (*Figure 4.12 D*).

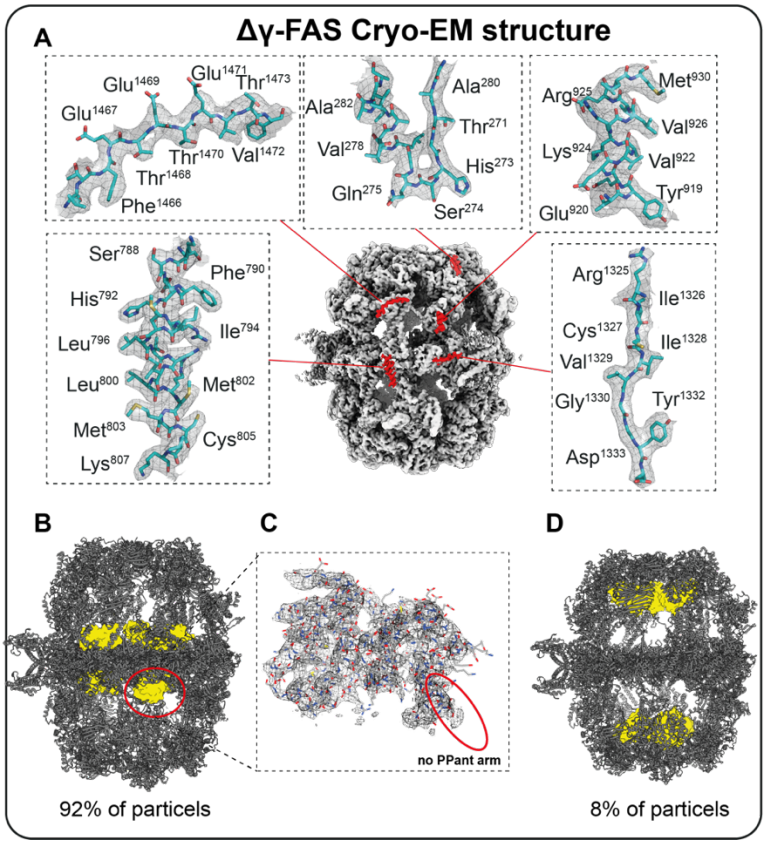

Figure 4.12: Cryo-EM structure of the Δγ-FAS at 2.9 Å A) *The density map of the whole Δγ-FAS molecule as surface structure (bottom mid). Representative for the quality of the density over the whole molecule, different areas are magnified (boxes 1-5 around the FAS molecule, highlighted in red). The quality of the density allowed the reliable modelling of most amino acid side chains over the whole molecule.* ***B)*** *The ACP domain (yellow) was found to be located at the central wheel for 92% of the particles within the Cryo-EM dataset.* ***C)*** *The density map allowed the modelling of most parts of the ACP domain. Other than in the X-ray structure we did not find any density resulting from PPant arm at the Ser^{180} residue of the ACP domain.* ***D)*** *The reconstruction of a model from the particles into the smaller group (8% of the particles) showed the ACP domains (yellow) located under the top of both halve domes.*

4.11 Structural heterogeneity of Δγ-FAS particles

Besides a rearrangement of the ACP domain (yellow) from the KS active sites (orange) at the central wheel (*Figure 4.12 B and Figure 4.13 A_i*) towards the outer areas of both halve domes, next to the AT active sites (blue) (*Figure 4.12 D and Figure 4.13 B_i*), we also found a rearrangement of the outer FAS domes. The comparison of the two structures with different location of the ACP domains shows a shift of the AT-domain in direction of the central-wheel coupled to a shift of the MPT domain towards the outer part of the molecule (*Figure 4.13 A_{ii} and B_{ii}*). A top-view inspection of this rearrangement revealed a relative rotation of 15° for both halve-domes along the three-fold symmetry axis (*Figure 4.13 Ai_{i} and B_{iii}*). According to this, we denoted the two different structural states as non-rotated state (*Figure 4.13 A*) and rotated state (*Figure 4.13 B*). While the non-rotated state is characterized by the location of its ACP domains in proximity to the KS active sites (orange), the ACPs in the rotated state are located next to the AT active sites (blue).

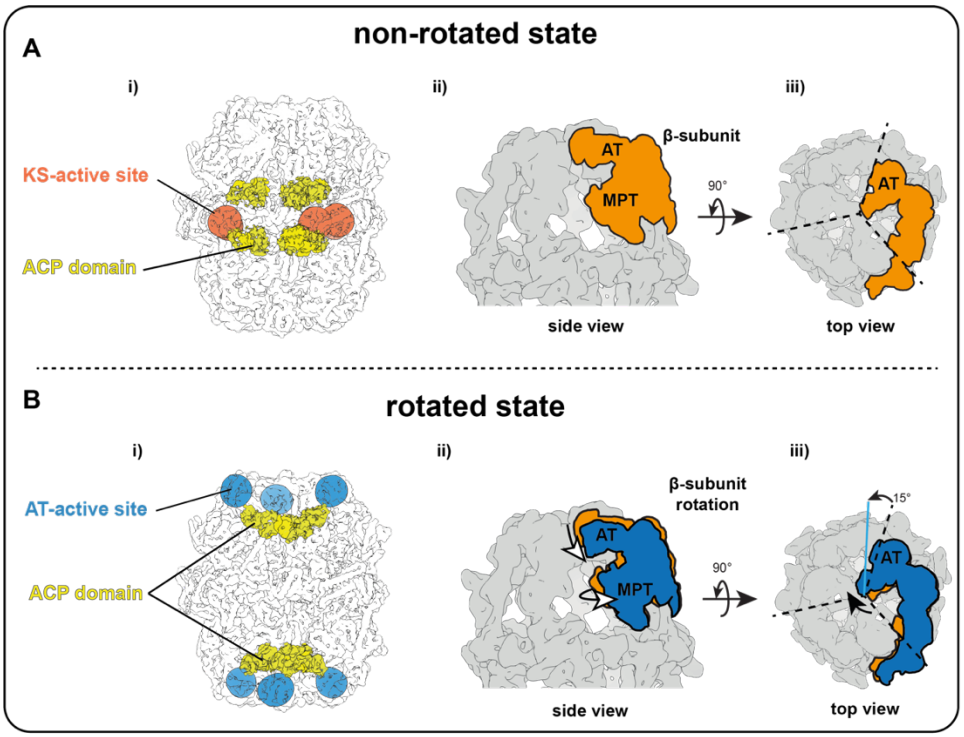

Figure 4.13: Cryo-EM data processing reveals two different states of the Δγ-FAS. A) *The non-rotated state was found in 92% of the Δγ-FAS particles in a Cryo-EM dataset. Within this state, the ACP domains (yellow) were found to be located at the central wheel in proximity to the KS active sites (orange).* ***B)*** *The rotated state was reconstructed from 8% of the Δγ-FAS particles in the same Cryo-EM dataset. Other than in the non-rotated state, the ACP (yellow) was found to be located right next to the AT active sites (blue).* ***$A_{ii\text{-}iii}$ & $B_{ii\text{-}iii}$)*** *Besides the rearrangement of the ACPs, the transition from non-rotated to the rotated state is characterized by an inward movement of the AT domain coupled to an outward movement of the MPT domain. In the top-view these movements appear as a 15° rotation around the three-fold axis of the FAS halve domes.*

After we could show that we can use Δγ-FAS for structural investigations using both, X-ray crystallography and Cryo-EM, we also wanted to investigate the role of the γ-subunit in the reconstituted Δγ-FAS$_{rec}$ complex. By a direct structural comparison with Δγ-FAS we hoped to get a better idea of the role and task of the γ-subunit within the FAS molecule.

4.12 X-ray structure of Δγ-FAS$_{rec}$

According to previous findings of the γ-subunit$_{rec}$ binding affinity to Δγ-FAS we grew protein crystals with a 7x molar excess of γ-subunit$_{rec}$ over Δγ-FAS. Using vapor diffusion, we managed to grow Δγ-FAS$_{rec}$ protein crystals up to a size of 150 µm x 150 µm x 200 µm and collected an X-ray crystallographic dataset with diffractions up to 4.6 Å. Other than the Δγ-FAS crystals, the Δγ-FAS$_{rec}$ crystal had two molecules in its asymmetric unit with unit cell constants of a = 234.9 Å, b = 430.3 Å, c = 422.6 Å and β = 97°. Due to the resolution of 4.6 Å we were only able to build a C_α-trace structure of the Δγ-FAS$_{rec}$ complex (Figure 4.14, left). To our surprise, the overall structure of the Δγ-FAS$_{rec}$ resembled those of the rotated state which we previously discovered in 8% of the particles Δγ-FAS in the Cryo-EM dataset (*Figure 4.12 D*). The ACP domains were also located in proximity to the AT domains under the top of both halve domes (Figure 4.14, right). Additionally, we found positive mFo-DFc densities inside the FAS cavity, when the model of the Δγ-FAS X-ray structure (*Figure 4.11*) was used for refinement of the 4.6 Å crystallographic Δγ-FAS$_{rec}$ dataset (data not shown). With additional information of protein-protein interactions from the XL-MS analysis (*Figure 4.10*) we managed to build a C_α-trace structure for parts of the γ-subunit$_{rec}$ into these additional densities (*Figure 4.14, right*). Within the whole FAS molecule, we found densities for six copies of the γ-subunit, three in each halve tome.

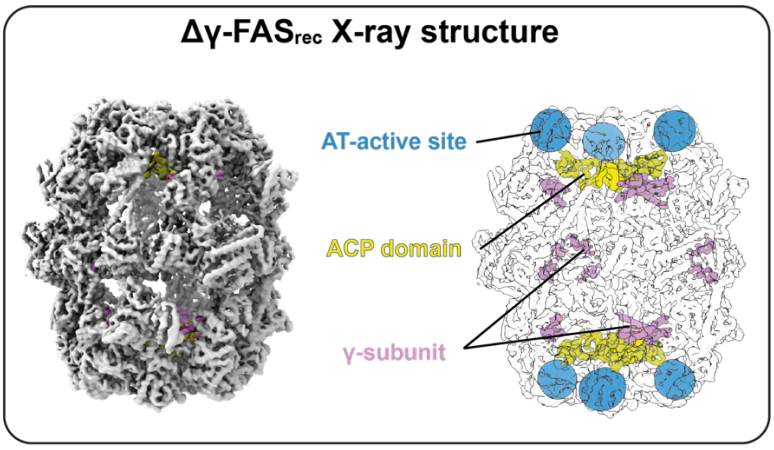

Figure 4.14: X-ray structure of Δγ-FAS$_{rec}$ reveals a rotated state with bound γ-subunit. left) *The 4.6 Å density map of the whole Δγ-FAS$_{rec}$ molecule as surface structure.* ***right)*** *as already described for the rotated state within the Cryo-EM dataset, the ACP domain (yellow) was in proximity to the AT active sites (blue). The additional densities of the γ-subunit were found next to the ACP domain and next to the central wheel (purple). In total six copies of the γ-subunit were found within each FAS molecule, three in each halve dome.*

4.13 Cryo-EM structure of $\Delta\gamma$-FAS$_{rec}$

We were also able to obtain a structure from a Cryo-EM dataset with $\Delta\gamma$-FAS and γ-subunit$_{rec}$ at 7x molar excess at a global resolution of 2.8 Å when D3 symmetry was applied. Reconstruction with an applied C3 and C1 symmetry resulted in lower resolutions of 2.9 Å and 3.2 Å, respectively. The global resolution of 2.8 Å allowed us a reliable modelling of all catalytic domains including most of the amino acid side chains. Surprisingly, we found 95% of the $\Delta\gamma$-FAS$_{rec}$ particles in a rotated state with an additional density of the γ-subunit$_{rec}$ inside the cavity of both halve domes (*Figure 4.15 A*). This rotational state with additional densities for the γ-subunit$_{rec}$ was the same as those described for the 4.8 Å X-ray structure (*Figure 4.14*). Other than in the Cryo-EM structure of the $\Delta\gamma$-FAS (*Figure 4.12*) we were able to also build the PPant modification of the ACP-domain Ser^{180} residue (data not shown). The density of the bound γ-subunit$_{rec}$ allowed us the modelling of the residues 3-59, 77-112 and 133-150 including most of the side chains. For the residues 60-76 and 114-132 no densities were found and thus we could not build a model of these regions (*Figure 4.15 B*). The reconstruction of a model from the second class containing the leftover 5% particles of the dataset showed the $\Delta\gamma$-FAS in its non-rotated state without additional γ-subunit$_{rec}$ and its ACP located in proximity to the AT domain (*Figure 4.15 C*).

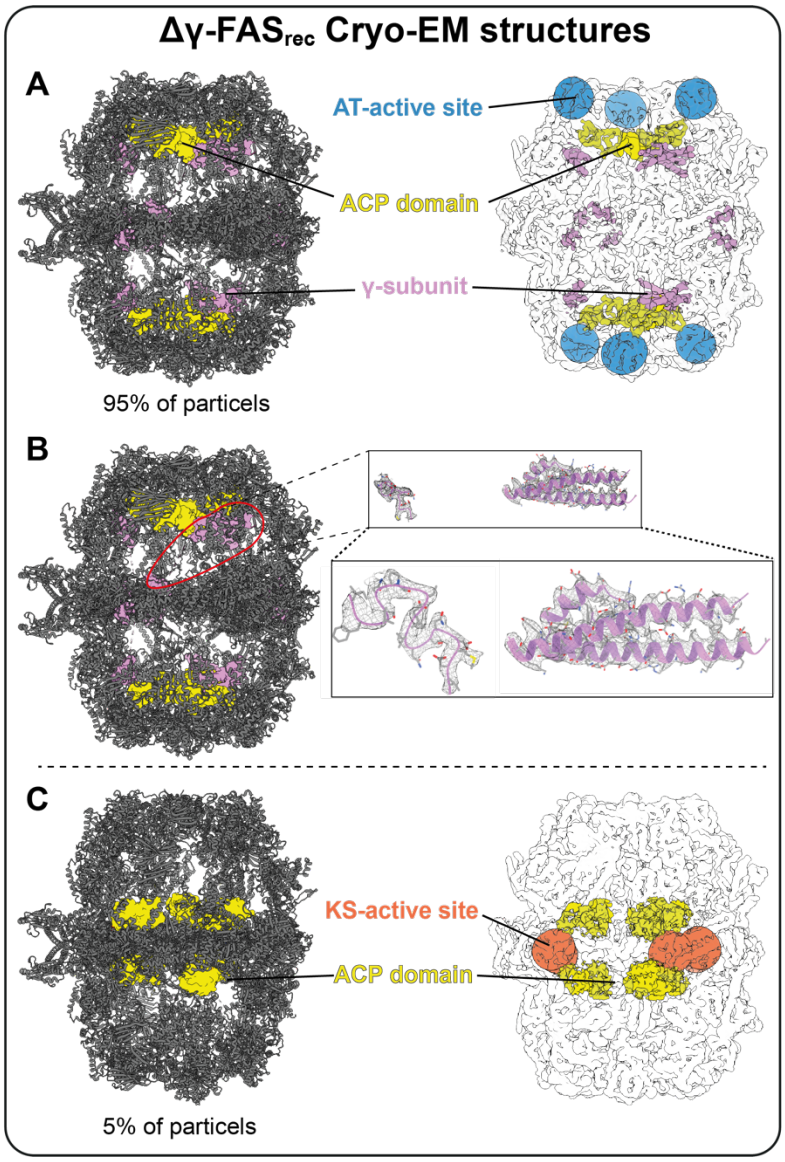

Figure 4.15: Cryo-EM structure of Δγ-FAS$_{rec}$ reveals two conformational states A) *The Cryo-EM structure resulting from 95% of the particles from the Δγ-FAS$_{rec}$ dataset shows the FAS in its rotated state. In addition to the ACP (yellow) in proximity to the AT domain (blue) density of the γ-subunit (purple) was found.* ***B)*** *The quality of the additional density map allowed to build a reliable model of the γ-subunit. Other than in the X-ray structure, also side chains of several amino acids were built.* ***C)*** *The smaller population including 5% of the particles from the Δγ-FAS$_{rec}$ Cryo-EM dataset led to a non-rotated FAS structure. The ACP domains (yellow) were found in proximity to the KAS active sites (orange). Other than for the rotated state, no additional densities of the γ-subunit appeared.*

4.14 The γ-subunit influences the structure of Δγ-FAS

After the discovery of two conformational states within a Cryo-EM dataset of Δγ-FAS particles (*Figure 4.12 B and D*), we could show that the rotated state is stabilized upon addition of γ-subunit$_{rec}$ at 7x molar excess over Δγ-FAS. While for the Δγ-FAS dataset, the non-rotated state was prominent, this ratio has reversed for Δγ-FAS$_{rec}$. Thus, we concluded that the binding of γ-subunit$_{rec}$ somehow induces a structural rearrangement stabilizing the rotated state of the FAS particles (*Figure 4.16*). These findings were further supported by the two crystal structures. In the crystals the Δγ-FAS was found in a non-rotated state (*Figure 4.11*) *and* the Δγ-FAS$_{rec}$ in a rotated state with additional densities of the γ-subunit$_{rec}$ (*Figure 4.14*).

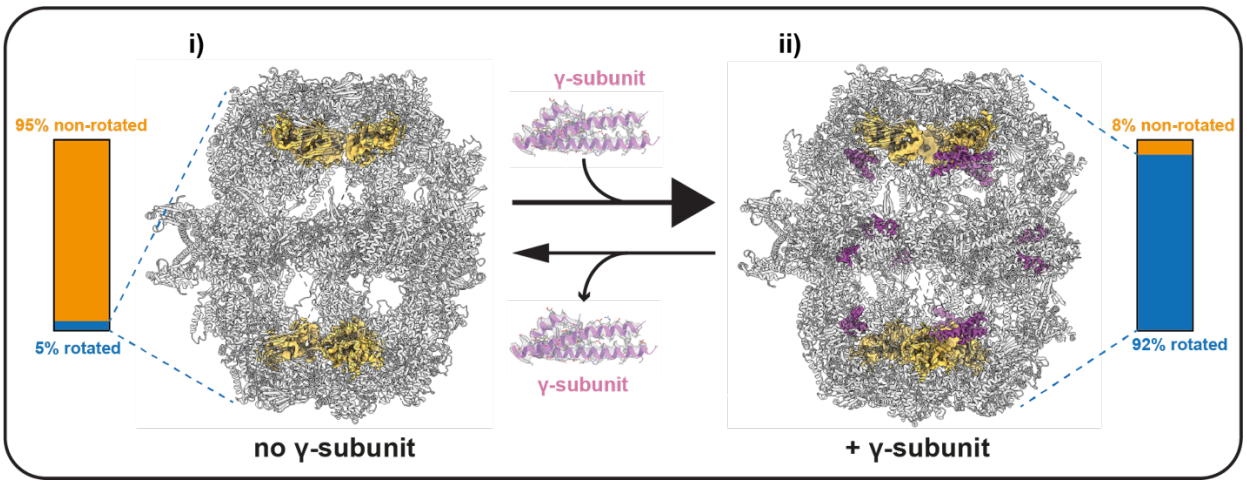

Figure 4.16: γ-subunit stabilizes the rotated state of FAS. i) *Without additional γ-subunit only 5% of the particles within a Cryo-EM dataset were found in a rotated state. The reconstruction of these particles (indicated in blue) led to the illustrated structure.* ***ii)*** *Upon addition of γ-subunit in 7x molar excess over the Δγ-FAS, 92% of the particles (indicated in blue) in the corresponding Cryo-EM dataset were found to be in a rotated state. Besides the shift of the ratios between the non-rotated and rotated state, we also found densities of the γ-subunit inside the FAS dome.*

4.15 Steady-state kinetic measurements of Δγ-FAS and Δγ-FAS$_{rec}$

Former studies have shown that the endogenous wtFAS purified from yeast cells is enzymatically active and synthesizes saturated fatty-acyl CoAs of different chain lengths. For this *de novo* synthesis it uses the two substrates acetyl-CoA and malonyl-CoA and the co-enzyme NADPH as reducing equivalent (Dietlein and Schweizer, 1975; Wakil et al., 1964). To investigate the role of the γ-subunit within the FAS complex, we decided to undergo an intensive steady-state kinetic analysis of the Δγ-FAS and the Δγ-FAS$_{rec}$ complex. Therefore, we used a spectrophotometric assay that monitors the consumption of NADPH over time (Aprahamian et al., 1982). With help from Dr. Viktor Sautner, we improved the spectrophotometric assay and characterized the steady-state kinetics of the Δγ-FAS complex in dependency of all three substrates. The kinetic measurements were performed for both complexes Δγ-FAS and Δγ-FAS$_{rec}$.

Acetyl-CoA concentration dependent activity measurements of Δγ-FAS and Δγ-FAS$_{rec}$ (*Figure 4.17*) showed a maximum enzymatic activity (V_{max}) at ~100 µM acetyl-CoA. For acetyl-CoA concentrations > 100 µM a substrate excess inhibition was found. Analysis of the steady-state rates using a substrate-excess inhibition modified Hill-equation (see 3.20) showed substrate affinity constants ($K_{0.5}$) of $K_{0.5}$ = 38.4 ± 9.9 µM for Δγ-FAS and $K_{0.5}$ = 54.8 ± 0.07 µM for Δγ-FAS$_{rec}$. The Hill-coefficients (n) for Δγ-FAS (n = 0.96 ± 0.16) and Δγ-FAS$_{rec}$ (n = 1.09 ± 0.07) indicate that the acetyl-CoA binding does not underly any cooperativity.

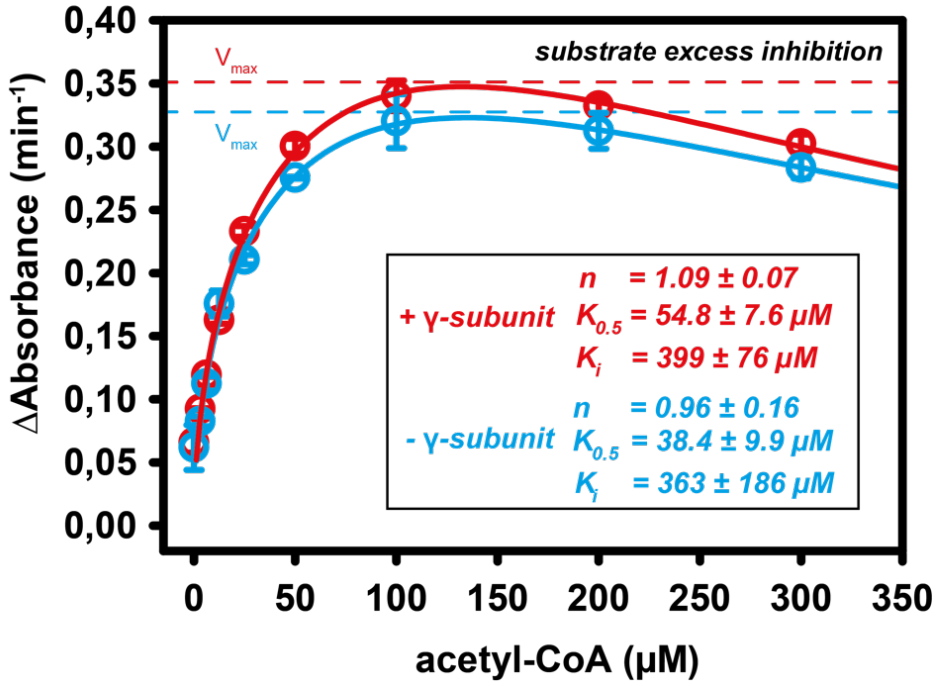

Figure 4.17: Steady-state kinetic analysis of acetyl-CoA dependent Δγ-FAS activity ± γ-subunit$_{rec}$. *The kinetic activities of Δγ-FAS ± γ-subunit$_{rec}$ in dependency of the acetyl-CoA concentration (0 µM – 300 µM) was detected by measurement of NADPH consumption over time (ΔAbsorbance/min). For each datapoint the initial velocities (t = 0-5s) of the reactions were taken. In both cases, with (red) and without (blue) γ-subunit a substrate excess inhibition was detected (> 140 µM acetyl-CoA). In presence of γ-subunit the maximum rate (V_{max}) of 0.35 min^{-1} was detected at 140 µM acetyl-CoA. The substrate affinity ($K_{0.5}$) with additional γ-subunit was determined to 54.8 ± 7.6 µM. While no cooperativity (n) was found for both reactions, the absence of γ-subunit showed a slight decrease of the acetyl-CoA affinity ($K_{0.5}$ = 38.4 ± 9.9 µM) and the maximum rate (V_{max} = 0.33 min^{-1}) at 140 µM acetyl-CoA. Each measuring point was measured as triplicate (n=3) and the error bars indicate the calculated standard deviation (SD).*

Malonyl-CoA dependent activity measurements (*Figure 4.18*) showed a V_{max} for both reactions at around 50 µM malonyl-CoA. For malonyl-CoA concentration exceeding 50 µM, a substrate excess inhibition was detected in both reactions, respectively. Evaluation of the steady-state rates with a substrate-excess inhibition modified Hill-equation (see 3.20) showed a $K_{0.5}$ of 35.2 ± 5.5 µM for Δγ-FAS$_{rec}$ and a significantly lower value ($K_{0.5}$ = 18.7 ± 2.2 µM) for Δγ-FAS. Other than for acetyl-CoA, the malonyl-CoA dependent activity measurements revealed a positive cooperativity (n > 1.0) for the malonyl-CoA binding in both reactions.

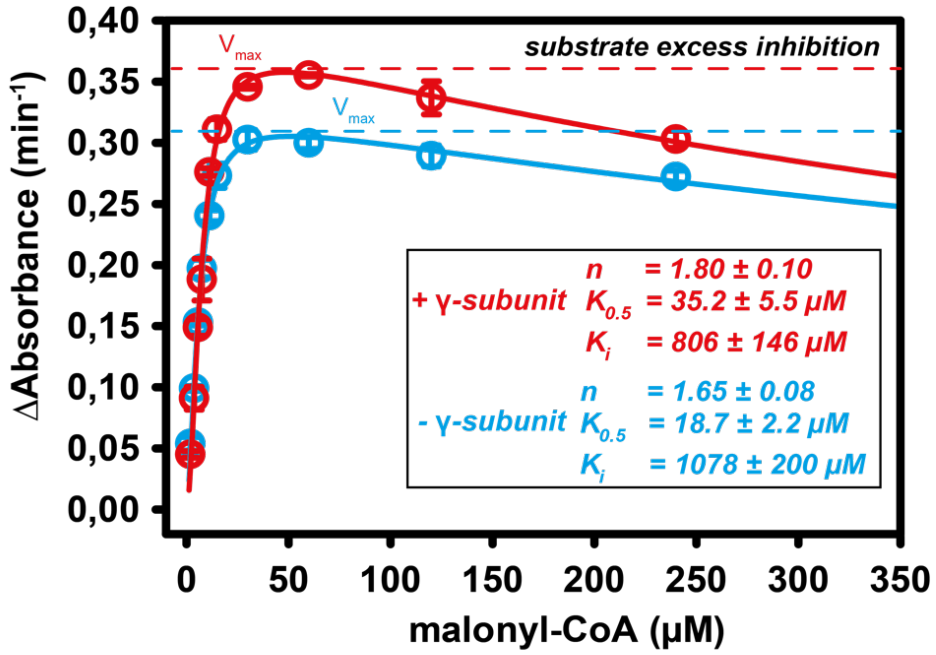

Figure 4.18: Malonyl-CoA dependent activity of FAS ± γ-subunit$_{rec}$. *The kinetic activities of Δγ-FAS ± γ-subunit$_{rec}$ in dependency of the malonyl-CoA concentration (0 µM – 250 µM) was detected by measurement of NADPH consumption over time (ΔAbsorbance/min). For each datapoint the initial velocities (t = 0-5s) of the reactions were taken. In both cases, with (red) and without (blue) γ-subunit a substrate excess inhibition was detected (> 50 µM acetyl-CoA). In presence of γ-subunit the maximum rate (V$_{max}$) of 0.35 min^{-1} was detected at 50 µM malonyl-CoA. The substrate affinity (K$_{0.5}$) with additional γ-subunit was determined to 35.2 ± 5.5 µM. Without γ-subunit$_{rec}$ a decreased V$_{max}$ of 0.30 min^{-1} at 50 µM malonyl-CoA as well as a decreased K$_{0.5}$ of 18.7± 5.5 µM was found. The Hill coefficient (n) of both reactions was found to be >1.0 which indicates a positive cooperativity for the binding of malonyl-CoA. Each measuring point was measured as triplicate (n=3) and the error bars indicate the calculated standard deviation (SD).*

After the first NADPH concentration dependent activity measurements, we discovered significantly differences between the kinetic progression curves of Δγ-FAS and Δγ-FAS$_{rec}$ at lower NADPH concentrations (< 100 µM). While for Δγ-FAS constant steady-state rates were observed from the start of the enzymatic reaction ($V_0 = V_{ss}$) (*Figure 4.19, blue*), the Δγ-FAS$_{rec}$ progression curve revealed two different kinetic phases (*Figure 4.19, red*). An activation phase V_0 with a lower initial activity, which is followed by a mono-exponential transition into a steady-state phase of increased activity rate (V_{ss}). The occurrence of such progression curves revealing different kinetic states is also known as kinetic hysteresis (Frieden, 1970).

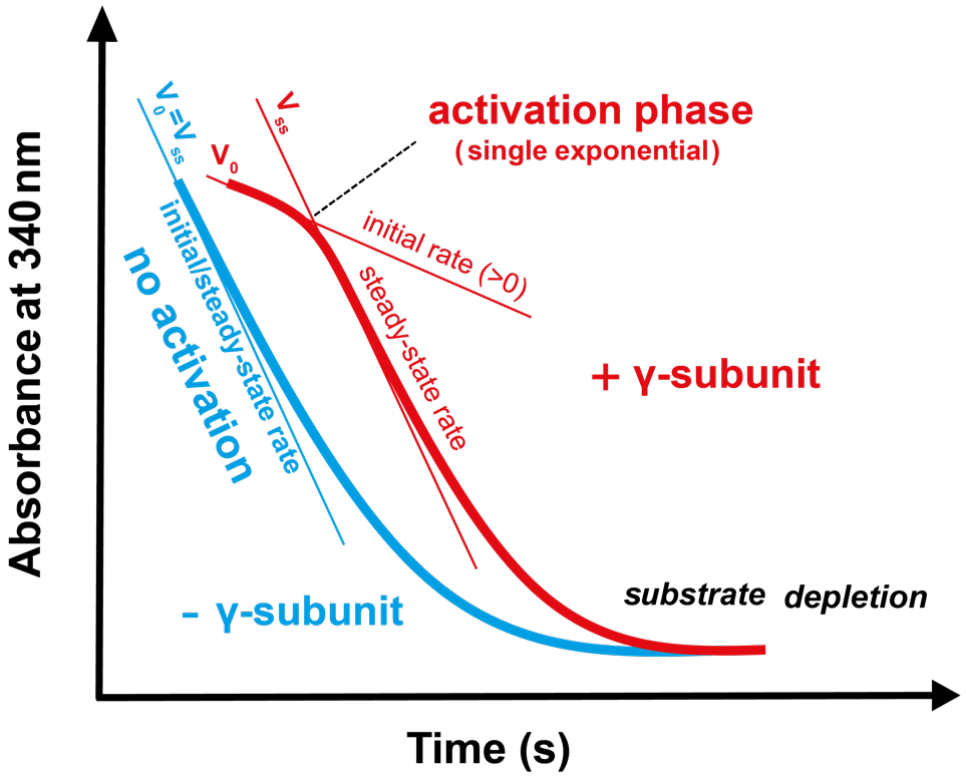

Figure 4.19: Schematic representation of Δγ-FAS and Δγ-FAS$_{rec}$ activity at low NADPH concentrations. *The FAS without γ-subunit (blue) showed a steady-state rate from the beginning of the enzymatic reaction (V_0=V_{ss}). Other than that, we observed two kinetical states of the progress curve in presence of γ-subunit (red). For the first seconds of the activity assay a lower initial activity (V_0) was observed. By a single exponential transition (activation phase) the rate increased and changed into a linear steady-state phase (V_{ss}).*

According to the different kinetic phases within the kinetic hysteresis, we distinguished between two different NADPH dependent activities for Δγ-FAS$_{rec}$. The initial activity rates V_0 (*Figure 4.20, red*) and the steady-state activity rates V_{ss} (*Figure 4.20, black*) were compared with the steady state activity rates V_0 = V_{ss} from Δγ-FAS (*Figure 4.20, blue*). The evaluation of the three progression curves using an unmodified Hill-equation (see 3.20) showed an increasing $K_{0.5}$ upon γ-subunit binding. From $K_{0.5}$ = 17.7 µM for Δγ-FAS, the addition γ-subunit induced an increase of the $K_{0.5}$ increased by a factor of 2.52 ($K_{0.5}$ = 44.7 µM) for the initial phase (V_0). After the mono-exponential transition into the steady-state phase (V_{ss}) the $K_{0.5}$ Δγ-FAS$_{rec}$ decreased to 34.7 µM, which corresponds to an increase of factor 1.96 compared to Δγ-FAS. The evaluation of the maximum rates for both complexes also revealed changes upon binding of the γ-subunit. Without γ-subunit the maximum rate of the NADPH consumption was 0.30 min^{-1}. In presence of the γ-subunit this was found to be increased within both kinetic states of the Δγ-FAS$_{rec}$ complex. During the activation phase the V_{max} was 0.35 min^{1}. After the mono-exponential transition into the steady-state phase the Vmax further increased to a maximum rate of V_{max} = 0.37 min^{-1}.

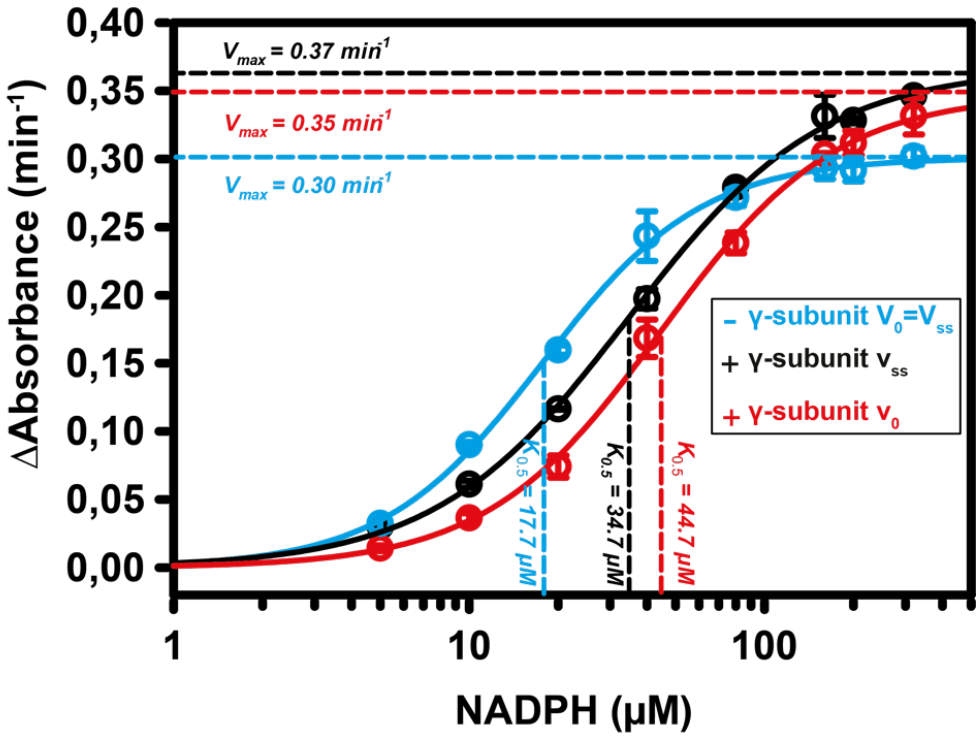

Figure 4.20: Binding of γ-subunit induces a NADPH concentration dependent kinetic hysteresis. *To analyze the impact of the γ-subunit binding on the NADPH dependent FAS activity, the rates without γ-subunit (blue, V_0=V_{ss}) were compared with the initial rate (V_0, red) and steady-state rate (V_{ss}, black) of the Δγ-FAS_{rec} complex. The NADPH affinity decreased in presence of the γ-subunit. Without γ-subunit the $K_{0.5}$ was determined to 17.7 µM, whereas both kinetic states in presence of the γ-subunit showed an increased $K_{0.5}$. During the activation phase a $K_{0.5}$ of 44.7 µM was found. After the mono-exponential transition into the steady-state phase the $K_{0.5}$ was determined to 34.7 µM. Evaluation of the maximum rates (Vmax) revealed an increase in the presence of γ-subunit. Without γ-subunit the V_{max} of the FAS activity was 0.30 min^{-1}. In the γ-subunit bound state the maximum rate was increased to 0.35 min^{-1} for the activation phase, followed by 0.37 min^{-1} for the steady-state phase. Each measuring point was measured as triplicate (n=3) and the error bars indicate the calculated standard deviation (SD).*

Within the FAS complex the hysteretic effect seemed to be introduced by binding of the γ-subunit, affecting both, the NADPH affinity as well as the maximum rate of NADPH consumption. We thus surmised, that the significant impact of the γ-subunit on the NADPH dependent kinetic activity, coupled to the introduction of an enzyme hysteretic effect could help us to decipher the role of the γ-subunit.

To exclude any artifacts of the γ-subunit binding, we repeated the substrate specific kinetic measurements for all three substrates under protein crowding conditions, using a protein of similar size and charge. Therefore, control measurement with high concentrations of 1 mM additional trypsin inhibitor were made. For none of the substrates the crowding control revealed any significant changes of the FAS kinetics. As an example, *Figure 4.21* shows the NADPH dependent FAS activities in presence (red) and absence (blue) under non-crowding and crowding conditions (lighter colors). Due to that, we concluded that the observed kinetic changes as well as the hysteretic effect induced by the γ- are indeed specific.

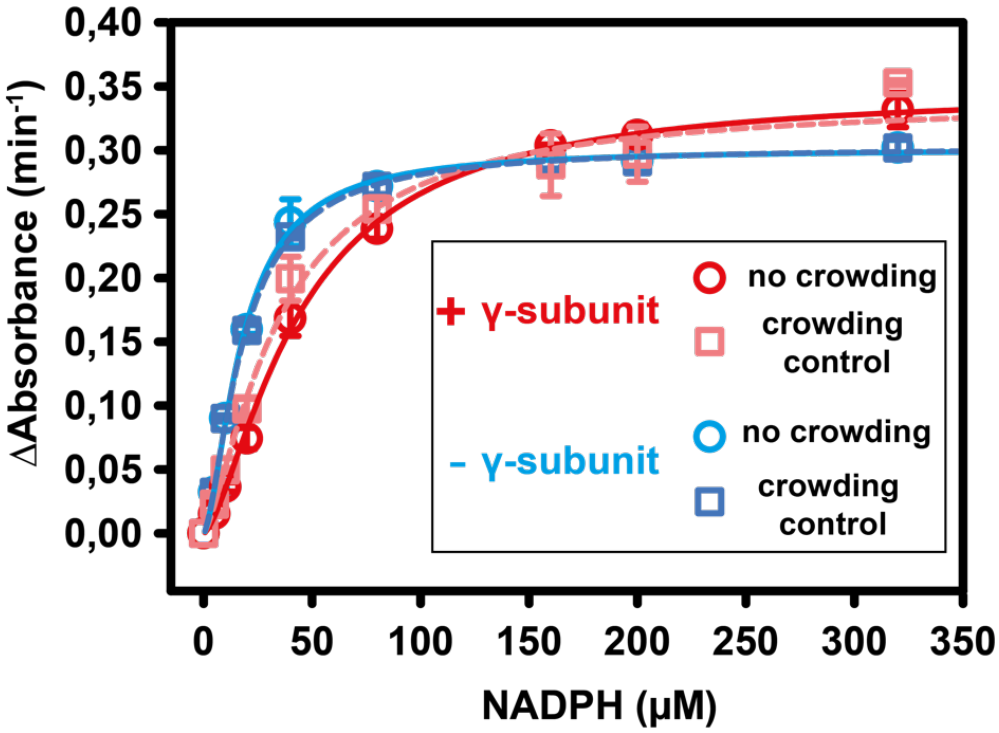

Figure 4.21: Impact of γ-subunit on the NADPH dependent FAS activity is specific. *To test whether the effect of the γ-subunit on NADPH dependent FAS activity is specific, control measurements under crowding conditions with 1 mM additional trypsin inhibitor (squares) were made. The overlay of the different NADPH dependent activities showed no changes for the reactions without γ-subunit (blue). For measurements with additional γ-subunit only minor changes were observed in the regime of 30-120 µM. Due to overlapping standard deviations, these differences were not significant. Each measuring point was measured as triplicate (n=3) and the error bars indicate the calculated standard deviation (SD).*

With the findings that the γ-subunit modulates the response of FAS to NADPH during enzymatic activity, we wanted to know whether a basal NADPH consumption also occurs in absence of malonyl-CoA and acetyl-CoA. Therefore, we measured the NADPH consumption of Δγ-FAS and Δγ-FAS_{rec} without malonyl-CoA and acetyl-CoA. Surprisingly, we indeed found a basal NADPH depletion in both reactions. This can be explained by a futile cycle reaction at the FMN-bound ER domain. In such a futile cycle reaction, electrons from NADPH can be transferred to free oxygen via the FMN co-factor molecule. This substrate independent loss of electrons leads to the production of reactive oxygen species (ROS) like H_2O_2 (Chaiyen et al., 2012; Morlock et al., 2018; Suzuki et al., 2017). A comparison of the futile cycle NADPH consumption rates in both reactions showed significant differences. Upon binding of the γ-subunit the futile cycle reaction was significantly reduced (*Figure 4.22*). The reduction of the futile cycle reaction by the γ-subunit was observed until a NADPH concentration of ≈ 100 µM. For higher NADPH concentrations identical rates of substrate independent NADPH depletion were found. Therefore, we concluded that the γ-subunit binding also reduced the rate of the ER futile cycle reaction. This helps to prevent an undesired consumption of NADPH and protects the cell from accumulation of toxic ROS. Determined *in vivo* NADPH concentrations of 50-150 µM in yeast cells also correlate with

the observed range of the futile cycle suppression of the γ-subunit (Gancedo and Gancedo, 1973; Polakis and Bartley, 1966).

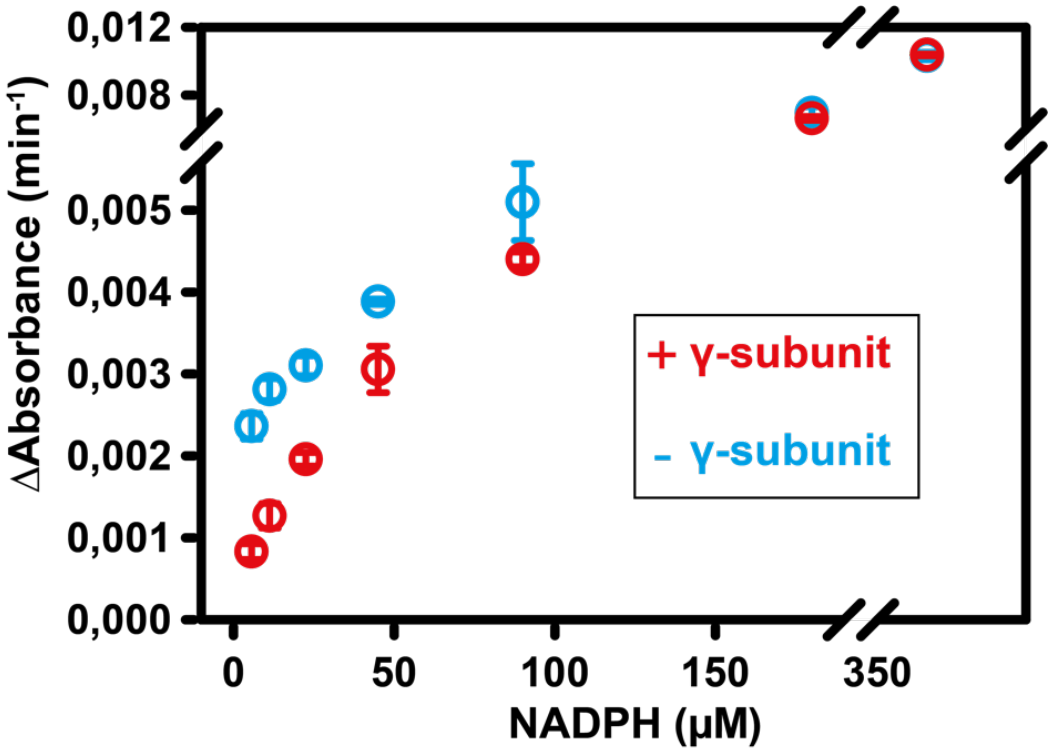

Figure 4.22: The γ-subunit reduces the Δγ-FAS futile cycle. *Kinetic measurements in absence of acetyl-CoA and malonyl-CoA revealed a significant decrease of the NADPH futile cycle at the ER active site upon addition of the γ-subunit (red) relative to the reaction without γ-subunit (blue). The effect of suppression of the futile cycle reaction was detected up to a NADPH concentration of 90 µM. At 180 µM and 360 µM NADPH, no differences between absence and presence of γ-subunit were detected. The error bars show the SD of each data point (n = 3).*

4.16 γ-subunit as a FAS specific protein shuttle

From native gel binding experiments, structural investigations, and enzyme kinetical assays we knew that the γ-subunit specifically binds to the inner cavity of the FAS dome. Within this specific binding, the two unstructured regions aa 1-25 and aa 117-150 of the γ-subunit were found to play a crucial role (*see 4.3*). Therefore, we asked ourselves whether these regions could be somehow used as modifications for other proteins. An addition of both regions to small FAS unspecific proteins could mediate their translocation into the inner FAS cavity – similar to import sequences found in other cellular processes (Kalderon et al., 1984). To establish a proof of concept, we designed synthetic proteins harboring 1x or 2x domains of UnaG which is a small (15 kDa) fluorescent bilirubin binding protein deriving from *A. japonica* (Kumagai et al., 2013). The idea of using a fluorescent protein was, that a potential translocation into the FAS complex could be easily optically detected. The two fluorescent UnaG constructs had a molecular weight of 31.2 kDa and 47.8 kDa, respectively (*Figure 4.23 A, top and middle*). As a third construct, we modified the small (23 kDa) *E. coli* thioesterase TesA with the same 1-25 and 117-150 regions (*Figure 4.23 A, bottom*). Other than the UnaG constructs, TesA is not fluorescent but has an

intrinsic acyl-chain thioesterase activity (Lennen and Pfleger, 2012). A translocation of an additional acyl-chain thioesterase into the FAS complex could have the potential to affect the acyl-chain elongation process inside the FAS cavity. To test whether the three synthetic proteins bind to Δγ-FAS, reactions containing Δγ-FAS and 50x molar excess of the three constructs were incubated and applied to sucrose density gradients. The gradients were fractionated and analyzed via SDS-PAGE. Indeed, all three synthetic proteins showed a co-sedimentation together with the FAS into the 40S region of the gradient (*Figure 4.23 B)*. Thus, we concluded that the both sequences deriving from the γ-subunit can be used as import sequences for other proteins.

The observation of the gradients with the fluorescent UnaG under UV-light also allowed an optical evaluation of the co-sedimentation with the FAS (*Figure 4.23 C*). A decreasing fluorescent intensity from 1x UnaG to 2x UnaG can be explained by the size difference. The site of the modified proteins could be the limiting factor for the translocation into the FAS cavity. Furthermore, we could show that also a small acyl-chain specific thioesterase (TesA) can be incorporated into the Δγ-FAS. The successful incorporation of the 2x UnaG construct led us conclude that constructs of a size corresponding to at least 47.8 kDa can be used.

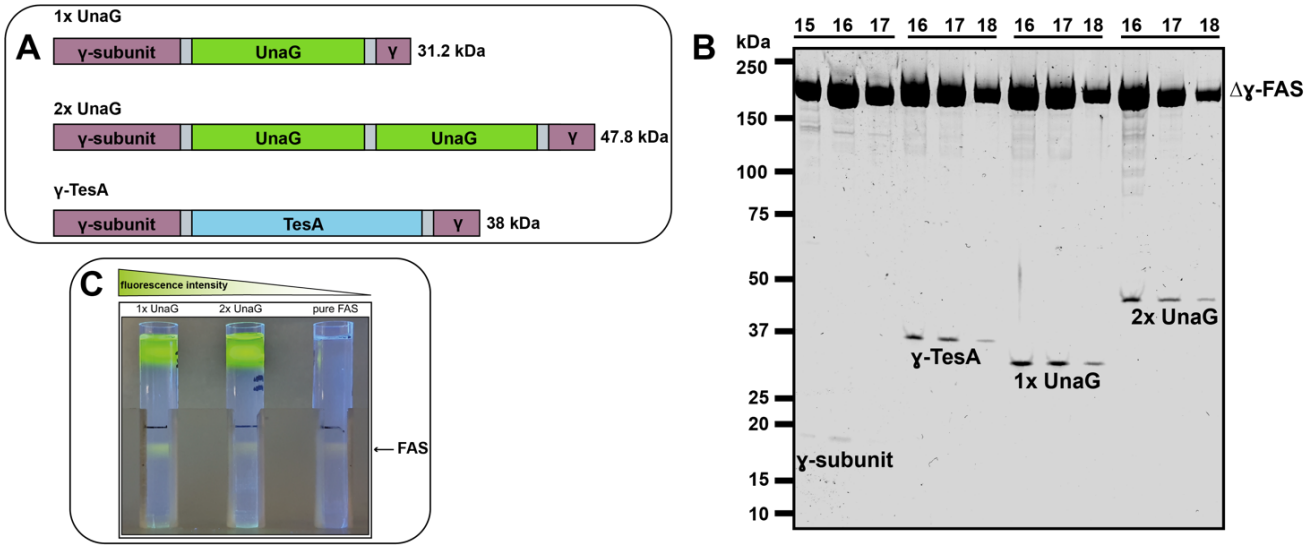

Figure 4.23: γ-subunit as a FAS specific protein shuttle. A) *Schematic illustration of the synthetic protein constructs with the γ-subunit N- and C- termini plus 1xUnaG, 2xUnaG and TesA domains.* ***B)*** *The 40S peak fractions of four Δγ-FAS sucrose density gradients were analyzed via SDS-PAGE. For the recombinant γ-subunit as well as for the three synthetic protein constructs a co-sedimentation with the Δγ-FAS into the 40S region was detected.* ***C)*** *Sucrose density gradients of Δγ-FAS with 1xUnaG, 2xUnaG and pure FAS under UV-light. The fluorescence intensity shows that the incorporation of 1xUnaG is stronger than for the 2xUnaG. Due to the bound FMN, also the pure Δγ-FAS shows a basal fluorescence.*

4.17 Product analysis of *in-vitro* FAS reactions

As reported in former studies of the yeast wtFAS most commonly palmitoyl-CoA (C_{16}-CoA) and steaoryl-CoA (C_{18}-CoA) are released as main products of the yeast fatty acid synthesis cycle. To test, whether this also holds true for $\Delta\gamma$-FAS and $\Delta\gamma$-FAS_{rec}, we analyzed the composition of acyl-CoA products in kinetic activity reactions, respectively. Additionally, we also analyzed reactions containing additional thioesterase TesA and the synthetic γ-TesA protein with the γ-subunit import sequences 1-25 and 117-150 (*see 4.16*). For the thioesterase reactions we wanted to investigate whether the translocation of γ-TesA in to the $\Delta\gamma$-FAS has an impact on the product composition of the FAS cycle. All activity assays were made with substrates at V_{max} concentrations to ensure a maximum enzymatic activity of FAS. The reactions were incubated until no further enzymatic activity was measurable due to complete substrate depletion (end-point reaction). The product analysis experiments were performed by our collaborator PD Dr. Meina Neumann-Schaal (DSMZ – Leibniz Institute, Braunschweig) using GC-MS. Each assay was analyzed in triplicates (n = 3) and the average signal readout for each acyl-CoA product was visualized in a bar chart (*Figure 4.24*).

In the reactions of $\Delta\gamma$-FAS and $\Delta\gamma$-FAS_{rec} we detected acyl-CoAs from C_4-CoA up to C_{14}-CoA in different quantities. While the amounts of C_4-, C_6-, C_{12}- and C_{14}-CoA were relatively low, C_8- and C_{10}-CoA turned out to be the most abundant products within the reactions. Surprisingly, we only detected C_{16}-CoA in the $\Delta\gamma$-FAS_{rec} reaction and no C_{18}-CoA in any reaction. Due to these results, we surmised that both FAS reactions were enzymatically active. The additional production of C_{16}-CoA in the $\Delta\gamma$-FAS_{rec} reaction indicates that the γ-subunit could have an impact on the product chain length. To further address this question additional product analysis investigations with γ-subunit titrations and internal control reactions are required. Since these experiments are currently conducted, we cannot present any results of these measurements.

The analyses of the reactions with TesA and the modified γ-TesA did not show any acyl-CoA products. Therefore, we concluded that the thioesterase domain must have been reactive to any acyl-CoAs and was most likely not specific to the ACP-bound growing acyl-chain inside the FAS cavity. To confirm this assumption, additional GC-MS measurements targeting free fatty acids would be required. These measurements are under current development and thus, not further results can be presented.

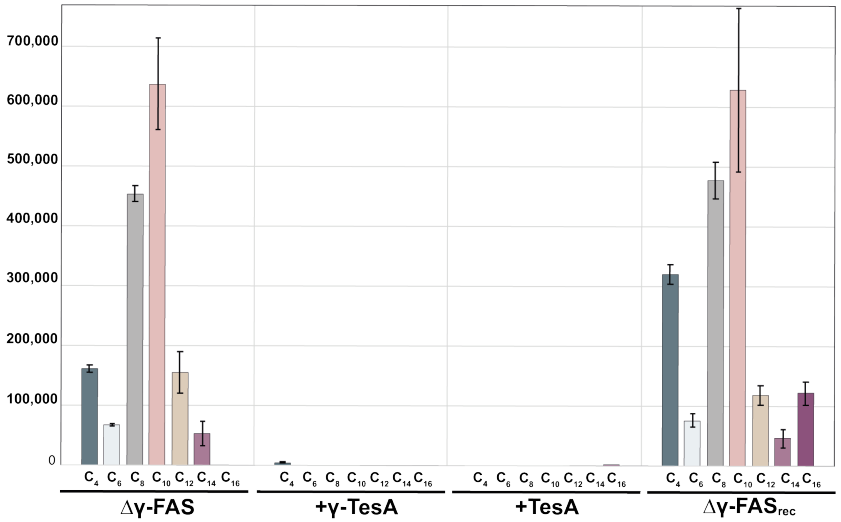

Figure 4.24: GC-MS analysis reveals the acyl-CoA portfolio of Δγ-FAS ± γ-subunit and in presence of γ-TesA/TesA. *For acyl-CoA product analysis of different Δγ-FAS assays end-point reactions were analyzed via GC-MS. While in the reactions in absence (Δγ-FAS) and presence (Δγ-FAS$_{rec}$) of γ-subunit different acyl-CoAs (C4-C16) were detected, the reactions with additional γ-TesA and TesA proteins did not contain any detectable acyl-CoAs. For each acyl-CoA the average of the absolute peak area resulting from three independent measurements is represented. For both reactions, with and without γ-subunit C_8- and C_{10}-CoA were found to be the most abundant acyl-CoA products. Other than Δγ-FAS, Δγ-FAS$_{rec}$ also showed the production of C_{16}-CoA.*

As an internal control of the different product analysis reactions, we also analyzed the abundance of the three substrates acetyl-CoA, malonyl-CoA, and NADPH as well as the released CoA and the oxidized $NADP^+$ (*Figure 4.25*). The comparable ratios of substrates within the separate reactions as well as the abundancy of $NADP^+$ and CoA in similar amounts, led us conclude that all reactions had comparable activities. Within all four reactions malonyl-CoA was almost depleted which indicates that malonyl-CoA was the limiting factor in each reaction.

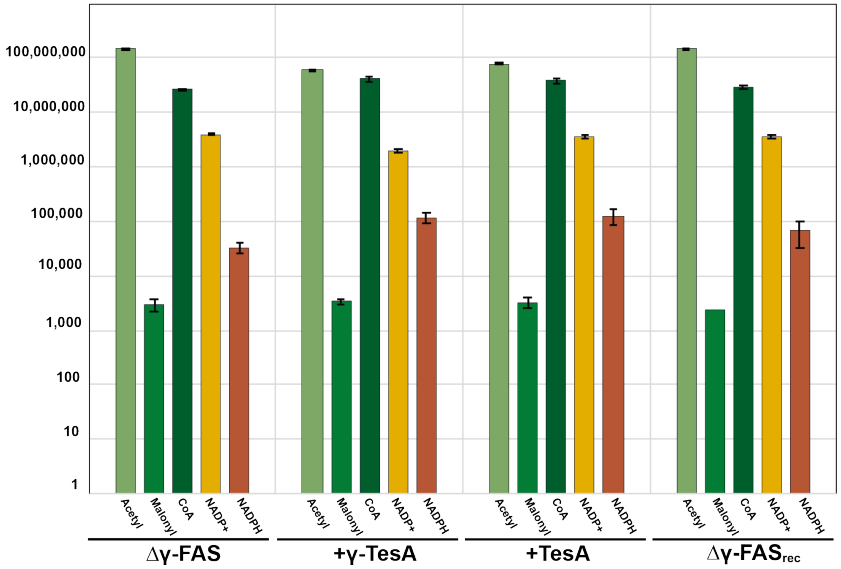

Figure 4.25: Substrate consumption of reaction with Δγ-FAS ± γ-subunit and in presence of γ-TesA/TesA is comparable. *For the three substrates acetyl-CoA, malonyl-CoA, and NADPH as well as for the side-products CoA and $NADP^+$ the average of the absolute peak area resulting from three independent measurements is represented. For all four reactions, comparable ratios between substrate consumption and the side-products $NADP^+$ and CoA were detected. Within all four reactions, the malonyl-CoA pool was found to be completely used up, indicating that all four reactions stopped due to malonyl-CoA limitations.*

In the previous chapters of part of this thesis the discovery of a novel, formerly unknown γ-subunit of the yeast FAS was described. Within a close collaboration with my colleague Kashish Singh it was possible to investigate the kinetics and visualize the γ-subunit binding by use of X-ray crystallography and Cryo-EM. The structural information revealed a direct impact on the FAS structure upon γ-subunit binding. Besides inducing a rotational movement of the FAS dome, the location of the ACP domain was also found to be influenced by the γ-subunit. Extensive steady-state kinetic measurements showed a direct impact of the γ-subunit to the NADPH turnover by kinetic hysteresis and suppression of a futile-cycle reaction. Product analysis could not completely clarify the impact of the γ-subunit to the internal chain-length control of FAS. Despite its impact on the localization of the ACP domain, the γ-subunit did not allow us to get any further detailed insights into the substrate shuttling process.

Our next goal was to get a further insight into the different transient ACP-enzyme interactions. Only with structural information of these states it would be possible to understand the molecular mechanism that controls the product chain lengths and other reactions related to the ACP-substrate shuttling. Based on the development of a biochemical method that allows the enzymatic modification of *E. coli* apo-AcpP with type II FAS mechanism-specific crosslinker substrates by Burkart and co-workers, we wanted to establish a method that allows the modification of yeast type I FAS (Mindrebo et al., 2020a). With such a tool in hand we wanted to trap the ACP of yeast FAS at specific active sites and solve its structure by X-ray crystallography.

4.18 Creation of a PPant-free FAS variant

Former studies showed that a specific serine residue of the ACP domain is post-translationally modified (Fichtlscherer et al., 2000a; Stoops et al., 1990). This transition from apo-ACP to activated holo-ACP is essential for the activity of FAS (*Figure 0.4*). To introduce different site-specific crosslinker to the ACP domain Burkart and co-workers designed different reactive pantetheineamide precursor molecules that can be enzymatically converted into crypto-CoAs (*Figure 0.8*). By use of the PPTase mediated activation reaction the reactive pantetheineamide residues can be transferred to apo-ACP, resulting a crypto-ACP. The crypto-ACP domain is then able to undergo a crosslink reaction with specific FAS domains (*Figure 0.9*).

To apply this method to the endogenous yeast FAS, the FAS must be purified in an enzymatic inactive apo-ACP state. Since the activity of FAS is crucial for the growth of yeast cells, only enzymatic active FAS (holo-ACP) can be purified from wild-type yeast cells. To solve this problem, we decided to create a recombinant yeast strain with a deletion of the PPTase domain encoded at the 3' terminus within the FAS2 gene. For deletion, a STOP-codon was introduced at the codon 1750 in the FAS2 gene using homologous recombination. To select for positive clones, a 3' KanMX resistance marker was introduced together with the STOP-codon (*Figure 4.26*). To compensate for the consequences of the fatty acid synthesis inactivation, the cells were rescued

by addition of external FAs to the growth medium. The successful replacement of the PPTase coding sequence with a STOP-codon and KanMX resistance cassette was verified by DNA sequencing the corresponding FAS2 region (data not shown).

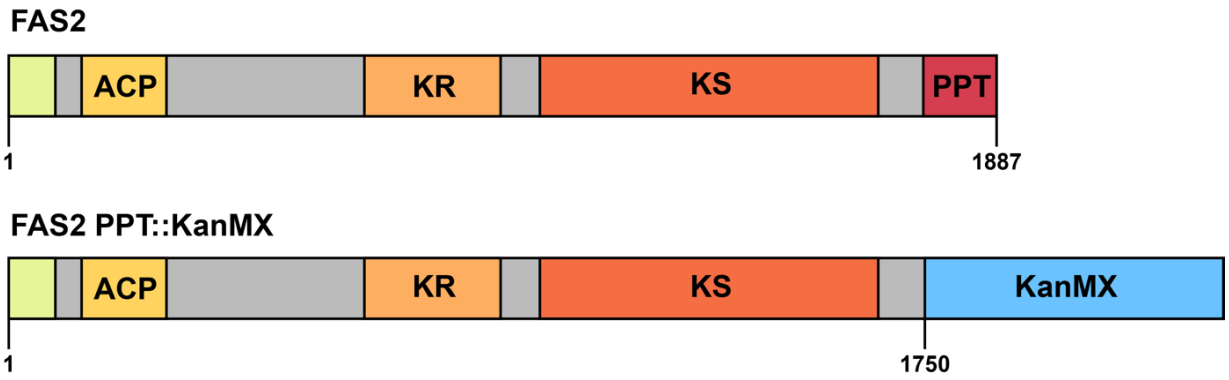

Figure 4.26: Schematic representation of wtFAS2 and FAS2 PPT::KanMX loci.Top) *The FAS2 locus of the wtBJ2168 yeast strain encodes for 1887 amino acids which build up the α-subunit containing parts of the MPT domain (green), the ACP (yellow), the KR (bright orange), the KS (orange) and the c-terminal PPT domain (red).* ***Bottom)*** *The modified FAS2 PPT::KanMX locus encodes for the amino acids 1-1750 containing parts of the MPT domain, the ACP, KR and KS, respectively. For deletion of the n-terminal PPT domain a STOP codon was introduced at position 1751. For antibiotic selection, a c-terminal KanMX open reading frame (blue) was added.*

To compare the growth rates of the wild-type BJ2168 strain with the modified BJ2168 FAS2 PPT::KanMX (ΔPPTase-BJ2168) strain we measured the development of cell density from both strains at 30 °C over time. To ensure a cell growth for the PPTase deficient strain, additional external fatty acids, and the selection antibiotic G418 were added to the medium. The optical cell density was spectrophotometrically determined in steps of 180 min at OD_{600} until the stationary phase was reached after 3000 min (*Figure 4.27*). The wild-type yeast strain (blue) showed a doubling time of 90 min during its exponential growth phase and reached a cell density of OD_{600} = 8.4 when the stationary phase was reached after 2300 min. For the ΔPPTase-BJ2168 strain the doubling time was increased to 300 min. The final cell density was decreased to OD_{600} = 5.0 after reaching the stationary phase after 3000 min.

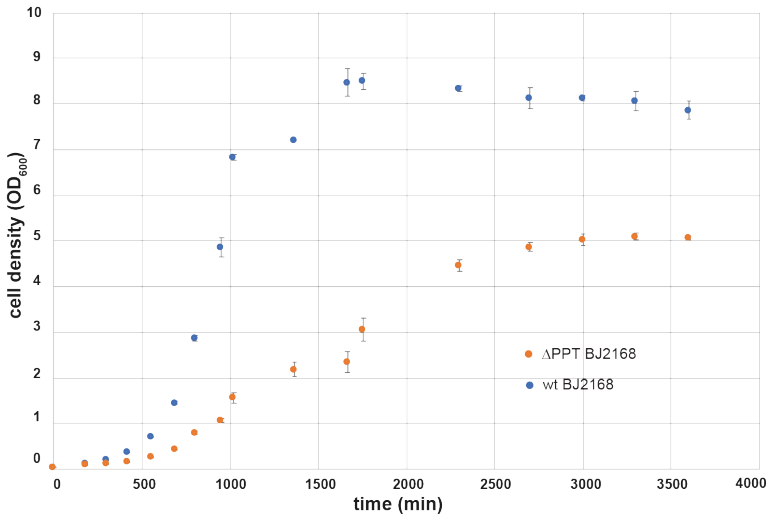

Figure 4.27: Growth experiments reveal a reduced cell growth of ΔPPT BJ2168 strain. *The wild-type yeast strain (blue) showed a doubling time 90 min during its exponential growth phase and reached a cell density of OD_{600} = 8.4 when the stationary phase was reached after 2300 min. The* ΔPPT BJ2168 strain had a doubling time of 300 min and only reached its final cell density of OD_{600} = 5.0 after 3000 min.

4.19 Purification of endogenous ΔPPTase-FAS

After successful generation of a ΔPPTase-BJ2168 yeast strain with a deletion, we asked ourselves whether the modified cells are still expressing the inactive ΔPPTase-FAS. In case they do so, we also wanted to know whether the expressed complex assembles correctly and could be purified from the cell lysate. For chromatography-free purification of ΔPPTase-FAS we used the similar protocol as already described for Δγ-FAS (*Figure 4.1*). By inducing of an additional initial purification step that to remove nucleic acids and nucleic acid binding proteins, we managed to dispense one sucrose density gradient (*Figure 4.28 A*). After application on two successive sucrose density gradients, we ended up with pure ΔPPTase-FAS according to SDS-PAGE analysis (*Figure 4.28 B*).

Due to the sedimentation of the ΔPPTase-FAS into the 40S region of the density gradients, we concluded that the complex was fully assembled. The shift of the ΔPPTase-FAS bands on the SDS-PAGE (*Figure 4.28 A*) compared to those of the Δγ-FAS (*Figure 4.1*) can be explained by deletion of the PPTase domain from the α-subunit. An additional indicator for the correct assembly of the purified ΔPPTase-FAS was the intense yellow color of the final protein solution (not shown).The color originates from the ER-bound FMN molecules (Lynen, 1980). With a total yield of 7.5 – 10 mg of ΔPPTase-FAS from 230 g ΔPPTase-BJ2168 cells, the final yield was ~25-50% lower than those of wtFAS and Δγ-FAS. The decrease of the yield can most likely be explained by a reduced expression of the ΔPPTase-FAS.

A kinetic activity assay of freshly purified ΔPPTase-FAS confirmed that the enzyme is indeed inactive (data not shown). Therefore, we have concluded that the ACP-domain of ΔPPTase-FAS is in its inactive apo-form and does most likely not have a post-translational PPant modification.

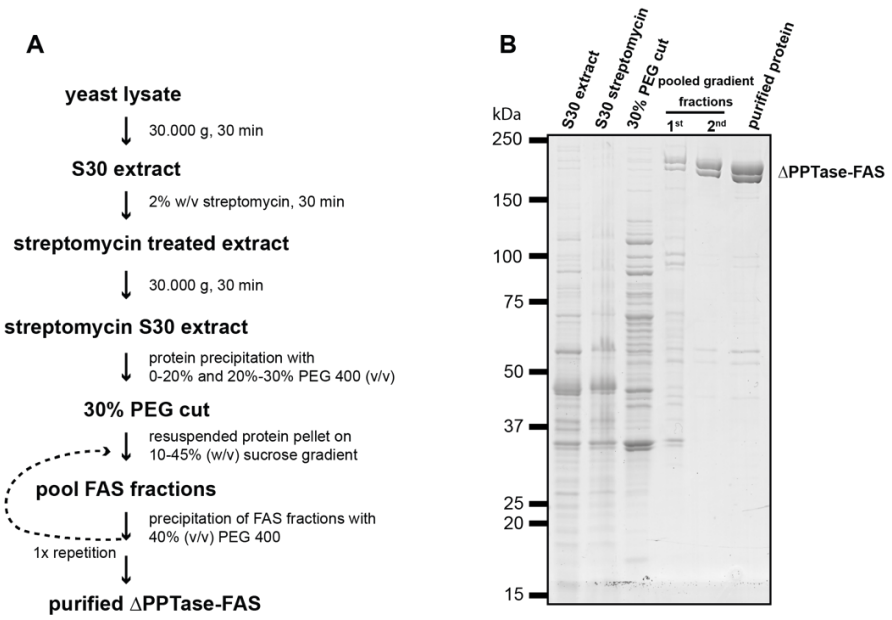

Figure 4.28: Chromatography-free purification of ΔPPTase-FAS. A) *Schematic representation of the chromatography-free purification of ΔPPTase FAS from ΔPPTase-BJ2168 lysate* ***B)*** *After a first centrifugation step for removal of cell debris (S30), nucleic acid binding proteins are removed by a streptomycin precipitation followed by centrifugation (S30 streptomycin). For after a 30% PEG cut, the resulting protein pellet containing the ΔPPTase-FAS was loaded on a linear 10%-45% sucrose gradient. For removal of unspecific proteins, the FAS containing fractions were pooled (1st) and further applied on a second linear sucrose gradient. The final ΔPPTase-FAS containing fractions (2nd) were pooled (purified protein). According to the SDS-PAGE analysis the resulting ΔPPTase-FAS protein was relatively pure.*

4.20 Enzymatic modification of apo-ACP

With the PPant-free ΔPPTase-FAS in hand we wanted to know whether the recombinant yeast PPTase domain can catalyze the *in-vitro* phosphopantetheinylation of recombinant apo-ACP. Therefore, we cloned the yeast PPTase (yPPTase) and ACP (yACP^{apo}) sequences in separate bacterial expression vectors and expressed them in *E. coli* expression strains. After successful purification of both proteins using affinity chromatography (data not shown) we incubated yACP^{apo} with yPPTase and CoA or C_{17}-CoA, respectively. As a control, we additionally used a S180A-ACP mutation which cannot be phosphopantetheinylated due to the exchange of Ser^{180} for Ala^{180}. SDS-PAGE analysis of both reactions revealed a visible shift yACP^{apo} upon binding of the PPant from CoA and C_{17}-PPant from C_{17}-CoA. The longer hydro-carbon chain deriving from C_{17}-CoA induced a larger shift than CoA (*Figure 4.29 left*). Within the S180A-ACP control reaction no shift of the ACP band was detected (*Figure* 4.29 *right).*

Thus, we have concluded that the recombinant yPPTase is indeed enzymatically active and specifically adds PPant to the Ser^{180} residue of yACP^{apo}. Since C_{17}-CoA can also be used as a substrate, we concluded that the yPPTase does not have a substrate specificity discriminating other CoA variants with alternating acyl-chain length.

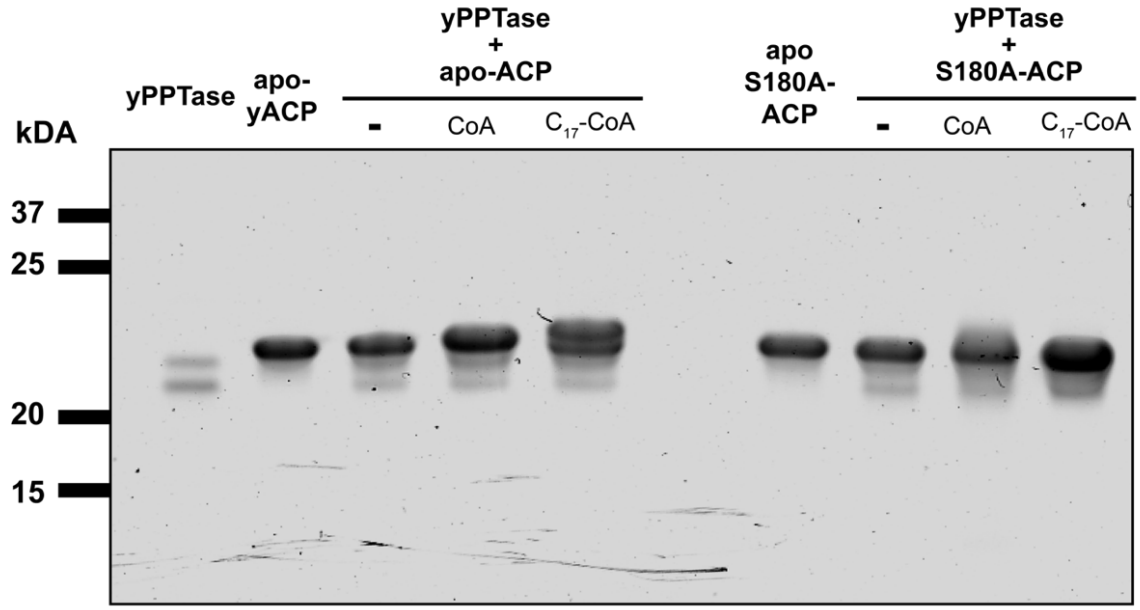

Figure 4.29: Phosphopantetheinylation of yACP by yPPTase. *SDS-PAGE analysis of the post-translational addition of a 4'-phosphopantetheine arm from CoA and C_{17}-CoA to yeast apo-ACP and a S180A-ACP mutant. The band shift of the apo-ACP upon addition of CoA and C_{17}-CoA indicates a successful 4'-phosphopantetheine transfer from the CoA substrates to the serine residue of apo-ACP. Thus, the apo-ACP can be converted into its holo-ACP form. For the S180A-ACP mutant no shift due to yPPTase mediated 4'-phosphopantetheine transfer from CoA and C_{17}-CoA was detected.*

4.21 *In-vitro* activation of ΔPPTase-FAS

With the knowledge that the recombinant yPPTase domain can transfer PPant from CoA to the Ser^{180} residue of recombinant $yACP^{apo}$, we sought to test whether yPPTase is able to catalyze the same reaction in the fully assembled ΔPPTase-FAS molecule.

To do so, we incubated freshly purified ΔPPTase-FAS with CoA and recombinant PPTase domains from different species (*Figure 4.30, left*). To test, whether the activation was successful, we compared the enzymatic activity of the ΔPPTase-FAS reactions with those of the Δγ-FAS (*Figure 4.30, right*). The kinetic measurements showed that only ΔPPTase-FAS incubated with yeast yPPTase was activated. Compared with the enzymatic activity of Δγ-FAS the activated ΔPPTase-FAS showed a restored activity of 80%. The activation reactions without additional PPTase or with PPTase domains originating from other organisms did not show any activation (*Figure 4.30 right*). To cross-verify the correct post-translational modification of the ACP-Ser^{180} in activated ΔPPTase-FAS, tandem mass spectrometry measurements were performed by Dr. Andreas Linden. In the activated ΔPPTase-FAS samples, one phosphopantetheine residue at position 180 within the α-chain was found. The untreated ΔPPTase-FAS did not show any phosphopantetheine modifications and thus, was not activated (*Table 4.2*).

We therefore concluded, that recombinant yPPTase can indeed be used for the post-translational *in-vitro* activation of ΔPPTase-FAS. Additionally, we have already shown that the length of acyl-CoA hydro-carbon chain is not limiting for the yPPTase activity (*Figure 4.29*). For

this reason, we decided to use yPPTase for all following ΔPPTase-FAS activation experiments using crypto-CoA derivatives.

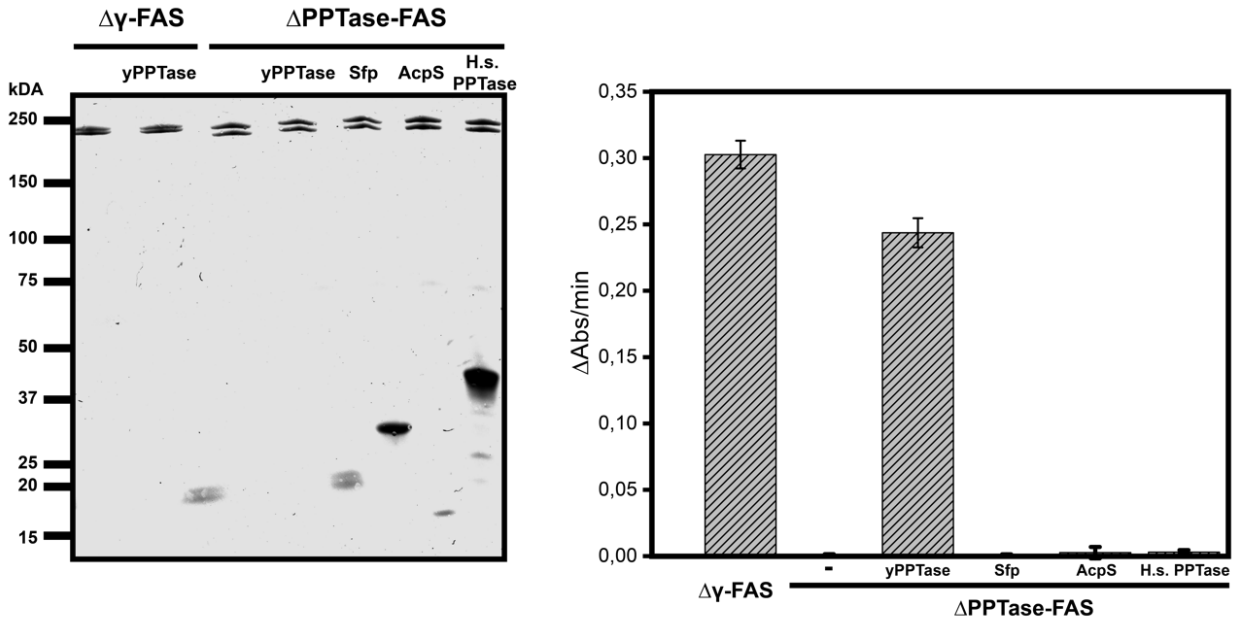

Figure 4.30: Recombinant yPPTase can be used for ΔPPTase-FAS activation. A) *SDS-PAGE analysis of different Δγ-FAS and ΔPPTase-FAS activation reactions. As the gel indicates, all reactions contained Δγ-FAS (control) or ΔPPTase-FAS and additional PPTases from yeast (yPPTase), B. subtilis (Sfp), E. coli (AcpS) and H. sapiens (H.s. PPTase). For all reactions CoA was used as substrate for the phosphopantetheine transfer. According to the SDS-PAGE none off the reactions contained any unspecific impurities.* ***B)*** *Enzyme kinetic measurements of the different activation reactions revealed a maximum activity of 0.30 min^{-1} for Δγ-FAS. For the ΔPPTase-FAS without additional PPTase (-) and with the PPTases Sfp, AcpS and H.s. PPTase no enzymatic activity was detected. The activation reaction of ΔPPTase-FAS with yPPTase resulted in a maximum activity of 0.25 min^{-1}. In all activity measurements, the substrates acetyl-CoA, malonyl-CoA, and NADPH were used at V_{max} concentrations as previously determined (see 4.15).*

Protein	Position within protein	Localization probability	Amino acid	Phosphopantetheine probability
α-chain of activated ΔPPTase-FAS	180	1	S	DLVGGKS(1)TVQNEILGDLGK
α-chain of ΔPPTase-FAS	No phosphopantetheine residues were detected in the ΔPPTase-FAS			

Table 4.2: Mass spectrometric analysis of ΔPPTase-FAS phosphopantetheinylation. *Mass spectrometric analysis of ΔPPTase-FAS before and after the phosphopantetheinylation reaction with yPPTase and CoA. While the α-subunit of activated ΔPPTase-FAS revealed a phosphopantetheine residue at the amino acid position 180 (Ser^{180}), no such phosphopantetheine modification was found on the untreated ΔPPTase-FAS.*

4.22 Chemo-enzymatic *in-vitro* CoA synthesis

After establishing the protocol for activation of ΔPPTase-FAS, we adapted an assay which allows the *in-vitro* chemo-enzymatic synthesis of crypto-CoA derivatives starting form modified pantetheineamide precursor probes. The chemo-enzymatic synthesis of such CoA variants has been formerly described by Burkart et al. (Mindrebo et al., 2020a) and requires the bacterial *E. coli* enzymes CoaA, CoaD, CoaE, ATP and pantetheine/pantetheineamide analogs (*Figure 0.8*).

To test the enzymatic activity and ensure the function of the chemo-enzymatic assay, we used commercially available pantethine, which was reduced to pantetheine by addition of reducing agent. The resulting pantetheine was further used as substrate for the chemo-enzymatic CoA synthesis by CoaA, CoaD and CoaE under consumption of ATP. All three enzymes used in this reaction were formerly cloned, expressed and purified by my colleague Kashish Singh. To verify whether CoA was produced within the reaction assay, we used the reaction product as substrate for the yPPTase mediated activation of the ΔPPTase-FAS (*see section above 4.21*). The activity of the activated ΔPPTase-FAS was measured and compared with the activation efficiency of commercially available CoA. These kinetic activity measurements showed identical enzymatic activity for both reactions (data not shown). Thus, we concluded that the chemo-enzymatic CoA synthesis starting from pantetheine was successful and can indeed be used for the *in-vitro* synthesis of other CoA substrates. Since we did not find any differences in the activity of ΔPPTase-FAS activated with commercial and enzyme-synthetic produced CoA, we also assumed that the chemo-enzymatic synthesis is highly efficient and produces CoA in sufficient amounts and quality for the ΔPPTase-FAS activation reaction.

4.23 Mechanism-based crosslinking of bacterial AcpP

With the knowledge that we can modify the apo-ACP from ΔPPTase-FAS and produce CoA from pantetheine we wanted to apply the chemo-enzymatic synthesis on reactive pantetheineamide derivatives. Therefore, we tested three different pantetheineamide probes (*Figure 0.10 i, Figure 0.11, Figure 0.12*) which were formerly designed by Burkart and co-workers and synthesized for us by the collaborating company NovAliX (Illkirch-Graffenstaden, France) (Milligan et al., 2019b; Nguyen et al., 2014a; Tallorin et al., 2016b; Worthington et al., 2006). Since the reactive groups of the pantetheineamide probes were originally designed for a crosslinking actvity with active site residues of the bacterial *E. coli* type II FAS system, we used these specific bacterial domains as reaction partners.

In one-pot reactions we first synthesized crypto-CoAs using the previously described chemoenzymatic assay (see 4.22). After incubation and centrifugation all three reactions separated into a liquid (SN) and a solid phase (pellet). The SN was carefully removed and both phases were independently tested as substrates for the phosphopantetheinylation reaction of *E. coli* apo-AcpP ($AcpP^{apo}$) by the *B. subtilis* phosphopantetheinyl transferase (Sfp). To test

whether the reactions produced AcpP^{crypto} with a reactive group, the respective bacterial domains were added (Figure 4.31). Products of the one-pot reactions were analyzed by SDS-PAGE. Reactions containing FabA (19 kDa) and FabB (42.6 kDa) reactive CoA analogues showed additional bands of molecular weights corresponding to hypothetical adducts of AcpP-FabA (33 kDa) and AcpP-FabB (60 kDa) for both, the SN and pellet fractions of crypto-CoA synthesis. In both cases the bands of AcpP-FabA and AcpP-FabB revealed a higher intensity for substrates deriving from SN than those of the pellet fractions. It therefore can be assumed that the soluble SN fractions revealed a higher crosslinking efficiency when used as substrate for the phosphopantetheinylation reaction. The reaction with FabI (27.8 kDa) only showed an additional band of an unexpected lower molecular weight (15 kDa) for the pellet fraction of crypto-CoA. This could be either caused by the structure of the reactive group which induces a significant change of the running behavior. Second, it is also possible that the interaction between FabI and AcpP^{crypto} is not stable under reducing and denaturing conditions of the SDS-PAGE. For the interaction of AcpP^{crypto} with FabA and FabB we concluded that the protein-protein interaction is stable under SDS-PAGE conditions and therefore most likely of covalent nature.

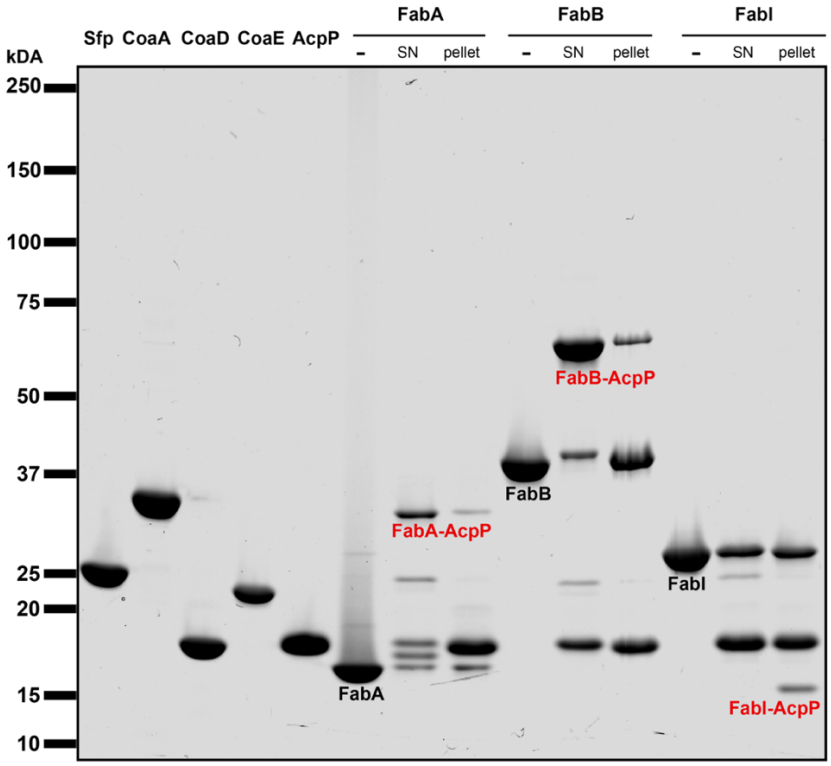

Figure 4.31:E. coli AcpP can be modified with crypto-CoAs and binds to type II FAS proteins. *SDS-PAGE analysis of enzymatic one-pot AcpP crosslinking reactions. First, crypto-CoAs with domain specific warheads against E coli FabA, FabB and FabI were in-vitro synthesized by CoaA, CoaD and CoaE. In a second step, the solid phase (pellet) and the liquid phase (SN) resulting from the chemo-enzymatic reactions were used as substrate for the Sfp mediated transfer of the modified phosphopantetheine residue of the crypto-CoAs to apo-AcpP. To test for a crosslinking reaction between the resulting crypto-AcpP with the corresponding type II domains all reactions were analyzed via SDS-PAGE. For FabA (19 kDa) a band corresponding to the size of the 33 kDa FabA-AcpP (red) was found for both, the SN as well as the pellet fraction. The FabB (42,6 kDa) reaction also revealed a protein band corresponding to the 60 kDa product of FabB-AcpP (red) for both fractions tested. For FabI (27.8 kDa) only an additional band of 15 kDa was found for the hypothetical 44kDa FabI-AcpP crosslinking product within the pellet fraction of the crypto-CoA substrate.*

4.24 *In-vitro* Modification of ΔPPTase-FAS

With the knowledge of being able to phosphopantetheinylate the apo-ACP of ΔPPTase-FAS *in vitro* and having an established protocol for the chemo-enzymatic synthesis of mechanism-based reactive crypto-CoAs, we decided to combine both biochemical tools. Therefore, we tested the crosslinking potential of three different crypto-CoAs with ΔPPTase-FAS. We first synthesized crypto-CoA substrates with chemo-enzymatic one-pot reactions and further used them as substrates for the yPPTase mediated phosphopantetheinylation reaction (*Figure 4.32 A*). All reactions were analyzed via SDS-PAGE (*Figure 4.32 B*). For reactions with the crypto-CoAs [Br-KS] and [Cl-KS] we detected a shift of the ΔPPTase-FAS bands (*Figure 4.32 B, Br-KS, and Cl-KS*). However, the use of the crypto-CoA analogue [SO-DH] did not show any band shift on the SDS-PAGE (*Figure 4.32 B, SO-DH*). Since a change of the running behavior on an SDS-gel is not implicit for a successful intramolecular crosslinking reaction, the use of analytical methods like protein mass spectrometry would be advantageous. We nevertheless assumed that the band-shift introduced by the [Br-KS] and [Cl-KS] probes could be explained by an intramolecular crosslinking reaction of the crypto-ACP to the active site cysteine of the KS domain. This assumption was supported by the successful use of [Br-KS] variants with alternating acyl-chain lengths for the structure determination of the crosslinked *E. coli* AcpP-FabB complex using X-ray crystallography (Mindrebo et al., 2020a). We therefore used [Br-KS] crypto-CoA as substrate for further ΔPPTase-FAS modifications.

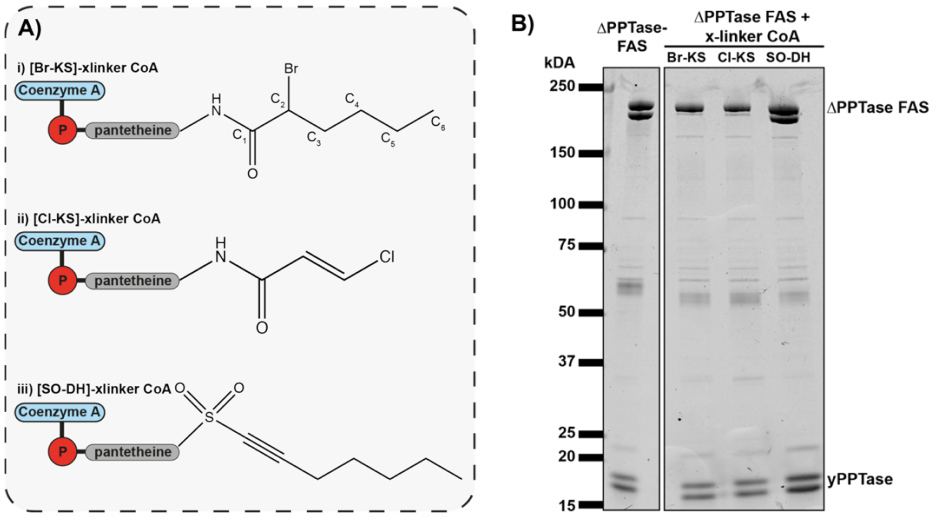

Figure 4.32: yPPTase mediated modification of ΔPPTase-FAS with crypto-CoAs induces a band shift on n SDS-gel. A) *Schematic representation the three different crypto-CoAs: i) [BR-KS] crypto-CoA and ii) [Cl-KS] crypto-CoA are both targeting the active site cysteine residue of the KS domain. The Br and Cl residues act as electrophilic leaving groups that allow the formation of a covalent linkage to the sulfur group of the active site cysteine. iii) The [SO-DH] crypto-CoA is designed to form a covalent crosslink with the active site histidine of the DH domain.* ***B)*** *SDS-PAGE analysis of ΔPPTase-FAS and ΔPPTase-FAS phosphopantetheinylation reactions with yPPTase and different crypto-CoAs. The ΔPPTase-FAS reaction without CoA analog (left) shows the characteristic ΔPPTase-FAS double band at 200 kDa and a yPPTase double band between 15 and 20 kDa. ΔPPTase-FAS reactions with [Br-KS] and [Cl-KS] crypto-CoA as substrate for the phosphopantetheinylation reaction show a change I the running behavior of the ΔPPTase-FAS bands. Instead of two separate band, only one single band appears for both crypto-CoAs. The reaction with the [SO-DH] crypto-CoA did not affect the running behavior of ΔPPTase-FAS.Structural investigation of crosslinked ΔPPTase-FAS*

To get a structural insight into the crosslinked ΔPPTase-FAS molecule we used ΔPPTase-FAS protein from the *in-vitro* phosphopantetheinylation reaction with the [Br-KS] crypto-CoA to grow protein crystals. The crystals grew up to a size of ~150x100x100 µm and for the best crystal we obtained an X-ray crystallographic dataset with reflections until 2.9 Å. The crystal belonged to the primitive monoclinic space group $P2_1$ with the unit cell constants a = 227.7 Å, b = 356.4 Å, c = 251.2 Å and β = 112.3°. For molecular replacement we used the X-ray structure of Δγ-FAS which was formerly solved by my colleague Kashish Singh (Figure 4.11 *B*). A comparison with the structure of Δγ-FAS confirms the deletion of the PPTase domain located outside of the central homo-hexameric central wheel (*Figure 4.33 A, PPTase domain highlighted in yellow*). The quality of the electron density map allowed us reliable modelling of all enzymatic ΔPPTase-FAS domains. For most amino acids we were able to also model the side chain residues (*Figure 4.33 B*). Additionally, we found electron density near the KS domain which allowed us to build the structure of the ACP domain together with a covalent crosslink between the modified Ser^{180} of the ACP and the KS active site cysteine (Cys^{1305}). The continuous electron density from the Ser^{180} residue of the ACP domain, along the attached PPant residue to the active site Cys^{1305} of the KS domain led us conclude that we indeed managed to introduce a covalent crosslink between ACP and the KS domain of the ΔPPTase-FAS (*Figure 4.33 C*).

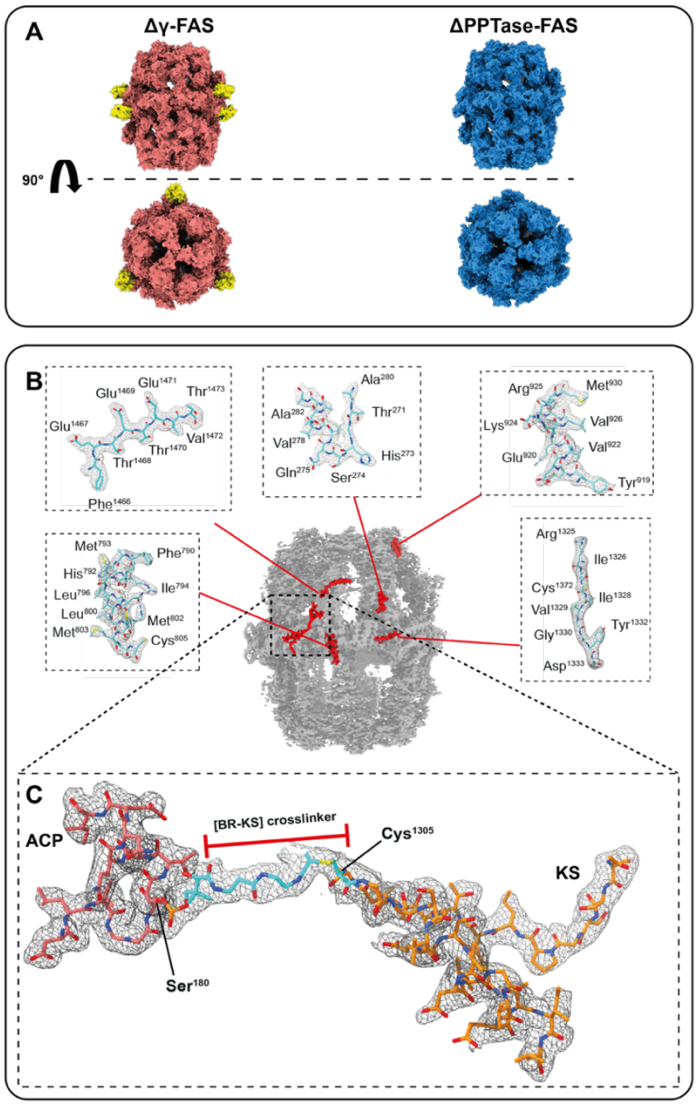

Figure 4.33: X-ray structure of the crosslinked ΔPPTase-FAS. A) *A direct comparison of the X-ray structures from the Δγ-FAS (left) with the ΔPPTase-FAS (right) shows that the PPTase domain (yellow) which is located outside of the hexameric central does not appear in the ΔPPTase-FAS structure.* ***B)*** *The 2.9 Å electron density map is shown as an envelope structure of the whole ΔPPTase-FAS molecule (middle). Representative for the quality of the electron density map over the whole particle, different areas of the molecule are highlighted (red) and magnified (boxes 1-5).* ***C)*** *The electron density map allowed the modelling of the ACP domain with its phosphopantetheine arm from the used [Br-KS] crosslinker. Due to the continuous electron density, we also modeled a covalent linkage to the active site Cys^{1305} of the KS-domain. Besides the phosphopantetheine arm and the covalent linkage we were also able to model carbon atoms C_1-C_3 of the crosslinker C_6-acyl chain (Figure 4.32 Ai). The electron densities in all figures are contoured at 1.5 σ.*

A closer inspection of the covalent linkage between the ACP domain and the active site Cys^{1305} showed that the ACP-KS interaction is formed between two distinct α-subunits (α_1 and α_2) of the α_6-central wheel (*Figure 4.34 A*). The PPant arm of the ACP-domain from the α_1-subunit (red) is covalently bound to the KS active site cysteine of the neighboring α_2-subunit (orange). Thus, the mechanism-based crosslinking of the ACP domain to the keto synthase resulted in an intramolecular crosslink between two distinct α-subunits. To our surprise we additionally found a non-covalent interaction of a third α-subunit (blue) in proximity to the crosslinked PPant at the KS active site (*Figure 4.34 A and B*). This suggest that in total three neighboring α-subunits are involved into substrate binding and the condensation reaction of the KS domain.

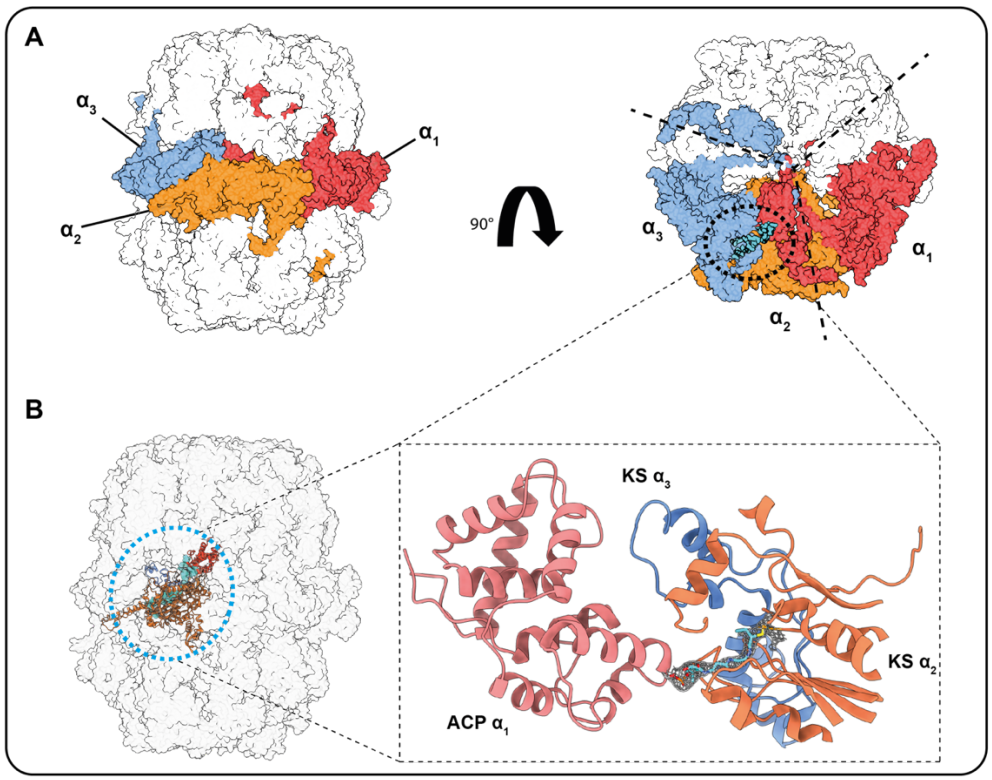

Figure 4.34: The crosslinked ACP domain reveals the interaction of three neighboring α-subunits. A) *The schematic representation of the ΔPPTase-FAS molecule in side-view (left) and top view (right). Three neighboring α-subunits are highlighted in colors α_1 (red), α_2 (orange) and α_3 (blue). The top-view also shows the three-fold symmetry axis as well as the location of the phosphopantetheine arm of the ACP domain from the α_1-subunit.* ***B)*** *In the side-view representation the location of the crosslinked ACP domain of the α_1-subunit (red), the KS active site of the α_2-subunit (orange) and the phosphopantetheine arm (cyan) is highlighted and magnified (box). The magnification of the crosslinked ACP domain shows the intra-molecular covalent linkage between the α_1-subunit and the α_2-subunit by the phosphopantetheine residue. In proximity to the phosphopantetheine arm also a part of a third α_3-subunit (blue) is found.*

With structural information of the intramolecular crosslinking between *in-vitro* modified ACP domain (*Figure 4.35 A, left*) we were able to build the model of the covalent linkage to the sulfur group of the active site cysteine from the neighboring KS domain (*Figure 4.35 A, right).* The continuous electron density allowed us the reliable modelling of the Br-KS crosslinker with its acyl-chain hydro-carbon atoms $C_{1\text{-}3}$ (Figure 4.35 *A – C)*. However, we could not localize the whole acyl-chain of the bound substrate. While the carbon atoms $C_{4\text{-}6}$ where not visible, we could show that two threonine residues (Thr^{1546} and Thr^{1544}) are stabilizing the pantetheine part of the cross-linked substrate (Figure 4.35 *B and C)*. Next to the active site Cys^{1305} two histidine residues (His^{1542} and His^{1585}) are located facing towards the covalent linkage between the PPant and Cys^{1305}. These two His residues were formerly proposed as part of the catalytic triad of the KS active site (von Wettstein-Knowles et al., 2006; Zhang et al., 2006). Even though, we did not find any structural information showing a direct interaction of the third α-subunit (Figure 4.35 *B and C, blue*) with the cross-linked PPant, its proximity is conspicuous.

From the structure of the crosslinked ΔPPTase-FAS we concluded that it is indeed possible to modify the ACP domain of macromolecular complexes like the yeast FAS *in vitro*. By use of structure determination methods like X-ray crystallography it is possible to investigate

intermediate states of interactions which are usually of a transient nature. Therefore, this biochemical tool can be also applied for other ACP dynamics within the FAS complex or transferred to other protein complexes that underly the same or a similar substrate shuttling mechanism.

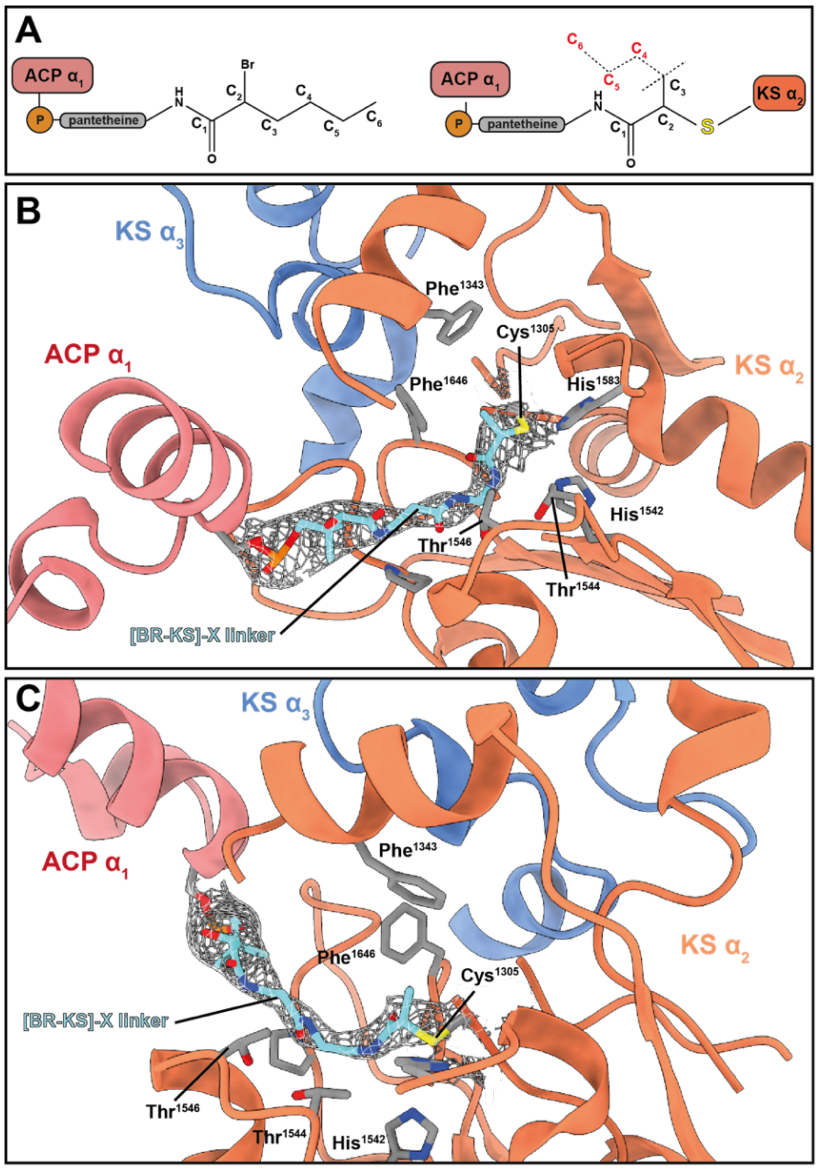

Figure 4.35: The covalent binding of the ACP allows an insight into the transient ACP-KS intermediate state: A) (left) *Schematic representation of the crypto-ACP modified with the pantetheine amide residue from [Br-KS] crypto-CoA. The Br residue acts as an electrophilic leaving group that allows the formation of a covalent linkage to the sulfur atom of the active site cysteine from the KS active site.* ***A) (right)*** *The schematic representation of the covalent bond between the crypto-ACP and the sulfur group of the active site cysteine. The carbon atoms C_{1-3} (black) can be modelled into the electron density, whereas no electron density was found to model the carbon atoms C_{4-6} of the [Br-KS] acyl-chain.* ***B) and C)*** *Detailed representation of the crosslinked KS active site. For the intra-molecular covalent linkage between the phosphopantetheine residue (cyan) of the ACP domain from α_1-subunit (red) and the active site Cys^{1305} of the α_2-subunit (orange) the electron density map is contoured at 1.5 σ. The two threonine residues Thr^{1546} and Thr^{1544} are stabilizing the pantetheine arm. In proximity to the covalent linked Cys^{1305} the two histidine residues His^{1542} and His^{1583} as parts of the catalytic triad are highlighted. In proximity to the acyl-chain of the crosslinker the two hydrophobic phenylalanine residues Phe^{1343} and Phe^{1646} are located.*

5 Discussion

The aim of this thesis was the development of novel biochemical techniques and tools that allow the specific manipulation of transient conformational states within large proteins and protein complexes. Conformational changes are often the basis for the catalysis of enzymatic reactions. Only the biochemical control of such different states allows to gain detailed structural information, which is essential to understand the biocatalytic mechanisms and their regulation. As protein of interest, we chose the large 2.6 MDa FAS from baker's yeast *S. cerevisiae*. Former structural and biochemical investigations showed that this protein complex undergoes different conformational changes which are directly connect to substrate processing by distinct intramolecular enzymatic domains (Leibundgut et al., 2007; Lomakin et al., 2007; Lynen et al., 1980). In a highly cooperative project, we managed to establish a novel chromatography-free purification method that allowed the purification of endogenous FAS under constant protein concentration, pH, and ionic strength. With the help of this method, we discovered a weakly bound and salt-labile FAS binding protein with an apparent size of 20 kDa. By mass spectrometric analysis and biochemical binding experiments we were able to show that this additional protein is a formerly overseen third subunit of the FAS complex. Following the previous designation of the FAS subunits, we termed the novel protein as γ-subunit. The combination of results from protein structure determination techniques like Cryo-EM and X-ray crystallography with intensive steady-state enzyme kinetic experiments allowed us to draw an image of how the γ-subunit binds to the FAS complex and influences its conformational and kinetic landscape. Furthermore, we identified sequences of the γ-subunit that are essential for its translocation into the FAS molecule. With help of these FAS specific import sequences, we could show that single proteins can be modified and imported into the FAS complex. Even though, the discovery of the γ-subunit allowed us to induce a conformational rearrangement of the FAS molecule, we wanted to have a biochemical tool that allows us the specific investigation of different transient ACP-enzyme interactions. Therefore, we created a recombinant yeast strain that allowed us the purification of a correctly assembled enzymatic inactive FAS molecule. On basis of a biochemical tool which was originally designed for the investigation of transient ACP-enzyme interactions within the bacterial FAS system (Mindrebo et al., 2020a), we successfully transferred the method to the yeast FAS system. This allowed us to manipulate the ACP domain of yeast FAS *in vitro* with mechanism specific crosslinker substrates. By vapor diffusion, we managed grow protein crystals of the FAS complex, modified with a keto synthase (KS) specific crosslinking substrate. From these crystals we managed to collect an X-ray crystallographic dataset with diffractions until 2.9 Å. The resulting electron density map allowed us the modelling of the covalent linkage between the ACP and the keto synthase active site together with three carbon atoms of the substrate's acyl-chain. This made it possible to get an insight into the usually transient intermediate state of the substrate-bound ACP-KS interaction.

5.1 Chromatography-free protein purification

A basic requirement for the biochemical and structural investigation of proteins or protein complexes is the presence of a pure and intact sample. Therefore, various methods were developed over the last decades. In the beginning people used protein-specific solubilities for selective precipitation by introducing changes into the solvent composition. By centrifugation, the precipitated protein was separated from the solvent and thereby unspecific proteins with deviating solubilities could be removed. The subsequent introduction of chromatographic methods allowed a separation of proteins and protein complexes due to protein-specific physical or biochemical differences. According to their charge, molecular size, or shape the use and combination of different chromatographic stationary phases allowed to establish tailor-made purification protocols for manifold different proteins. The development of molecular biological methods further allowed the manipulation of desired proteins with additional sequences having the property to undergo specific interactions with the stationary phase of chromatographic columns. The use of such chromatographic methods is still the most common method to purify protein and protein complexes from a cellular lysate (Hallberg, 2008; Scopes, 2001). Although, chromatography has many obvious advantages for the protein purification, there are also significant disadvantages. Like the induced overexpression of proteins in bacterial or eukaryotic cells, also the addition of affinity tags to the protein sequence can lead to assembly problems resulting in misfolding or aggregation of the desired protein (Ledent et al., 1997; Majorek et al., 2014). For eukaryotic proteins that are recombinantly expressed in procaryotic systems, the absence of essential chaperones that usually support their correct assembly can lead to aggregation or misfolding (Saibil, 2013). Moreover, procaryotic expression systems are not able to induce protein-specific post-translational modifications to eukaryotic proteins. For many proteins, such modifications are crucial for their functionality and regulation (Shental-Bechor and Levy, 2009; Tripodi et al., 2015). A characterization of proteins with missing post-translational modifications could potentially lead to unspecific activities and artificial effects.

To avoid such potential problems for the yeast FAS protein complex, we decided to purify the endogenous protein from wild-type yeast cells. As formerly described for other protein complexes, the use of chromatographic purification step can introduce damages like the dissociation of complexes or loss of single subunits (Tsumoto et al., 2007; Vassylyeva et al., 2017). We therefore decided to adapt a chromatography-free purification method which was formerly described for the human 20S and 26S proteasome complexes to yeast FAS (Haselbach et al., 2017; Schrader et al., 2016).

5.2 Chromatography-free purification reveals a novel γ-subunit

Since the beginning of structural research on the yeast FAS it was firmly assumed that the FAS is a hetero-dodecameric complex of six α-subunits and six β-subunits (Lynen et al., 1980). This assumption was further confirmed by the X-ray crystallographic structure which was simultaneously solved in 2007 by two groups (Leibundgut et al., 2007; Lomakin et al., 2007). Surprisingly, the chromatography-free purification of endogenous FAS from yeast cell lysate resulted in a co-sedimentation of an unknown protein with a molecular weight of 20 kDa. By use of tandem protein mass spectrometric analysis (*Figure 4.3*) we were able to show that the co-sedimenting protein band belongs to the product of the YDL110C locus. Former studies designated this protein as ribosome-binding translation-machinery-associated protein 17 (Tma17p) or ATPase dedicated chaperone 17 (Adc17) with a role in proteasome assembly. (Fleischer et al., 2006; Hanssum et al., 2014; Rousseau and Bertolotti, 2016). With help of a ΔYDL110C knockout yeast strain, recombinant Tma17p/Adc17, mass spectrometric and SDS-PAGE analyses we could show that Tma17p/Adc17 indeed specifically binds and co-sediments with FAS (*Figure 4.4 and Figure 4.7*). Since we also did not find any ribosomal or proteasomal proteins in the final FAS fractions after three consecutive density gradients *(*Figure 4.2 *and Figure 4.5 c)*, we concluded that Tma17p/Adc17 is a third, previously undiscovered subunit of the $\alpha_6\beta$ FAS complex. According to the previous naming of the FAS subunits, we decided to rename Tma17p/Adc17 as γ-subunit.

5.3 How did the γ-subunit escape its discovery?

After the first description of the yeast FAS by Lynen and co-workers it finally took more than fifty years until a third subunit of this complex was discovered (Lynen, 1962). The question of how and why the γ-subunit escaped its discovery for so many decades and different groups is fundamental. During the history of FAS research, many different purification protocols were reported. The first protocols were based on purification of the endogenous FAS protein from yeast lysate using ammonium sulfate precipitation in combination with density gradient centrifugation (Karam and Arslanian, 1984; Lynen, 1962). Later on, yeast strains were genetically modified by introducing affinity tags to the α- or β-subunit, which allowed affinity based chromatographic purification of the FAS complex (Fichtlscherer et al., 2000b; Johansson et al., 2008). Furthermore, the development of recombinant bacterial expression systems allowed the recombinant heterologous co-expression of both FAS subunits, resulting in fully assembled enzymatic active FAS (Fischer et al., 2020). The two groups that solved the first crystal structures of the yeast FAS purified endogenous protein from wild-type *S. cerevisiae* cells by ammonium sulfate precipitation (Leibundgut et al., 2007) or pelleting by ultra-centrifugation (Lomakin et al., 2007). For further purification steps, both groups continued with ion-exchange chromatographic steps that require ionic-strength dependent elution of proteins from the chromatographic column.

By comparing all different protocols which were formerly used for endogenous yeast FAS purification it is striking that each of them contained at least one step of chromatographic purification or ammonium sulfate precipitation. As chromatographic purification methods require a direct interaction of the protein with the stationary phase, the protein separation is either a size-dependent diffusion-based process or relies on the use of an eluent. Both can lead to dilution of the protein during the chromatographic process (Jungbauer, 2005). If proteins or protein complexes drop below their certain dissociation constant they can lose single subunits or even fully dissociate (Schreiber, 2002). Our binding experiments of the γ-subunit with the Δγ-FAS complex revealed a relatively high dissociation constant of 3.1 ± 0.1 µM (*Figure 4.8*) and showed its salt-dependent dissociation from FAS at an ionic strength corresponding to 150 mM KCl (*Figure 4.4 and Figure 4.7*). It could be speculated that the γ-subunit was previously lost due to dilution or high-salt conditions during different steps of purification. Other than the protein precipitation by salting-out with ammonium sulfate (Green and Hughes, 1955), our chromatography-free purification protocol is based on polyethylene glycol (PEG) precipitation. The use of this polymer allows protein precipitation at constant ionic strength which could explain why we did not lose the salt-labile γ-subunit (Atha and Ingham, 1981).

Knowing that the γ-subunit is indeed a FAS binding protein, we went back to literature research and to our surprise found hints for an earlier discovery of the γ-subunit as a FAS binding protein. A closer inspection of mass-spectrometric based proteomic screens from Fleischer and co-workers revealed an association of the γ-subunit to the α- and β-subunit of yeast FAS and not to ribosomes or ribosomal subunits. However, they did not further discuss these findings and thus the γ-subunit was most likely misinterpreted as a ribosomal binding protein (Fleischer et al., 2006). In a second study that investigated the ACP shuttling process within the yeast FAS using Cryo-EM, an additional density was found inside the FAS reaction chamber (*Figure 5.1 A*). Besides the theory that this density could potentially belong to the flexible linker domain of the ACP, they also discussed the option that it could belong to an uncharacterized protein molecule (Gipson et al., 2010b). To test whether the additional densities could have belonged to the γ-subunit, we tried to fit our structure of the γ-subunit (*Figure 5.1 B*) into the density map appearing in their Cryo-EM map of the FAS (*Figure 5.1 C*). Since the structure of the γ-subunit perfectly fitted into their density map one can conclude that they indeed observed the FAS molecule in a γ-subunit bound state. Additional protein mass-spectrometric analyses of their purified FAS protein could have helped them to discover the additional γ-subunit. Literature research showed that they used an affinity-based purification protocol for their FAS. Thus, it could be speculated that the protein concentration as well as the ionic strength of their buffers never exceeded a critical threshold which would have led to the loss of the γ-subunit. We originally discovered the γ-subunit by the closer inspection of SDS-PAGE analysis of density gradients (*Figure 4.1 and Figure 4.2*). It is important to mention that we used pre-casted 4-15% SDS-gels. These gradient gels allow a

reliable separation of protein bands in a size range from 10 kDa to 250 kDa. Thus, use of non-gradient SDS-gels would have led to the loss of the small 17 kDa band of the γ-subunit. Due to missing information about protein concentrations, SDS-gels as well as buffer conditions used in the purification protocol from Gipson *et al.* the reason why they have overlooked the γ-subunit remains speculative.

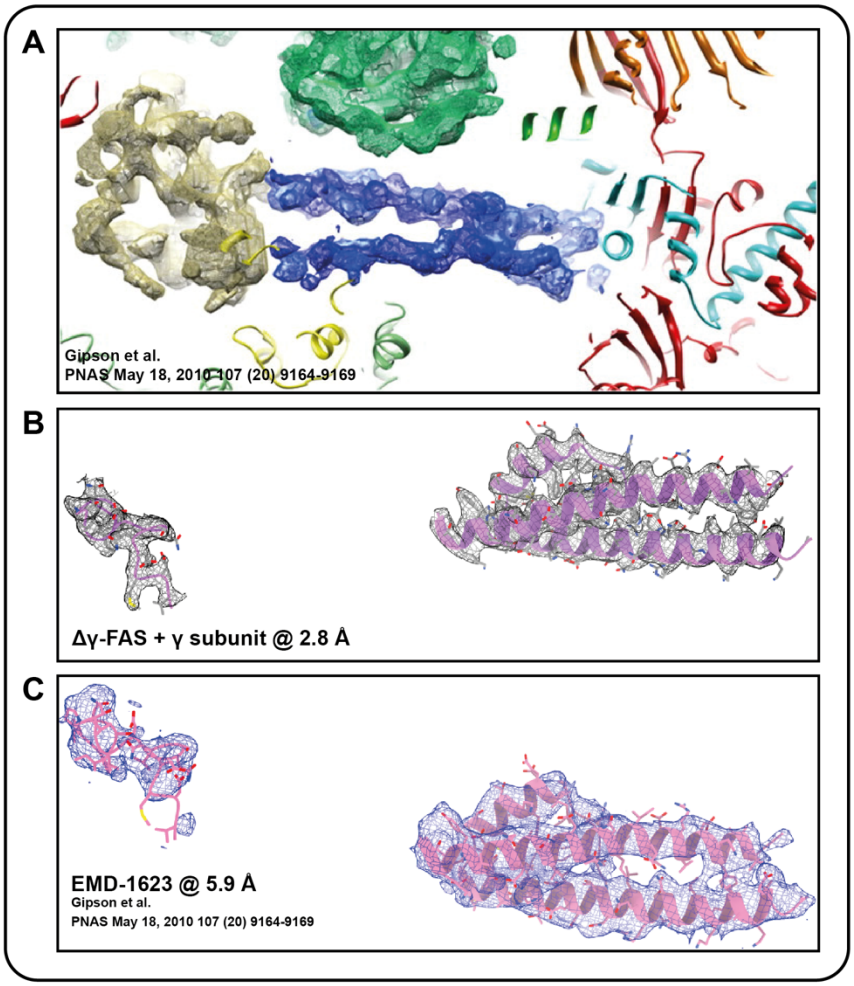

Figure 5.1: Density map of the γ-subunit in former studies: A) *The additional density as it was found in Cryo-EM studies of the FAS complex by Gipson and co-workers* (Gipson et al., 2010b). *According to the location between the ACP domain (yellow), the MPT domain (red) and other α-subunit segments (cyan) they speculated that the additional density (blue) could belong to the ACP linker peptides. B) Structure model of the γ-subunit (purple) into the 2.8 Å Cryo-EM density map. The map quality allowed the modelling of side chains for most of the amino acids.* ***C)*** *The structure model of the γ-subunit (purple) (see B) was fit into the 5.9 Å density map from Gipson and co-workers* (Gipson et al., 2010b). *Despite the lower resolution all parts of the γ-subunit that were built with information of the 2.8 Å density could be fit into the 5.9 Å map.*

5.4 Role of the γ-subunit domain

Structural investigations of Δγ-FAS and the reconstituted Δγ-FAS$_{rec}$ using X-ray crystallography and Cryo-EM showed that the FAS complex can adopt different conformational states. The difference between the two states is a relative rotational movement of the outer FAS halve domes together with the rearrangement of the ACP from the central wheel towards the AT domain. As we were able to show that the ratio between the rotated and non-rotated state is directly coupled

to addition of γ-subunit, we concluded that the γ-subunit binding stabilizes the rotated state. Similar findings were also described by Gipson *et al.* (Gipson et al., 2010b). Although, they concluded that the different conformational states within their dataset could be explained by different intermediate states, our findings indicate that they most likely investigated a mixture of Δγ-FAS and Δγ-FAS_{rec} particles. Since they have used FAS particles which were synchronized by addition of NADPH and malonyl-CoA followed by inhibition with the fungal keto synthase binding inhibitor cerulenin, one can assume that their particles must have had a relatively low heterogeneity. An observation of two different intermediate states as it was discussed in their conclusions is therefore rather unlikely.

With additional information from extensive kinetic characterization of the Δγ-FAS and Δγ-FAS_{rec} we could show that the γ-subunit moreover has a direct impact on the FAS kinetics. Is binding introduces of a kinetic hysteresis effect which directly impacts the NADPH binding behavior according to the NADPH concentration. Since only Δγ-FAS_{rec} revealed this hysteretic transition, it is very likely that this kinetic effect is directly coupled to the conformational transition between the rotated and the non-rotated state. The hysteretic behavior of Δγ-FAS_{rec} allows a direct feedback regulation according to the current intra-cellular NADPH concentration. The binding of γ-subunit increases the $K_{0.5}$ of NADPH by a factor of 2.5. This prevents a NADPH depletion at lower NADPH concentrations (<100 µM). At the same time the V_{max} of NADPH is also modulated and increased by up to 23 % for NADPH concentrations higher than 100 µM (*Figure 4.20*). Together with findings that the γ-subunit additionally suppresses a futile cyclic NADPH depletion reaction at the FMN bound enoyl reductase domain for NADPH concentrations ≤ 100 µM, we concluded that the γ-subunit is a regulator of the FAS activity. Studies of intracellular NADPH concentrations within yeast cells showed that the concentration can vary between different phases of the cell cycle. These concentrations were determined to lie in the range between 50 µM and 150 µM (Gancedo and Gancedo, 1973; Polakis and Bartley, 1966). The description of the γ-subunit as a regulator of the NADPH dependent FAS activity within the lower micromolar concentration regime can be further supported by these numbers. Since acyl-CoAs are the main precursor for the energy storage medium triacylglycerol, a tight regulation of its production is beneficial for the cell (Jain et al., 2016). While the production at low energy levels would be a waste, the up regulation during phases of energy excess can help the cell to store chemical energy for future starvation phases.

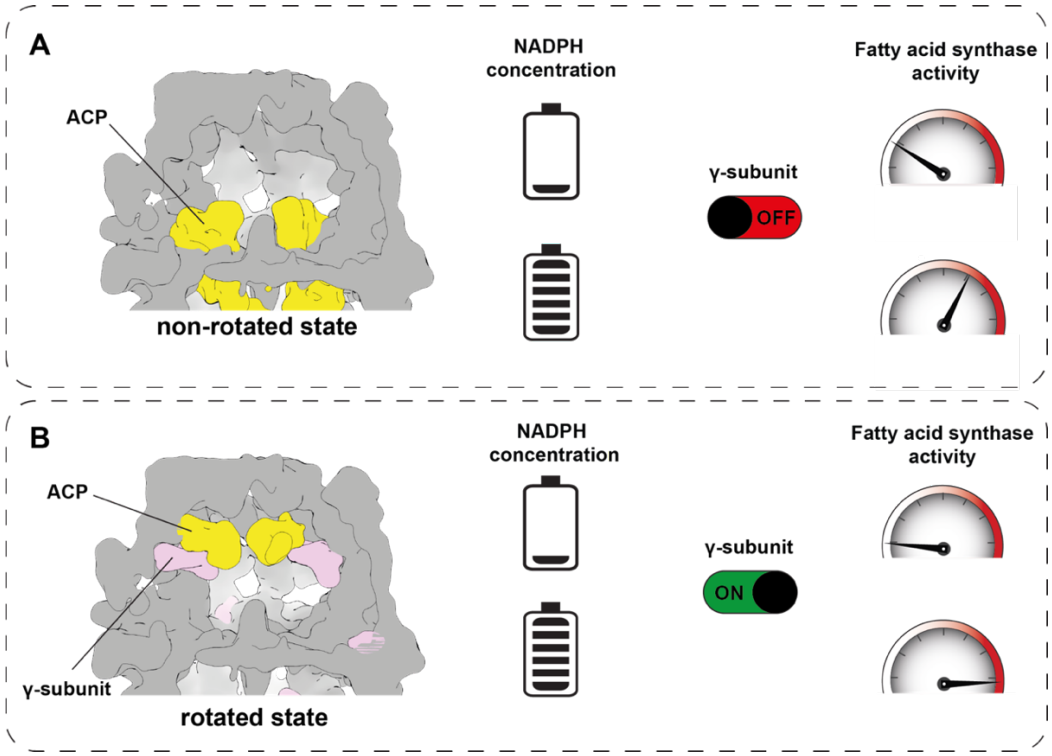

Figure 5.2: γ-subunit as a regulator of the NADPH dependent FAS activity. *The combination of structural investigations with steady-state kinetic measurements led us conclude that the γ-subunit stabilizes a rotated state of the FAS which is directly coupled to a kinetic hysteresis effect.* ***A)*** *In the absence of γ-subunit (γ-OFF) the FAS is predominantly in its non-rotated state. In this state, the ACP domains (yellow) are in proximity to the central wheel. At low cellular NADPH concentrations (empty battery) the FAS molecule has a moderate activity which results in the consumption of NADPH despite its limitation. At high NADPH levels (battery full) the FAS activity increases to a moderate level. This allows an increased production of fatty-acyl chains in case of high energy levels.* ***B)*** *In presence of the γ-subunit (γ-ON) the rotated state of the FAS is stabilized. In this state, the γ-subunit (pink) is bound to the interior of the FAS cavity. The ACP domains (yellow) are located at the outer parts of both halve domes. In case of low cellular NADPH concentrations (empty battery) the FAS activity is reduced to a minimum. This prevents the waste of NADPH resources at low energy levels. At high NADPH levels (battery full) the γ-subunit induces an upregulation of the FAS activity. In this scenario the high levels of NADPH can preferably be used for the synthesis of fatty-acyl chains.*

5.5 γ-subunit as a FAS import sequence

With the help of the two γ-subunit truncations $\gamma^{\Delta 1\text{-}25}$ and $\gamma^{\Delta 117\text{-}150}$ we could show that both, the N-terminal, and C-terminal regions are essential for the binding to Δγ-FAS (*Figure 4.9*). The manipulation of other proteins with these two sequences led to the Δγ-FAS specific binding which was verified by a co-sedimentation into the 40S region of density gradients (*Figure 4.23*). With the use of two fluorescent constructs of different size we could show that the also other proteins can be imported into the FAS and the binding efficiency is also size dependent (*Figure 4.23*). This could be explained by the physical barrier of the FAS dome. The space between the openings (see *Figure 5.3*) as well as the volume of the inner cavity is limited. Thus, it is most likely not possible to import proteins of any size into the FAS.

Since the fluorescent constructs were used as a proof of concept, we wanted to show that the γ-subunit import sequences can also be used to import proteins with enzymatic activity into the FAS. The presence of additional acyl-chain specific enzymes inside the FAS reaction chamber could potentially affect the acyl-CoA synthesis and thus open the possibility for modifications of

the acyl-CoA products. Zhu et *al.* successfully introduced such an additional enzmye (TesA) into the FAS cavity by incorporation into the sequence of the flexible ACP linker regions (Zhu et al., 2017). This additional thioesterase activity induced the release of short and medium fatty acyl chains by the FAS prior to their final transfer to CoA by the MPT domain. With the addition of the γ-subunit import sequences to TesA (γ-TesA) we could show that we are also able to mediate its import into the FAS. Other than Zhu and colleagues we managed this without genetic modification of the FAS genes (*Figure 4.23 B*). GC-MS product analyses of the acyl-CoA composition of Δγ-FAS activity assays containing additional TesA and γ-TesA could show that no acyl-CoAs were detectable in any of the reactions (*Figure 4.24*). While this shows that the TesA domain was indeed enzymatic active, we could not conclude whether the modified γ-TesA induced a change within the chain length of free fatty acids. To investigate this, additional GC-MS analyses targeting free fatty acids instead of acyl-CoAs are required. These experiments are already planned but are waiting to be carried out.

The discovery of the γ-subunit import sequences is also of potential biotechnological interest. Free fatty acids from renewable feedstocks like yeast cultures can be used as precursor molecules for the production of biodiesel, biological pyrolysis oil and other fine chemicals (Lu et al., 2008; Nikolau et al., 2008; Shin et al., 2016). Besides a chain-length control of the produced fatty acids as it was shown for TesA (Zhu et al., 2017) also other fatty-acyl chain specific enzymes could be modified with the γ-subunit import domains. The addition of domains harboring e.g., desaturase or cyclase activity could expand the possibilities to produce other biotechnological interesting precursor molecules with the yeast FAS complex (Bellou et al., 2016; Ji and Huang, 2019).

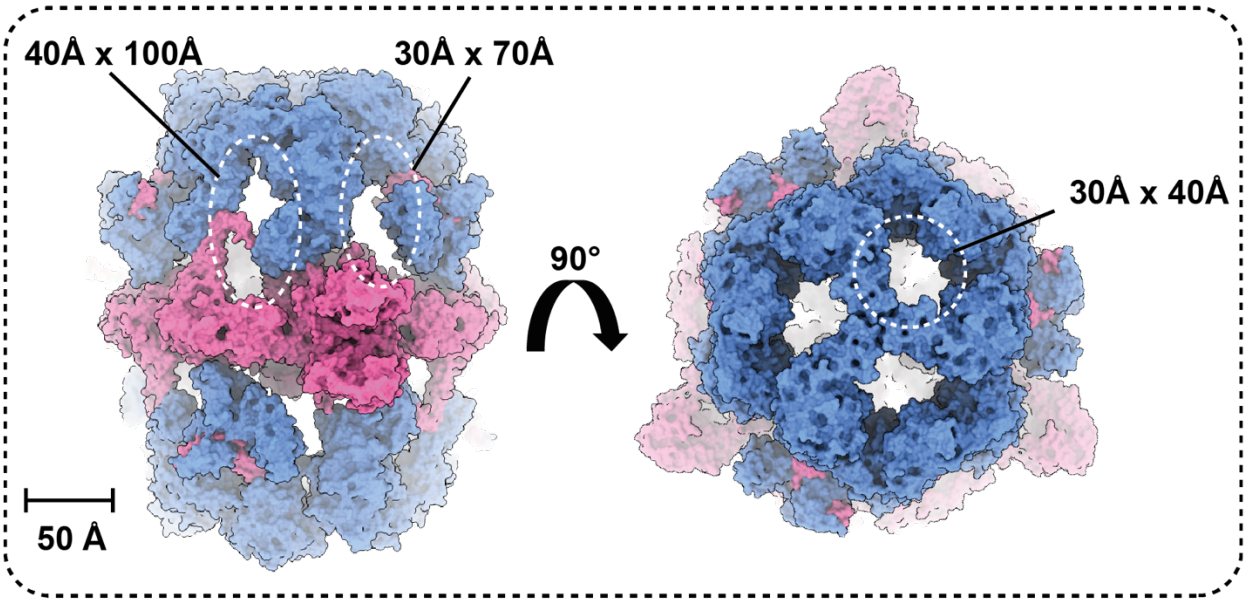

Figure 5.3: The FAS molecule has openings of different size. (left) *Side-view of the yeast FAS molecule. Between the central (purple) and the two halve domes (blue) several openings of different size allow an exchange between the inner cavity of the FAS and the solvent.* ***(right)*** *The top-view of the FAS molecule reveals three openings per halve dome with dimensions of 30Å x 40Å.*

5.6 Product analysis of Δγ-FAS and Δγ-FAS$_{rec}$ reactions

To test whether the deletion of the γ-subunit has an impact on the chain length of the final acyl-CoA products we compared the acyl-CoA composition of end point reactions from *in vitro* activity assays containing Δγ-FAS or Δγ-FAS$_{rec}$. The evaluation of GC-MS measurements showed that in both reactions, acyl-CoAs of chain length between C_4 and C_{14} were released. While CoAs of chain length between C_6 – C_{14} were produced in comparable amounts, we found significantly more C_4-CoA in the Δγ-FAS$_{rec}$ reaction. Furthermore, we only detected palmitoyl-CoA (C_{16}-CoA) in the Δγ-FAS$_{rec}$ reaction (*Figure 4.24*). As the only difference between both reaction assays ways the presence/absence of γ-subunit it is possible that the change of the product composition is caused by binding of the γ-subunit to the FAS complex.

Additional analyses of the substrate consumption of the end point reactions (*Figure 4.25*) showed that within both reactions, malonyl-CoA was the limiting factor. In literature it was already described that the ratio between malonyl-CoA and acetyl-CoA the reaction assay has a direct impact on the chain length of the final acyl-CoAs that are released to the solvent. A decreasing malonyl-CoA concentration with no change in the acetyl-CoA concentration results in a shift towards acyl-CoAs of shorter chain length (Lynen et al., 1964; Sumper et al., 1969). This could explain why mainly medium and short chain acyl-CoAs were produced. By consumption of malonyl-CoA during the enzymatic reaction, the ration between malonyl-CoA and acetyl-CoA shifts towards acetyl-CoA. Since acetyl-CoA is only used for the priming reaction of the iterative chain elongation reaction, one molecule of malonyl-CoA is consumed per elongation cycle (*Figure 0.5*). To prevent the analysis of a mixture that represents the acyl-CoA product composition from different time points with alternating malonyl-CoA/acetyl-CoA ratios, additional time dependent product analyses could be made.

Since we performed the *in vitro* activity assays without additional crowding agents, findings from earlier product analyses of the mycobacterial and FAS could also explain the presence of C_{16}-CoA in the Δγ-FAS$_{rec}$ reaction. Within these studies it was shown that the addition of a crowding agent like BSA induces a shift towards longer fatty acyl CoAs compared to non-crowding conditions (Bloch and Vance, 1977; Schjerling et al., 1996).However, the molecular basis for this crowding effect is not fully understood. One explanation could be a reduced product inhibition in presence of BSA. BSA was shown to bind acyl-CoAs and thus could prevent an accumulation of inhibitory products within the assay (Spector et al., 1969). Besides the ratio between malonyl-CoA and acetyl-CoA it was also shown that the reaction velocity has a direct impact on the final product chain length (Sumper et al., 1969).

It is likely that the γ-subunit in the Δγ-FAS$_{rec}$ also acts as a crowding agent and thus induces the production C_{16}-CoA. To exclude the crowding effect as the reason for a shift towards longer acyl-CoAs, further control reactions with additional crowding agents are required. Since these

analyses are still in progress, we are currently unable to conclusively assess whether the γ-subunit binding induces a change within the product composition of the FAS complex.

5.7 Creation of an apo-ACP FAS complex

From former studies of the yeast FAS complex, it was already known that the ACP domain of the α-subunit is modified by a post-translational addition of PPant from CoA to a specific Ser^{180} residue (Stoops and Wakil, 1978; Stoops et al., 1978). This post-translational modification is essential for the FAS driven *de novo* fatty acids synthesis reaction in yeast cells and catalyzed by the FAS internal PPTase-domain, located at the C-termius of the α-subunit. It was also shown that this essential activation reaction takes place prior to the full assembly of the FAS complex (Chirala et al., 1987; Fichtlscherer et al., 2000; Mohamed et al., 1988). Therefore, it is not possible to purify inactive FAS molecules harboring an ACP in its apo-state. Since the *in vitro* modification of the ACP domain requires FAS molecules with an apo-ACP domain, we successfully created a PPTase deficient yeast strain. To compensate the breakdown of the essential *de novo* fatty acid synthesis the cells were rescued by addition of external fatty acids into the growth medium. By replacing a first detergent-based lysate clarification step with the precipitation of nucleic acid and nucleic acid bindings proteins by streptomycin, we could dispense one density gradient centrifugation step. This allowed us to shorten the chromatography-free purification of ΔPPTase-FAS by a whole working day, compared to the initially established protocol of Δγ-FAS (*Figure 4.1 and Figure 4.28*). Given the fact that the ΔPPTase-FAS molecules also sedimented in the 40S region of the density gradients, we concluded that the PPTase deletion did not affect the assembly of the complex. The enzymatic inactivity and protein mass spectrometric analyses of freshly purified ΔPPTase-FAS confirmed that the ACP domain of the ΔPPTase-FAS molecule was in its inactivated apo-state (*Figure 4.30 and Table 3.1*). Therefore, we concluded that we could use the ΔPPTase-FAS for further experiments targeting the *in vitro* modification of the apo-ACP.

Although, other molecular biological methods for the modification and expression of recombinant FAS molecules were developed in the past we decided to create a genetically modified yeast strain. This ensured that all potential chaperones for a proper complex assembly are present within the cell. Furthermore, the recombinant expression in bacterial cells would result in FAS protein lacking potential post-translational modifications. The purification of the endogenous complex enabled us to rule out such problems.

5.8 In vitro activation of the ΔPPTase-FAS

For the *in vitro* activation of non-phosphopantetheinylated ΔPPTase-FAS we tested four individual PPTase domains deriving from different species. The separate domain of the yeast FAS complex (yPPTase), Sfp from *B. subtilis*, AcpS from *E. coli* and the single PPTase domain

of the *H. sapiens* FAS complex (H.s. PPTase). First trials using all mentioned PPTases did not lead to any activation of the ΔPPTase-FAS complex. Since it was previously shown that most PPTase domains are relatively unspecific and can activate ACP domains from different organisms (Beld et al., 2014) we speculated that the halve domes of the FAS act as a physical barrier that shields the apo-ACP in the cavity from any interaction with external proteins (*Figure 5.3*). Findings from Johansson et *al.* supported this theory as they showed that the single yPPTase domain only shows enzymatic activity in its dimeric (26 kDa) state and crystalizes in a trimeric (39 kDa) form (Johansson et al., 2009a). Therefore, we surmised that the yPPTase domain is either too large or due to its surface charges not capable to diffuse into the ΔPPTase-FAS cavity. The *E. coli* AcpS has the same size (13 kDa) as the single yPPTase domain and was also shown to be active in its trimeric (39 kDa) state. Other than that, the *B. subtilis* Sfp is active in its monomeric state (26 kDa) and is able to activate ACP domains from various organisms and complexes (Quadri et al., 1998). Its lack of activity towards the yeast apo-ACP could potentially be explained by the special architecture of the ACP domain from yeast FAS (*Figure 0.6*).

However, in further activation experiments we decided to titrate different PPTase concentrations. While this was not successful for Sfp, AcpS and H.s. PPTase, we detected an activation of the ΔPPTase-FAS in assays containing a 180x molar excess of yPPTase. Since we lack experimental data of how the over-titration led to the activation reaction of the ACP domain the exact mechanism remains elusive. From structural data we concluded that the inner volume of the ΔPPTase-FAS with dimensions of 260Å x 230Å x 230Å would allow the formation of enzymatic active yPPTase dimers and trimers.

The comparison of the enzymatic activity of *in vitro* activated ΔPPTase-FAS with Δγ-FAS showed an activation efficiency of 85% (*Figure 4.30*). This could be explained by an incomplete modification of all apo-ACP domains into their enzymatically active holo-ACP state. Another possible explanation for the reduced enzymatic activity could be the activation protocol. Since the activation reaction was incubated and dialyzed over night at 18 °C it is possible that the ΔPPTase-FAS activity declined due to aging processes like oxidation. To exclude such problems, the protocol for the activation reaction will be further optimized in future experiments.

5.9 Enzymatic synthesis of CoA and crypto-CoAs

To achieve an enzymatic *in vitro* activation/modification of ΔPPTase-FAS with help of the yPPTase domain, CoA/crypto-CoA is required as substrate. While the pantetheine residue of the CoA molecule can vary in its chemical structure, the adenosine-3,5-bisphosphate backbone was shown to be mainly responsible for the substrate recognition in PPTase from *S. cerevisiae*, *M. tuberculosis*, *H. sapiens* and *B. subtilis* (Bunkoczi et al., 2007; Reuter et al., 1999; Vickery et al., 2014). Based on this finding, Burkart and co-workers designed and synthesized various pantetheineamide probes with mechanism based reactive groups targeting different type II FAS

domains (Mindrebo et al., 2020a). Using a chemo-enzymatic one-pot reaction, the pantetheineamide precursors were enzymatically processed by the bacterial enzymes CoaA, CoaD and CoaE. Within subsequent reactions, these enzymes transfer phosphate and adenosine monophosphate groups from ATP to the pantetheineamide crosslinker, to finally release crypto-CoA analogs harboring reactive groups (*Figure 0.8*). Based on this protocol we successfully adapted a one-pot reaction that allowed us the enzymatic synthesis of CoA from pantetheine and crypto-CoA from pantetheinamide analogs (*Figure 0.8*, *Figure 4.29*, Worthington and Burkart, 2006). In all tested chemo-enzymatic crypto-CoA synthesis reactions an insoluble precipitant accumulated. This could be explained by the emergence of magnesium pyrophosphate as a side product of the CoaD reaction (*Figure 0.8*). To test the reactivity of crypto-CoAs, we further used them as substrates for subsequent PPTase reactions. In these test-reactions, *E. coli* apo-AcpP was converted to crypto-AcpP catalyzed by *B. subtilis* Sfp. To test the crosslinking-reactivity of the different crypto-AcpP domains we added their corresponding target enzme.

While SDS-PAGE analysis showed successful crosslinking reactions for FabA and FabB, resulting in AcpP-FabA and AcpP-FabB constructs, we could not detect any protein band indicating a covalent linkage between AcpP and FabI (*Figure 4.31*). According to the SDS-PAGE the FabA and FabB crosslinking reaction to crypto-ACP was not 100% efficient. There are different possible reasons that could explain the reduced crosslinking reactivity. First, the one-pot reaction could also contain crypto-CoA precursor molecules or the structurally related adenosine diphosphate (ADP) which accumulates as by-product during the CoaA and CoaE reactions (*Figure 0.8*). Their structural similarity to crypto-CoA could explain a reduced efficiency of the Sfp reaction due to substrate inhibition. Further, the magnesium pyrophosphate which accumulates during the chemo-enzymatic crypto-CoA synthesis could somehow impair the Sfp reaction. Another problem was that we were not able to quantify the final crypto-CoA concentration within the chemo-enzymatic synthesis reactions. Since each reaction was a mixture of different optically active compounds like ATP, ADP, the reactive pantetheinamide substrates and crypto-CoA it was not possible to determine the concentration by spectrophotometric measurements. For the optimization of enzymatic assays, the knowledge about the concentration all reactants and substrates would be an advantage. To solve such basic problems crypto-CoAs and other chemo-enzymatic synthesized substrates should be purified by high-performance liquid chromatography (HPLC) in the future. This would also allow the removal of potentially inhibiting side-products as discussed above.

5.10 Modification of ΔPPTase-FAS

With the knowledge that we can modify the apo-ACP of ΔPPTase-FAS with an activation assay *in vitro* we decided to test different chemo-enzymatic synthesized crypto-CoAs as substrates. Due to structural similarities and the conservation of catalytic active site residues between the single bacterial enzymes and the yeast FAS domains we assumed that the mechanism-based

crosslinking reaction should also work for ΔPPTase-FAS. While the two keto synthase reactive probes were designed to form a covalent linkage with the active site cysteine of the KS domain, the dehydratase probe aims for a histidine residue (*Figure 4.32 A*) (Lomakin et al., 2007; Mindrebo et al., 2020b; Nguyen et al., 2014b). To test whether the crosslinking reactions with the three different reactive crypto-CoAs worked, we analyzed different one-pot reactions via SDS-PAGE. The reactions with the keto synthase reactive crypto-CoAs showed a band shift of the ΔPPTase-FAS bands on the gel. However, for the reaction with dehydratase specific crypto-CoA no change of the running behavior was visible (*Figure 4.32 B*). Based on these observations we concluded that the two keto synthase reactive probes most likely induced an intramolecular covalent linkage between the modified ACP domain and the KS active site. For the dehydratase probe we could not make any conclusions since it is also conceivable that a successful crosslink reaction is not visible as a band-shift on the SDS-PAGE. Aside from this it is also possible that the dehydratase crosslinking reaction did not work due to impurities within the chemo-enzymatic synthesized crypto-CoA substrate as discussed above. To further investigate whether all crosslinking reactions were in fact successful and resulted in a covalent linkage between the ACP domain and the keto synthase or dehydratase active site residues, the final reactions should further be analyzed via protein mass spectrometry for future experiments. Despite the missing information of additional mass spectrometric analyses, we assumed that the band shift upon addition of the keto synthase probes was indeed induced by an intramolecular crosslinking reaction. According to previous structural findings we assumed that the covalent linkage was formed between the ACP domain of one α-subunit and the keto synthase domain of a distinct neighboring α-subunit (Gipson et al., 2010a; Johansson et al., 2008). This could also explain the shift of the lower ΔPPTase-FAS band which belongs most likely to the truncated α-subunit.

Because the natural occurring substrate of the holo-ACP domain contains a PPant arm and an acyl-chain moiety of alternating length we decided to use the [BR-KS] crosslinker as substrate for further structural investigations of the modified ΔPPTase-FAS. While both keto synthase probes bind to the active site cysteine, only the additional C_6-acyl chain of the [BR-KS] crosslinker corresponds to an exact intermediate occurring during the catalytic condensation reaction at the KS domain. By use of [BR-KS] as substrate we hoped to get an insight into the architecture of the keto synthase domain with the covalently bound ACP and the C_6-acyl chain intermediate. Information of the acyl-chain location within this usually transient interaction is required to understand the chain-length control mechanism which is thought to be controlled by its translocation to an acyl-tunnel within the keto synthase domain (Gipson et al., 2010a; Johansson et al., 2008; Quadri et al., 1998; Sumper et al., 1969). Furthermore, Burkart and co-workers already successfully used the [Br-KS] probe with varying acyl-chain length for the investigation of the interaction between the *E. coli* keto synthase FabB (Mindrebo et al., 2020b).

5.11 Solving the structure of modified ΔPPTase-FAS

We managed to grow protein crystals of the ΔPPTase-FAS which was previously modified with the [Br-KS] crypto-CoA substrate. For the best crystal, we obtained a crystallographic dataset with detectable reflections until 2.9 Å. As already expected, we found the ACP domain in proximity to the KS domain. The overall structure of the ΔPPTase-FAS revealed the missing PPTase which is usually located outside of the hexameric central wheel (*Figure 4.33 A*). Since the overall structures of both, the Δγ-FAS and the ΔPPTase-FAS were otherwise identical we concluded that the deletion of the PPTase domain did not affect the assembly of the ΔPPTase-FAS complex. Within the enoyl reductase domain we further found a density that allowed us the modelling of the co-substrate FMN (data not shown). This supports the findings that the ΔPPTase-FAS structure assembly was not influenced. In closer detail, the electron density map allowed us also to build the PPant modification of the Ser^{180} residue from the ACP as well as a covalent linkage to the sulfur group of the Cys^{1305} residue within the keto synthase active site. As already expected, the covalent linkage was formed between two distinct α-subunits (*Figure 4.33 C and Figure 4.34*). Although only the C_{1-3} carbon atoms of the [Br-KS] acyl-chain could be modelled we were confident that the ACP domain was arrested at the keto synthase. This led us conclude that we managed to image the first snapshot showing the transient interaction of the ACP with the keto synthase domain in a substrate bound state. Since we used a crosslinker with a defined acyl-chain length one can assume that the acyl-chain modification of all ACP domains is identical. As already mentioned in the section above, Burkart and co-workers recently managed to solve the crystal structure of the *E. coli* AcpP-FabB complex using a similar [Br-KS] probe with different acyl-chain length. To test whether one could compare their findings with the structure of our ΔPPTase-FAS intermediate state, we analyzed the sequence and structure identities of crosslinked FabB and the extracted ΔPPTase-FAS keto synthase domain. The sequence comparison of the yeast keto synthase domain with the *E. coli* keto synthase FabB revealed 82 conserved identical residues, which corresponds to 20% sequence identity (*Figure 8.1*). The superposition of both structures revealed structural homologies over the whole domain (*Figure 5.4*). The only striking structural differences were found in the additional helix-turn helix motifs which are thought to play a role in the assembly of the yeast FAS complex (Lomakin et al., 2007). From these findings we concluded that we could indeed compare the architecture of the substrate bound AcpP-FabB complex with our crosslinked ΔPPTase-FAS intermediate.

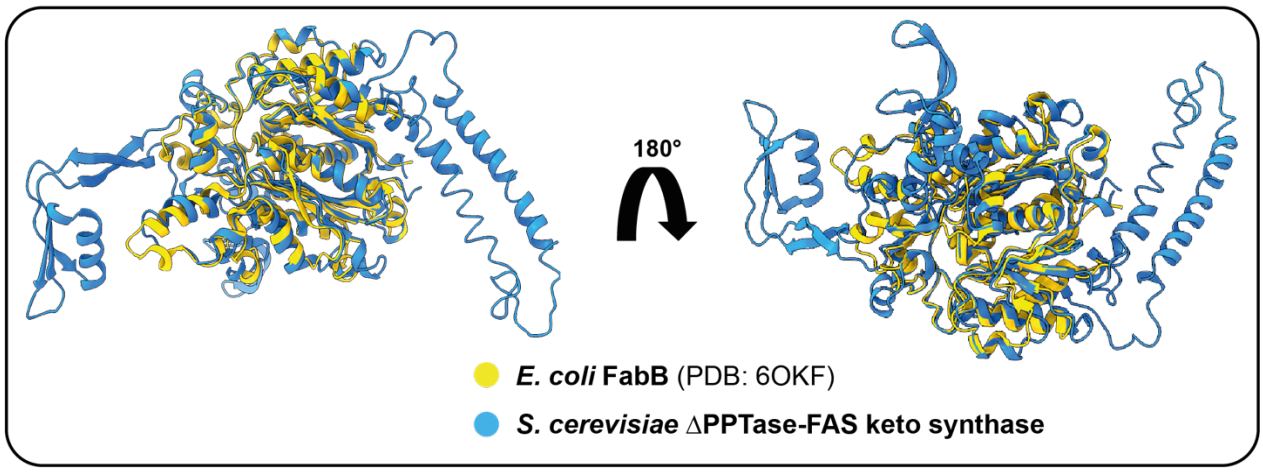

Figure 5.4: Overlay of S. cerevisiae KS domain with E. coli FabB. *The overlay of the keto synthase domain from the yeast FAS (blue) with the bacterial FabB (yellow; PDB: 6OKF) reveals a highly conserved structural homology.*

A direct comparison of the substrate bound keto synthase active sites revealed several structural similarities between the modified ΔPPTase-FAS and AcpP-FabB (*Figure 5.5*). Besides the covalent linkage between the ACP-bound substrate and the active site cysteine residues (Cys^{1305} and Cys^{163}) both structures also show an interaction of in total three distinct domains. Like ACPα_1, KSα_2 and KSα_3 from the ΔPPTase-FAS structure (*Figure 5.5 A*) the AcpP-FabB structure showed an interaction between AcpP and two FabB molecules (*Figure 5.5 B*). A closer inspection of the side chain architecture also showed several homologies. In both structures the pantetheine arm is stabilized by two threonine residues (Thr^{1546} and Thr^{1544}; *Figure 5.5 A*) and (Thr^{302} and Thr^{300}; *Figure 5.5 B*). In proximity to the active site cysteine residues with the covalent bound substrates we found the active site histidine residues (His^{1542} and His^{1583}) in the same orientation as how they were modelled for the AcpP-FabB structure (His^{298} and His^{333}). The acyl-tunnel of the ΔPPTase-FAS which is built up by four phenylalanine residues (Phe^{1376}, Phe^{1646}, Phe^{1343} and Phe^{1279}) and the residues of Ala^{1304}, Glu^{1378} and Lys^{1585} was empty since we were not able to model the carbon atoms $C_{4\text{-}6}$ of the substrate acyl-chain. A direct comparison of the C_{16} acyl-chain localization within the FabB acyl tunnel shows striking differences. While the overall composition of the acyl tunnel with hydrophobic residues (Phe^{229}, Phe^{201}, Phe^{392} and Ala^{162}) is similar, there are two methionine residues (Met^{197} and Met^{138}) which are both flipped out of the hydrophobic acyl-tunnel. In contrast, the Met^{1251} from ΔPPTase-FAS is flipped into the acyl-tunnel facing towards the Phe^{1279}. A second striking difference is the loop of the Cα-backbone between Cys^{1305} and Ala^{1304} within the ΔPPTase-FAS structure. The loop reaches into the entrance of the acyl-tunnel and seems to close or at least narrows its entrance. Within the AcpP-FabB structure this is not the case and Ala^{162} seems to contribute to the stabilization of the acyl-chain inside the acyl-tunnel.

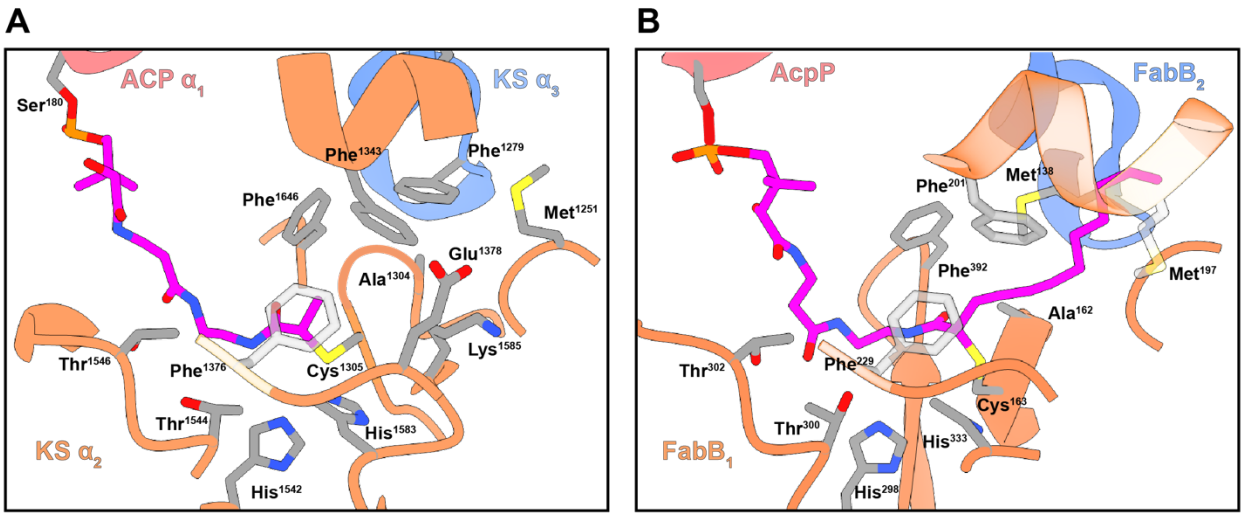

Figure 5.5: Substrate bound KS domain shows a comparable architecture in yeast and E. coli. A) *Detailed view of the yeast ΔPPTase-FAS keto synthase active site. The ACP domain (red) is linked to the KS active site Cys^{1305} via a covalent bond between the modified phosphopantetheine arm (pink). The two residues Thr^{1546} and Thr^{1544} stabilize the pantetheine-part of the substrate. The two His^{1542} and His^{1583} are parts of the catalytic triad together with the covalent bound Cys^{1305}. Due to missing information, we were not able to model the C_{4-6} carbon atom of the acyl-chain. Within the acyl-tunnel which is built of hydrophobic residues and the terminal gate keeper Met^{1251} we did not find any electron density. Therefore, we concluded that the acyl-chain was most likely not inside the tunnel. The loop-region between Cys^{1305} and Ala^{1304} could potentially work as an additional regulator for the open/closed state of the acyl-tunnel.* ***B)*** *Detailed structure of the E. coli keto synthase FabB active site with crosslinked C_{16}-AcpP (PDB: 6OKF). The electron density allowed a modelling of the C_{1-12} carbon atoms of the substrate acyl-chain. Besides the covalent linkage between the FabB active site Cys_{163} and the C_2 atom of the substrate, the acyl-chain was found to be located inside the hydrophobic acyl-tunnel. The gate keeper Met^{187} and Met^{138} are flipped out of the tunnel which allows a binding of the acyl-chain. Like the structure of the yeast keto synthase, the pantetheine part of the substrate ist also stabilized by two threonine residues (Thr^{302} and Thr^{300}) and the histidine residues (His^{298} and His^{333}) of the catalytic triad are facing towards the active site Cys^{163}.*

With the findings of an empty acyl-tunnel that additionally seems to be closed by a loop region one could speculate where the C_{4-6} atoms of the acyl-chain are located. One could assume that a localization inside the tunnel would stabilize the acyl chain, which most likely would improve the electron density. Since this is not the case, we speculate that the C_6 acyl-chain of the substrate did not enter the acyl tunnel at all.

Former studies also showed that Met^{1251} has a gate keeper role, controlling the final chain length of the FAS. Also, the point mutations G1250S and F1279K of acyl-tunnel residues had an impact on the chain length of the released acyl-CoAs. In both cases the released chains were shorter than in the wild-type strain. Based on our structural findings one could also test whether a point-mutations of the Ala^{1304} have an impact on the chain length control. Point-mutations of I1306A showed to have a strong impact on the product chain length. FAS molecules with this mutation mainly produced C_6- and C_8-CoA (Gajewski et al., 2017). Since the exchange of the hydrophobic Ile^{1306} to arginine revealed a huge impact, we assume that the loop region between Cys^{1305} and Ala^{1304} is most likely also part of the internal chain length control. However, these interpretations are rather speculative and would require additional experimental information from product analyses or protein structures.

To gain further information of the acyl-chain location at different chain length it is inevitable to expand the above-described protocol for alternative [BR-KS] crosslinkers with varying acyl-chain

length. Further, additional efforts should also be spent on the optimization of the protein crystals. Since we were able to collect a dataset with diffractions until 2.9 Å, a higher resolution will most likely give us more information about the location and architecture of the missing acyl-chain atoms.

6 Conclusion

In this thesis, we describe the discovery of a third subunit of the yeast FAS and the successful modification of the FAS complex with a mechanism based reactive substrate that allows the first insight into the transient interaction of the substrate-bound ACP with an enzymatic domain.

In the first part, the chromatography-free purification of endogenous FAS from wild-type yeast cells revealed a co-sedimentation of an additional protein together with the FAS complex. In this highly cooperative project with my colleague Kashish Singh we were able to show that this additional protein belongs to a third subunit (γ-subunit) which was overlooked for more than sixty years of FAS research. By a combination of protein mass spectrometric analyses, protein binding assays, structural investigations by X-ray crystallography and Cryo-EM and intensive steady-state enzyme kinetic characterizations we could show that the γ-subunit binds to the FAS in a salt-labile manner with a binding affinity in the micromolar range. Its binding to the FAS complex revealed a translocation to the inner cavity of the FAS. While without γ-subunit the FAS was predominantly found in a non-rotated conformation, the γ-subunit binding showed a stabilization of a rotational conformational change (rotated state) of the whole FAS complex. The transition between both states was coupled to the translocation of the ACP domain from the keto synthase domain at the central wheel (non-rotated) to the outer parts of both halve domes (rotated state). The enzyme kinetic steady-state measurements showed an impact of the γ-subunit to the turnover and binding kinetics of all three substrates acetyl-CoA, malonyl-CoA, and NADPH. While the impact on acetyl-CoA and malonyl-CoA was rather low, we could show that the NADPH processivity was modified by a kinetic hysteresis and the suppression of a futile cycle reaction at the FMN-bound enoyl reductase domain. Together with the structural findings we concluded that the transition from the rotated to the non-rotated state conditions the hysteretic effect of the NADPH turnover. We therefore suggested the γ-subunit as a regulator domain of the FAS complex. It allows a finer regulation of the FAS activity in response to the NADPH level within the cell. While the NADPH turnover is down-regulated at lower NADPH concentrations, the γ-subunit binding allows a higher fatty acyl production at high energy levels. In further experiments we could show that the N- and C-terminal sequences of the γ-subunit can be used to incorporate proteins into the FAS cavity which are usually not able to translocate into the FAS.

In the second part we successfully adapted a chemo-enzymatic protocol which was formerly developed for the modification of *E. coli* type II FAS proteins. With help of this protocol, we were able to modify the apo-ACP domain of inactive ΔPPTase-FAS with alternative substrates wearing a mechanism based reactive warhead *in vitro*. Using X-ray crystallography, we obtained a crystallographic data set with reflections until 2.9 Å of a ΔPPTase-FAS complex which was formerly modified with a keto synthase reactive substrate. The electron density map allowed us the modelling of the ΔPPTase-FAS in a formerly unseen intermediate state. The ACP domain was found to be covalently linked to the keto synthase active site. Further, we were able to model

the C_{1-3} carbon atoms of the substrate acyl-chain. This, to our knowledge is the first time that it was possible to specifically modify and image the yeast FAS complex in a usually transient intermediate state of the ACP-keto synthase interaction. Besides the arresting of this transient interaction, we were able to introduce an acyl-chain of defined length to the ACP domain. Although, we were not able to model the whole C_6-acyl chain of the substrate, the structure allowed us to get an insight into the overall conformation of the keto synthase domain with a medium-chain length substrate intermediate.

Based on these findings, we conclude that the yeast FAS complex is a suitable object for the development of novel biochemical tools that allow the modification dynamic macromolecular processes. The successful modification of the ΔPPTase-FAS can be seen as a proof of concept which confirms that biochemical assays which were developed for single bacterial enzymes can also be adapted to eukaryotic macromolecular complexes.

7 Outlook

The discoveries described in this thesis can make a valuable contribution to the research field of the yeast FAS and in parts have the potential to also influence structural investigations of other macromolecular complexes. The discovery of the γ-subunit as well as the identification of its role as a regulator domain of the FAS can be used for a better understanding of how the synthesis of fatty acyl chains is regulated in yeast. This is also of high biotechnological interest since the production of fatty acids by microorganism is a well developing field which has the potential to cover a significant need of lipid-derived precursor molecules for the chemical industry and the production of biofuels (Park et al., 2018; Rigouin et al., 2018; Sheng and Feng, 2015). While this mostly counts for oleaginous yeast strains like *Yarrowia lipolytica*, the understanding of the regulation of the yeast FAS system can most likely also be transferred to other type I FAS systems. Furthermore, the discovery that the γ-subunit can also be used as an import shuttle for other proteins into the type I FAS complex opens the door for manifold possibilities to modify the fatty acid production system *in vitro* and *in vivo*. This, for example could potentially allow to engineer yeast organisms for the production of renewable oleochemicals, fatty acids of defined chain length and other derivatives (Biermann et al., 2021).

The development of a chemo-enzymatic assay which allowed us to image the interaction of a transient intermediate state within the FAS complex has the potential to get a better insight of how enzymatic reactions at different enzymatic domains are controlled. With a better understanding of these catalytic processes, it could be possible to engineer the FAS complex for production of specific fatty acids. Further, the proof of concept that it is indeed possible to modify the ACP domain of macromolecular complexes *in vitro* can also be transferred to other complexes that rely on the use of acyl carrier or other carrier proteins. This, for example could potentially help to understand the mechanism of polyketide synthases (PKS) which are known to produce a huge variety of complex chemical compounds (Herbst et al., 2018).

8 Supplementary Information

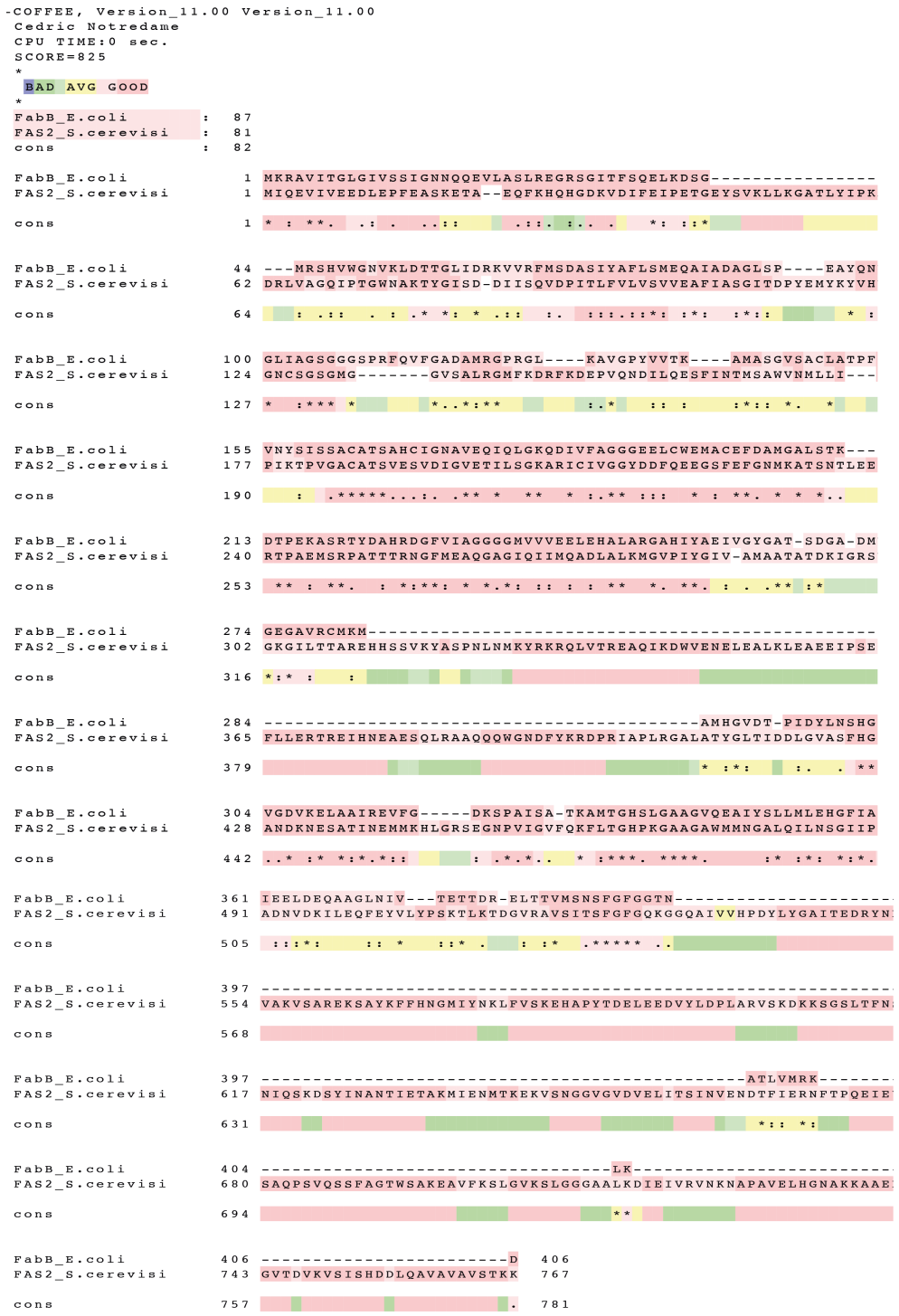

Figure 8.1: Sequence alignment of yeast KS domain and E. coli FabB*Sequence alignment results of the E. coli FabB and the keto synthase domain from the S. cerevisiae α-subunit. The alignment revealed a conservation of 82 amino acid residues between both sequences. Conserved residues are indicated by (*) and were mostly found in the n-terminal region of both proteins.*

Crystallographic data collection and refinement statistics

Name	Δγ-FAS	Δγ-FAS + γ-subunit	ΔPPTase-FAS
Data Collection			
Wavelength	0.976		0.68881
Resolution range (Å)	191.5 - 2.9 (3.0 - 2.9)	192.5 - 4.6 (4.7 - 4.6)	197.6 - 2.89 (2.89)
Space group	$P2_1$		
Unit cell			
a (Å)	217,6	234,9	227.7
b (Å)	347,5	430,3	357.6
c (Å)	265,2	422,6	250.7
β (°)	107,88	97,01	112.2
Total reflections	5950624 (592351)	3314706 (336434)	124444774 (621396)
Unique reflections	822268 (81944)	458021 (45686)	579145 (28958)
Multiplicity	7.2 (7.2)	7.2 (7.4)	21.5 (21.5)
Completeness (%) (Spherical truncation)	99.64 (99.58)	99.51 (99.71)	70.7 (13.4)
Completeness (%) (ellipsoidal truncation)	-	-	96.4 (76.3)
Mean I/sigma(I)	11.81 (0.87)	7.95 (0.87)	14.2 (1.7)
R_{pim}	0.06705 (0.8368)	0.08786 (0.8292)	0.081 (1.150)
$CC_{1/2}$	0.997 (0.341)	0.998 (0.364)	0.998 (0.577)
Refinement in Refmac5			
Number of TLS groups	59	-	
R-work	0.1969 (0.377)	0.2516 (0.4139)	0.18804 (0.339)
R-free	0.2183 (0.382)	0.3098 (0.4161)	0.21154 (0.318)
Number of non-hydrogen atoms	179483	231312	173152
Protein	178242	231312	
Ligands	913	-	
Solvent	328	-	
Protein residues	22778	46920	
Average B-factor (TLS/Isotropic refinement)($Å^2$)	49.69/92.72	256,34	
Protein	49.53/92.72	256,34	
Ligands	78.74/100.82	-	
Solvent	56.07/56.07	-	
Wilson	78,87	218,11	
R.m.s.d. bond length (Å)	0,014	0,016	0,008
R.m.s.d. bond angles (Å)	1,95	1,87	1,57
Ramachandran favored (%)	94,1	93,86	
Ramachandran allowed (%)	5,25	5,79	
Ramachandran outliers (%)	0,64	0,35	
Rotamer outliers (%)	13,8	-	
Clashscore	7,49	0,41	

Figure 8.2: Statistics of the crystallographic data collections and refinement processes

Cryo-EM data collection and refinement statistics

Sample	Δγ-FAS	Δγ-FAS + γ-subunit
Data collection and processing		
Microscope	Titan Krios	
Voltage (kV)	300	300
Camera	Falcon 3EC	
Slit width (ev)	-	-
Magnification	132000X	132000X
Pixel size (Å)	1,06	1,06
No. of Frames	20	30
Electron exposure (e^{-}/ $Å^2$)	62	48
Defocus range (μm)	43.525	0.7-3
Micrographs acquired	5441	4593
Initial particle images	1189206	856940
Particle images after 2D classification	834204	642703
Final particle images	144526	110597
Symmetry imposed	D3	D3
No. of Classes for conformational landscapes	-	-
Resolution (Å)	2,9	2,8
FSC threshold	0,143	0,143
Map-sharpening B factor ($Å^2$)	-120	-60
Refinement in Refmac5		
Initial model used	PDB: 2UV8	x-ray model from Δγ-FAS
Model composition		
Non-hydrogen atoms	178392	183564
Protein residues	178092	183216
Ligands	300	348
Fit to map		
Correlation coefficient (entire box)	0,886	0,896
Correlation coefficient (around atoms)	0,889	0,9
Fourier shell correlation (entire box)(Å)	3,23	3,17
Fourier shell correlation (around atoms)(Å)	3,05	2,97
Protein Geometry		
RMSD deviation bonds (Å)	0,0084	0,0089
RMSD deviation angles (°)	1,64	1,65
Favored rotamers (%)	92,29	92,78
Poor rotamers (%)	7,71	7,22
Ramachandran favored (%)	93,38	93,42
Ramachandran allowed (%)	7,7	7,58
Ramachandran outliers (%)	1,08	1
Clashscore	3,49	4,31
MolProbity score	2,33	2,39
EMRinger score	3,95	4,2

Figure 8.3: Statistics of the Cryo-EM datasets

9 Abbreviations

Å *Angström*
Abs *Absorbance*
ACC *Acetyl CoA Carboxylase*
ACP *Acyl Carrier Protein*
AcpS *Acyl Carrier Protein Synthase*
AT *Acetyltransferase*
ATP *Adenosine Triphosphate*
BC *Biotin Carboxylase*
BCCP *Biotin Carboxyl Carrier Protein*
BLAST *Basic Local Alignment Search Tool*
BSA *Bovine Serum Albumin*
CMN *Cyanobacteria-Mycobacteria-Nocardia*
CoA *Coenzyme A*
CT *Carboxyl Transferase*
CTF *Contrast Transfer Function*
CV *Column Volume*
DESY *Deutsches Elektronen Synchrotron*
DH *Dehydratase*
DNA *Deoxyreibonucleic Acid*
DSMZ *Deutsche Sammlung von Mikroorganismen und Zellkulturen*
Elo *Elongase*
EM *Electron Microscopy*
EMDB *Electron Microscopy Data Bank*
ER *Enoyl Reductase*
FAS *Fatty Acid Synthase*
FMN *Flavin mononucleotide*
FSC *Fourrier Shell Correlation*
GC *Gas Chromatography*
HPLC *High Performance Liquid Chromatography*
IPTG *Isopropyl-ß-D-thiogalactopyranosid*
Kan *Kanamycin*
kDa *Kilodalton*
KS *Ketoacyl Synthase*
MD *Molecular dynamic*
MDa *Megadalton*
ml *mililiter*
MPT *Malonyl Palmitoyl Transferase*
MS *Mass Spectrometry*
MSA *Multiple Sequence Alignment*
MWCO *Molecular Weight Cut-Off*
NAD(P)H *Nicotinamide adenine dinucleotide (phosphate)*
NAFLD *non-alcoholic fatty liver disease*
NHS *N-Hydroxysuccinimide*
NRPS *Non-ribosomal peptide synthesis*
NTA *Nitrilotriacetic Acid*
PCR *Polymerase Chain Reaction*
PDB *Protein Data Bank*
PEG *Polyethylene Glycol*
PKS *Polyketide Synthase*
PPTas *Phosphopantetheinyl Transferase*
PSI *Pound-force per square inch*
S *Svedberg*, *Svedberg*
SDS-PAGE *Sodium dodecyl sulphate-polyacrylamide gel electrophoresis*
SN *Supernatant*
TBE *TRIS-Borat-EDTA Buffer*
TCEP *Tris-(2-carboxyethyl)-phosphin Hydrochlorid*
TesA *Acyl-CoA Thioestarase A*
TEV *Tobacco Etch Virus*
UAS *Upstream activating sequences*
V *Volt*
wt *Wild Type*
XL-MS *Cross Linking Mass Spectrometry*
YP *Yeast Peptone*
YPD *Yeast Peptone Dextrose*
µl *microlit*

10 References

Alberts, A., Of, P.V.-P. of the N.A., and 1968, U. (1968). Acetyl CoA carboxylase. I. Requirement for two protein fractions. Ncbi.Nlm.Nih.Gov.

Altschul, S.F., Gish, W., Miller, W., Myers, E.W., and Lipman, D.J. (1990). Basic local alignment search tool. J. Mol. Biol. *215*, 403–410.

Anselmi, C., Grininger, M., Gipson, P., and Faraldo-Gómez, J.D. (2010). Mechanism of Substrate Shuttling by the Acyl-Carrier Protein within the Fatty Acid Mega-Synthase. J. Am. Chem. Soc. *132*, 12357–12364.

Aprahamian, S.A., Arslanian, M.J., and Wakil, S.J. (1982). Comparative studies on the kinetic parameters and product analyses of chicken and rat liver and yeast fatty acid synthetase. Comp. Biochem. Physiol. B. *71*, 577–582.

Atha, D.H., and Ingham, K.C. (1981). Mechanism of precipitation of proteins by polyethylene glycols. Analysis in terms of excluded volume. J. Biol. Chem. *256*, 12108–12117.

Beld, J., Sonnenschein, E.C., Vickery, C.R., Noel, J.P., and Burkart, M.D. (2014). The phosphopantetheinyl transferases: catalysis of a post-translational modification crucial for life. Nat. Prod. Rep. *31*, 61–108.

Bellou, S., Triantaphyllidou, I.-E., Aggeli, D., Elazzazy, A.M., Baeshen, M.N., and Aggelis, G. (2016). Microbial oils as food additives: recent approaches for improving microbial oil production and its polyunsaturated fatty acid content. Curr. Opin. Biotechnol. *37*, 24–35.

Beltran-Alvarez, P., Arthur, C.J., Cox, R.J., Crosby, J., Crump, M.P., and Simpson, T.J. (2009). Preliminary kinetic analysis of acyl carrier protein–ketoacylsynthase interactions in the actinorhodin minimal polyketide synthase. Mol. Biosyst. *5*, 511–518.

Biermann, U., Bornscheuer, U.T., Feussner, I., Meier, M.A.R., and Metzger, J.O. (2021). Fatty Acids and their Derivatives as Renewable Platform Molecules for the Chemical Industry. Angew. Chem. Int. Ed. Engl. *60*, 20144–20165.

Bloch, K., and Vance, D. (1977). Control mechanisms in the synthesis of saturated fatty acids. Annu. Rev. Biochem. *46*, 263–298.

Boom, T. Vanden, and Cronan, J.E. (1989). GENETICS AND REGULATION OF BACTERIAL LIPID METABOLISM. Annu. Rev. Microb. *43*, 317–360.

Brodersen, D.E., Clemons, W.M., Carter, A.P., Morgan-Warren, R.J., Wimberly, B.T., and Ramakrishnan, V. (2000). The Structural Basis for the Action of the Antibiotics Tetracycline, Pactamycin, and Hygromycin B on the 30S Ribosomal Subunit. Cell *103*, 1143–1154.

Brown, A.P., Slabas, A.R., and Rafferty, J.B. (2009). Fatty Acid Biosynthesis in Plants — Metabolic Pathways, Structure and Organization. 11–34.

Bunkoczi, G., Pasta, S., Joshi, A., Wu, X., Kavanagh, K.L., Smith, S., and Oppermann, U. (2007). Mechanism and substrate recognition of human holo ACP synthase. Chem. Biol. *14*, 1243–1253.

Bushnell, D.A., Cramer, P., and Kornberg, R.D. (2002). Structural basis of transcription: α-Amanitin–RNA polymerase II cocrystal at 2.8 Å resolution. Proc. Natl. Acad. Sci. *99*, 1218–1222.

Chaiyen, P., Fraaije, M.W., and Mattevi, A. (2012). The enigmatic reaction of flavins with oxygen. Trends Biochem. Sci. *37*, 373–380.

Chan, D.I., and Vogel, H.J. (2010). Current understanding of fatty acid biosynthesis and the acyl carrier protein. Biochem. J. *430*, 1–19.

Chan, D., Journal, H.V.-B., and 2010, U. (2010). Current understanding of fatty acid biosynthesis and the acyl carrier protein. Portlandpress.Com.

Chirala, S.S., Kuziora, M.A., Spector, D.M., and Wakil, S.J. (1987). Complementation of mutations

and nucleotide sequence of FAS1 gene encoding beta subunit of yeast fatty acid synthase. J. Biol. Chem. *262*, 4231–4240.

Chirala, S.S., Chang, H., Matzuk, M., Abu-Elheiga, L., Mao, J., Mahon, K., Finegold, M., and Wakil, S.J. (2003). Fatty acid synthesis is essential in embryonic development: Fatty acid synthase null mutants and most of the heterozygotes die in utero. Proc. Natl. Acad. Sci. *100*, 6358–6363.

Chun, P.W., Fried, M., and Ellis, E.F. (1967). Use of water-soluble polymers for the isolation and purification of human immunoglobulins. Anal. Biochem. *19*, 481–497.

La Clair, J., Foley, T.L., Schegg, T.R., Regan, C.M., and Burkart, M.D. (2004). Manipulation of carrier proteins in antibiotic biosynthesis. Chem. Biol. *11*, 195–201.

Cronan, J.E., and Waldrop, G.L. (2002). Multi-subunit acetyl-CoA carboxylases. Prog. Lipid Res. *41*, 407–435.

Crosby, J., and Crump, M.P. (2012). The structural role of the carrier protein – active controller or passive carrier. Nat. Prod. Rep. *29*, 1111–1137.

D'Agnolo, G., Rosenfeld, I.S., Awaya, J., Omura, S., and Vagelos, P.R. (1973). Inhibition of fatty acid synthesis by the antibiotic cerulenin. Specific inactivation of beta-ketoacyl-acyl carrier protein synthetase. Biochim. Biophys. Acta *326*, 155–156.

Dibrova, D. V., Galperin, M.Y., and Mulkidjanian, A.Y. (2014). Phylogenomic reconstruction of archaeal fatty acid metabolism. Environ. Microbiol. *16*, 907.

Dietlein, G., and Schweizer, E. (1975). Control of Fatty-Acid-Synthetase Biosynthesis in Saccharomyces cerevisiae. Eur. J. Biochem. *58*, 177–184.

Ducat, D., Way, J., biotechnology, P.S.-T. in, and 2011, undefined Engineering cyanobacteria to generate high-value products. Elsevier.

Duggar, B.M. (1948). Aureomycin; a product of the continuing search for new antibiotics. Ann. N. Y. Acad. Sci. *51*, 177–181.

Elad, N., Baron, S., Peleg, Y., Albeck, S., Grunwald, J., Raviv, G., Shakked, Z., Zimhony, O., and Diskin, R. (2018). Structure of Type-I Mycobacterium tuberculosis fatty acid synthase at 3.3 Å resolution. Nat. Commun. 2018 91 *9*, 1–6.

Emsley, P., and Cowtan, K. (2004). Coot: model-building tools for molecular graphics. Acta Crystallogr. D. Biol. Crystallogr. *60*, 2126–2132.

Farmer, R., Thomas, C.M., and Winn, P.J. (2019). Structure, function and dynamics in acyl carrier proteins. PLoS One *14*, e0219435.

Fichtlscherer, F., Wellein, C., Mittag, M., and Schweizer, E. (2000a). A novel function of yeast fatty acid synthase. Subunit α is capable of self-pantetheinylation. Eur. J. Biochem. *267*, 2666–2671.

Fichtlscherer, F., Wellein, C., Mittag, M., and Schweizer, E. (2000b). A novel function of yeast fatty acid synthase. Eur. J. Biochem. *267*, 2666–2671.

Fischer, M., Joppe, M., Mulinacci, B., Vollrath, R., Konstantinidis, K., Kötter, P., Ciccarelli, L., Vonck, J., Oesterhelt, D., and Grininger, M. (2020). Analysis of the co-translational assembly of the fungal fatty acid synthase (FAS). Sci. Rep. *10*, 895.

Fleischer, T.C., Weaver, C.M., McAfee, K.J., Jennings, J.L., and Link, A.J. (2006). Systematic identification and functional screens of uncharacterized proteins associated with eukaryotic ribosomal complexes. Genes Dev. *20*, 1294–1307.

Frieden, C. (1970). Kinetic aspects of regulation of metabolic processes. The hysteretic enzyme concept. J. Biol. Chem. *245*, 5788–5799.

Gajewski, J., Buelens, F., Serdjukow, S., Janßen, M., Cortina, N., Grubmüller, H., and Grininger, M. (2017). Engineering fatty acid synthases for directed polyketide production. Nat. Chem. Biol. *13*, 363–365.

Gancedo, J.M., and Gancedo, C. (1973). Concentrations of intermediary metabolites in yeast. Biochimie *55*, 205–211.

Gipson, P., Mills, D.J., Wouts, R., Grininger, M., Vonck, J., and Kühlbrandt, W. (2010a). Direct structural insight into the substrate-shuttling mechanism of yeast fatty acid synthase by electron cryomicroscopy. Proc. Natl. Acad. Sci. U. S. A. *107*, 9164–9169.

Gipson, P., Mills, D.J., Wouts, R., Grininger, M., Vonck, J., and Kuhlbrandt, W. (2010b). Direct structural insight into the substrate-shuttling mechanism of yeast fatty acid synthase by electron cryomicroscopy. Proc. Natl. Acad. Sci. U. S. A. *107*, 9164–9169.

Green, A.A., and Hughes, W.L. (1955). Protein fractionation on the basis of solubility in aqueous solutions of salts and organic solvents. In Methods in Enzymology, pp. 67–90.

Hahn, M., and Stachelhaus, T. (2004). Selective interaction between nonribosomal peptide synthetases is facilitated by short communication-mediating domains. Proc. Natl. Acad. Sci. U. S. A. *101*, 15585–15590.

Hallberg, M.B. (2008). Protein production and purification. Nat. Methods *5*, 135–146.

Han, G., Gable, K., Kohlwein, S.D., Beaudoin, F., Napier, J.A., and Dunn, T.M. (2002). The Saccharomyces cerevisiae YBR159w gene encodes the 3-ketoreductase of the microsomal fatty acid elongase. J. Biol. Chem. *277*, 35440–35449.

Hanssum, A., Zhong, Z., Rousseau, A., Krzyzosiak, A., Sigurdardottir, A., and Bertolotti, A. (2014). An inducible chaperone adapts proteasome assembly to stress. Mol. Cell *55*, 566–577.

Haselbach, D., Schrader, J., Lambrecht, F., Henneberg, F., Chari, A., and Stark, H. (2017). Long-range allosteric regulation of the human 26S proteasome by 20S proteasome-targeting cancer drugs. Nat. Commun. *8*, 15578.

Haselbach, D., Komarov, I., Agafonov, D.E., Hartmuth, K., Graf, B., Dybkov, O., Urlaub, H., Kastner, B., Lührmann, R., and Stark, H. (2018). Structure and Conformational Dynamics of the Human Spliceosomal Bact Complex. Cell *172*, 454-464.e11.

Hasslacher, M., Ivessa, A.S., Paltauf, F., and Kohlwein, S.D. (1993). Acetyl-CoA carboxylase from yeast is an essential enzyme and is regulated by factors that control phospholipid metabolism. J. Biol. Chem. *268*, 10946–10952.

Heath, R.J., Rubin, J.R., Holland, D.R., Zhang, E., Snow, M.E., and Rock, C.O. (1999). Mechanism of Triclosan Inhibition of Bacterial Fatty Acid Synthesis. J. Biol. Chem. *274*, 11110–11114.

Helmkamp, G.M., Brock, D.J., and Bloch, K. (1968). Beta-hydroxydecanoly thioester dehydrase. Specificity of substrates and acetylenic inhibitors. J. Biol. Chem. *243*, 3229–3231.

Herbst, D.A., Townsend, C.A., and Maier, T. (2018). The architectures of iterative type I PKS and FAS. Nat. Prod. Rep. *35*, 1046–1069.

Huang, X., Holden, H.M., and Raushel, F.M. (2001). Channeling of substrates and intermediates in enzyme-catalyzed reactions. Annu. Rev. Biochem. *70*, 149–180.

Jackowski, S., and Rock, C. (1983). Ratio of active to inactive forms of acyl carrier protein in Escherichia coli. J. Biol. Chem. *258*, 15186–15191.

Jain, S., Dholakia, H., Kirtley, W., and Oelkers, P. (2016). Energy Storage in Yeast: Regulation and Competition with Ethanol Production. Curr. Microbiol. *73*, 851–858.

Jensen-Urstad, A.P.L., and Semenkovich, C.F. (2012). Fatty acid synthase and liver triglyceride metabolism: housekeeper or messenger? Biochim. Biophys. Acta *1821*, 747.

Ji, X.-J., and Huang, H. (2019). Engineering Microbes to Produce Polyunsaturated Fatty Acids. Trends Biotechnol. *37*, 344–346.

Johansson, P., Wiltschi, B., Kumari, P., Kessler, B., Vonrhein, C., Vonck, J., Oesterhelt, D., and Grininger, M. (2008). Inhibition of the fungal fatty acid synthase type I multienzyme complex. Proc. Natl. Acad. Sci. *105*, 12803–12808.

Johansson, P., Mulinacci, B., Koestler, C., Vollrath, R., Oesterhelt, D., and Grininger, M. (2009a). Multimeric Options for the Auto-Activation of the Saccharomyces cerevisiae FAS Type I Megasynthase. Structure *17*, 1063–1074.

Johansson, P., Mulinacci, B., Koestler, C., Vollrath, R., Oesterhelt, D., and Grininger, M. (2009b). Multimeric Options for the Auto-Activation of the Saccharomyces cerevisiae FAS Type I Megasynthase. Structure.

Jungbauer, A. (2005). Chromatographic media for bioseparation. J. Chromatogr. A *1065*, 3–12.

Kabsch, W. (2010). XDS. Acta Crystallogr. D. Biol. Crystallogr. *66*, 125–132.

Kalderon, D., Roberts, B.L., Richardson, W.D., and Smith, A.E. (1984). A short amino acid sequence able to specify nuclear location. Cell *39*, 499–509.

Karam, G.A., and Arslanian, M.J. (1984). A rapid method for the purification of fatty acid synthetase from the yeast Saccharomyces cerevisiae. Int. J. Biochem. *16*, 667–673.

Keating, D.H., and Cronan, J.E. (1996). An isoleucine to valine substitution in Escherichia coli acyl carrier protein results in a functional protein of decreased molecular radius at elevated pH. J. Biol. Chem. *271*, 15905–15910.

Kumagai, A., Ando, R., Miyatake, H., Greimel, P., Kobayashi, T., Hirabayashi, Y., Shimogori, T., and Miyawaki, A. (2013). A bilirubin-inducible fluorescent protein from eel muscle. Cell *153*, 1602–1611.

Lambalot, R.H., Gehring, A.M., Flugel, R.S., Zuber, P., LaCelle, M., Marahiel, M.A., Reid, R., Khosla, C., and Walsh, C.T. (1996). A new enzyme superfamily - the phosphopantetheinyl transferases. Chem. Biol. *3*, 923–936.

Ledent, P., Duez, C., Vanhove, M., Lejeune, A., Fonzé, E., Charlier, P., Rhazi-Filali, F., Thamm, I., Guillaume, G., Samyn, B., et al. (1997). Unexpected influence of a C-terminal-fused His-tag on the processing of an enzyme and on the kinetic and folding parameters. FEBS Lett. *413*, 194–196.

Leibundgut, M., Jenni, S., Frick, C., and Ban, N. (2007). Structural basis for substrate delivery by acyl carrier protein in the yeast fatty acid synthase. Science (80-.). *316*, 288–290.

Lennen, R.M., and Pfleger, B.F. (2012). Engineering Escherichia coli to synthesize free fatty acids. Trends Biotechnol. *30*, 659–667.

Lim, J., Kong, R., Murugan, E., Ho, C.L., Liang, Z.-X., and Yang, D. (2011). Solution Structures of the Acyl Carrier Protein Domain from the Highly Reducing Type I Iterative Polyketide Synthase CalE8. PLoS One *6*, e20549.

Lindell, T., Weinberg, F., Morris, P., Roeder, R., and Rutter, W. (1970). Specific inhibition of nuclear RNA polymerase II by alpha-amanitin. Science *170*, 447–449.

Lomakin, I.B., Xiong, Y., and Steitz, T.A. (2007). The Crystal Structure of Yeast Fatty Acid Synthase, a Cellular Machine with Eight Active Sites Working Together. Cell *129*, 319–332.

Lu, X., Vora, H., and Khosla, C. (2008). Overproduction of free fatty acids in E. coli: implications for biodiesel production. Metab. Eng. *10*, 333–339.

Lust, G., and Lynen, F. (1968). The Inhibition of the Fatty Acid Synthetase Multienzyme Complex of Yeast by Long-Chain Acyl Coenzyme A Compounds. Eur. J. Biochem. *7*, 68–72.

Lynen, F. (1962). Fatty acid synthesis from malonyl CoA. In Methods in Enzymology, pp. 443–451.

Lynen, F. (1969). Yeast fatty acid synthase. Methods Enzymol. *14*, 17–33.

Lynen, F. (1980). On the Structure of Fatty Acid Synthetase of Yeast. Eur. J. Biochem. *112*, 431–442.

Lynen, F., Hopper-Kessel, I., and Eggerer, H. (1964). Fatty acid synthethase in yeast and the conformation of enzyme bound acetoacetic acid. Biochem. Z. *340*, 95–124.

Lynen, F., Engeser, H., Foerster, E. -C, Fox, J.L., Hess, S., Kresze, G. -B, Schmitt, T., Schreckenbach, T., Siess, E., Wieland, F., et al. (1980). On the Structure of Fatty Acid Synthetase of Yeast. Eur. J. Biochem. *112*, 431–442.

Maier, T., Leibundgut, M., and Ban, N. (2008). The Crystal Structure of a Mammalian Fatty Acid Synthase. Science (80-.). *321*, 1315–1322.

Majorek, K.A., Kuhn, M.L., Chruszcz, M., Anderson, W.F., and Minor, W. (2014). Double trouble-Buffer selection and His-tag presence may be responsible for nonreproducibility of biomedical experiments. Protein Sci. *23*, 1359–1368.

Mandel, A.L., La Clair, J.J., and Burkart, M.D. (2004). Modular synthesis of pantetheine and phosphopantetheine. Org. Lett. *6*, 4801–4803.

Medes, G., Thomas, A., research, S.W.-C., and 1953, undefined (1953). Metabolism of neoplastic tissue. IV. A study of lipid synthesis in neoplastic tissue slices in vitro. AACR.

Milligan, J.C., Lee, D.J., Jackson, D.R., Schaub, A.J., Beld, J., Barajas, J.F., Hale, J.J., Luo, R., Burkart, M.D., and Tsai, S.-C. (2019a). Molecular basis for interactions between an acyl carrier protein and a ketosynthase. Nat. Chem. Biol. *15*, 669–671.

Milligan, J.C., Lee, D.J., Jackson, D.R., Schaub, A.J., Beld, J., Barajas, J.F., Hale, J.J., Luo, R., Burkart, M.D., and Tsai, S.C. (2019b). Molecular basis for interactions between an acyl carrier protein and a ketosynthase. Nat. Chem. Biol. *15*, 669–671.

Mindrebo, J.T., Patel, A., Misson, L.E., Kim, W.E., Davis, T.D., Ni, Q.Z., La Clair, J.J., and Burkart, M.D. (2020a). Structural Basis of Acyl-Carrier Protein Interactions in Fatty Acid and Polyketide Biosynthesis. Compr. Nat. Prod. III 61–122.

Mindrebo, J.T., Patel, A., Kim, W.E., Davis, T.D., Chen, A., Bartholow, T.G., La Clair, J.J., McCammon, J.A., Noel, J.P., and Burkart, M.D. (2020b). Gating mechanism of elongating β-ketoacyl-ACP synthases. Nat. Commun. *11*, 1727.

Moche, M., Schneider, G., Edwards, P., Dehesh, K., and Lindqvist, Y. (1999). Structure of the complex between the antibiotic cerulenin and its target, beta-ketoacyl-acyl carrier protein synthase. J. Biol. Chem. *274*, 6031–6034.

Mohamed, A.H., Chirala, S.S., Mody, N.H., Huang, W.Y., and Wakil, S.J. (1988). Primary structure of the multifunctional alpha subunit protein of yeast fatty acid synthase derived from FAS2 gene sequence. J. Biol. Chem. *263*, 12315–12325.

Morlock, L.K., Böttcher, D., and Bornscheuer, U.T. (2018). Simultaneous detection of NADPH consumption and H2O2 production using the Ampliflu^{TM} Red assay for screening of P450 activities and uncoupling. Appl. Microbiol. Biotechnol. *102*, 985–994.

Murphy, D.J. (1996). Engineering oil production in rapeseed and other oil crops. Trends Biotechnol. *14*, 206–213.

Murshudov, G.N., Skubák, P., Lebedev, A.A., Pannu, N.S., Steiner, R.A., Nicholls, R.A., Winn, M.D., Long, F., and Vagin, A.A. (2011). REFMAC5 for the refinement of macromolecular crystal structures. Acta Crystallogr. D. Biol. Crystallogr. *67*, 355–367.

Nelson, D.L., and Cox, M.M. (1993). Principles Of Biochemistry. J. Chem. Educ. *70*, A223.

Nguyen, C., Haushalter, R.W., Lee, D.J., Markwick, P.R.L., Bruegger, J., Caldara-Festin, G., Finzel, K., Jackson, D.R., Ishikawa, F., O'Dowd, B., et al. (2014a). Trapping the dynamic acyl carrier protein in fatty acid biosynthesis. Nature *505*, 427–431.

Nguyen, C., Haushalter, R.W., Lee, D.J., Markwick, P.R.L., Bruegger, J., Caldara-Festin, G., Finzel, K., Jackson, D.R., Ishikawa, F., O'Dowd, B., et al. (2014b). Trapping the dynamic acyl carrier protein in fatty acid biosynthesis. Nature *505*, 427–431.

Nguyen, C., Haushalter, R.W., Lee, D.J., Markwick, P.R.L., Bruegger, J., Caldara-Festin, G., Finzel, K., Jackson, D.R., Ishikawa, F., O'Dowd, B., et al. (2014c). Trapping the dynamic acyl carrier protein in fatty acid biosynthesis. Nature *505*, 427–431.

Nikolau, B.J., Perera, M.A.D.N., Brachova, L., and Shanks, B. (2008). Platform biochemicals for

a biorenewable chemical industry. Plant J. *54*, 536–545.

Oesterhelt, D., Bauer, H., Kresze, G. -B, Steber, L., and Lynen, F. (1977). Reaction of Yeast Fatty Acid Synthetase with Iodoacetamide: 1. Kinetics of Inactivation and Extent of Carboxamidomethylation. Eur. J. Biochem. *79*, 173–180.

Omura, S., Katagiri, M., Nakagawa, A., Sano, Y., and Nomura, S. (1967). Studies on cerulenin. V. Structure of cerulenin. J. Antibiot. (Tokyo). *20*, 349–354.

Ookhtens, M., Kannan, R., Lyon, I., and Baker, N. (1984). Liver and adipose tissue contributions to newly formed fatty acids in an ascites tumor. Https://Doi.Org/10.1152/Ajpregu.1984.247.1.R146 *16*.

Park, Y.-K., Dulermo, T., Ledesma-Amaro, R., and Nicaud, J.-M. (2018). Optimization of odd chain fatty acid production by Yarrowia lipolytica. Biotechnol. Biofuels *11*, 158.

Parris, K.D., Lin, L., Tam, A., Mathew, R., Hixon, J., Stahl, M., Fritz, C.C., Seehra, J., and Somers, W.S. (2000). Crystal structures of substrate binding to Bacillus subtilis holo-(acyl carrier protein) synthase reveal a novel trimeric arrangement of molecules resulting in three active sites. Structure *8*, 883–895.

Peralta-Yahya, P.P., Zhang, F., del Cardayre, S.B., and Keasling, J.D. (2012). Microbial engineering for the production of advanced biofuels. Nature *488*, 320–328.

Pettersen, E.F., Goddard, T.D., Huang, C.C., Couch, G.S., Greenblatt, D.M., Meng, E.C., and Ferrin, T.E. (2004). UCSF Chimera--a visualization system for exploratory research and analysis. J. Comput. Chem. *25*, 1605–1612.

Pettersen, E.F., Goddard, T.D., Huang, C.C., Meng, E.C., Couch, G.S., Croll, T.I., Morris, J.H., and Ferrin, T.E. (2021). UCSF ChimeraX: Structure visualization for researchers, educators, and developers. Protein Sci. *30*, 70–82.

Pirson, W., Schuhmann, L., and Lynen, F. (1973). The specificity of yeast fatty-acid synthetase with respect to the “priming” substrate. Decanoyl-coA and derivatives as “primers” of fatty-acid synthesis in vitro. Eur. J. Biochem. *36*, 16–24.

Polakis, E.S., and Bartley, W. (1966). Changes in the intracellular concentrations of adenosine phosphates and nicotinamide nucleotides during the aerobic growth cycle of yeast on different carbon sources. Biochem. J. *99*, 521–533.

Polson, A., Potgieter, G.M., Largier, J.F., Mears, G.E., and Joubert, F.J. (1964). THE FRACTIONATION OF PROTEIN MIXTURES BY LINEAR POLYMERS OF HIGH MOLECULAR WEIGHT. Biochim. Biophys. Acta *82*, 463–475.

Price, A.C., Choi, K.H., Heath, R.J., Li, Z., White, S.W., and Rock, C.O. (2001). Inhibition of beta-ketoacyl-acyl carrier protein synthases by thiolactomycin and cerulenin. Structure and mechanism. J. Biol. Chem. *276*, 6551–6559.

Quadri, L.E.N., Weinreb, P.H., Lei, M., Nakano, M.M., Zuber, P., and Walsh, C.T. (1998). Characterization of Sfp, a Bacillus subtilis Phosphopantetheinyl Transferase for Peptidyl Carrier Protein Domains in Peptide Synthetases. Biochemistry *37*, 1585–1595.

Reuter, K., Mofid, M.R., Marahiel, M.A., and Ficner, R. (1999). Crystal structure of the surfactin synthetase-activating enzyme sfp: a prototype of the 4’-phosphopantetheinyl transferase superfamily. EMBO J. *18*, 6823–6831.

Rigouin, C., Croux, C., Borsenberger, V., Ben Khaled, M., Chardot, T., Marty, A., and Bordes, F. (2018). Increasing medium chain fatty acids production in Yarrowia lipolytica by metabolic engineering. Microb. Cell Fact. *17*, 142.

Rock, C.O., and Cronan, J.E. (1979). Re-evaluation of the solution structure of acyl carrier protein. J. Biol. Chem. *254*, 9778–9785.

Rousseau, A., and Bertolotti, A. (2016). An evolutionarily conserved pathway controls proteasome homeostasis. Nature *536*, 184–189.

Saibil, H. (2013). Chaperone machines for protein folding, unfolding and disaggregation. Nat.

Rev. Mol. Cell Biol. *14*, 630–642.

Scheres, S.H.W. (2012). RELION: implementation of a Bayesian approach to cryo-EM structure determination. J. Struct. Biol. *180*, 519–530.

Schjerling, C.K., Hummel, R., Hansen, J.K., Borsting, C., Mikkelsen, J.M., Kristiansen, K., and Knudsen, J. (1996). Disruption of the gene encoding the acyl-CoA-binding protein (ACB1) perturbs acyl-CoA metabolism in Saccharomyces cerevisiae. J. Biol. Chem. *271*, 22514–22521.

Schneider, C.A., Rasband, W.S., and Eliceiri, K.W. (2012). NIH Image to ImageJ: 25 years of image analysis. Nat. Methods *9*, 671–675.

Schrader, J., Henneberg, F., Mata, R.A., Tittmann, K., Schneider, T.R., Stark, H., Bourenkov, G., and Chari, A. (2016). The inhibition mechanism of human 20S proteasomes enables next-generation inhibitor design. Science *353*, 594–598.

Schreiber, G. (2002). Kinetic studies of protein–protein interactions. Curr. Opin. Struct. Biol. *12*, 41–47.

Schüller, H., A, S., S, K., B, H., and E, S. (1994). Importance of general regulatory factors Rap1p, Abf1p and Reb1p for the activation of yeast fatty acid synthase genes FAS1 and FAS2. Eur. J. Biochem. *225*, 213–222.

Schuster, H., Rautenstrauss, B., Mittag, M., Stratmann, D., and Schweizer, E. (1995). Substrate and Product Binding Sites of Yeast Fatty Acid Synthase. Eur. J. Biochem. *228*, 417–424.

Schweizer, H.P. (2001). Triclosan: a widely used biocide and its link to antibiotics. FEMS Microbiol. Lett. *202*, 1–7.

Schweizer, E., and Hofmann, J. (1990). Microbial Type I Fatty Acid Synthases (FAS): Major Players in a Network of Cellular FAS Systems. Microbiol. Mol. Biol. Rev. *68*, 501–517.

Schweizer, E., and Hofmann, J. (2004a). Microbial type I fatty acid synthases (FAS): major players in a network of cellular FAS systems. Microbiol. Mol. Biol. Rev. *68*, 501–517, table of contents.

Schweizer, E., and Hofmann, J. (2004b). Microbial type I fatty acid synthases (FAS): major players in a network of cellular FAS systems. Microbiol. Mol. Biol. Rev. *68*, 501–517, table of contents.

Scopes, R.K. (2001). Overview of protein purification and characterization. Curr. Protoc. Protein Sci. *Chapter 1*, Unit 1.1.

Sheng, J., and Feng, X. (2015). Metabolic engineering of yeast to produce fatty acid-derived biofuels: bottlenecks and solutions. Front. Microbiol. *6*, 554.

Shental-Bechor, D., and Levy, Y. (2009). Folding of glycoproteins: toward understanding the biophysics of the glycosylation code. Curr. Opin. Struct. Biol. *19*, 524–533.

Shi, S., Chen, Y., Siewers, V., and Nielsen, J. (2014). Improving production of malonyl coenzyme A-derived metabolites by abolishing Snf1-dependent regulation of Acc1. MBio *5*.

Shin, K.S., Kim, S., and Lee, S.K. (2016). Improvement of free fatty acid production using a mutant acyl-CoA thioesterase I with high specific activity in Escherichia coli. Biotechnol. Biofuels *9*, 208.

Shirra, M.K., Patton-Vogt, J., Ulrich, A., Liuta-Tehlivets, O., Kohlwein, S.D., Henry, S.A., and Arndt, K.M. (2001). Inhibition of Acetyl Coenzyme A Carboxylase Activity Restores Expression of the INO1 Gene in a snf1 Mutant Strain of Saccharomyces cerevisiae . Mol. Cell. Biol. *21*, 5710–5722.

Singh, N., Wakil, S.J., and Stoops, J.K. (1985). Yeast fatty acid synthase: structure to function relationship. Biochemistry *24*, 6598–6602.

Smith, J.L., and Sherman, D.H. (2008). An Enzyme Assembly Line. Science *321*, 1304.

Spector, A.A., John, K., and Fletcher, J.E. (1969). Binding of long-chain fatty acids to bovine serum albumin. J. Lipid Res. *10*, 56–67.

Stoops, J.K., and Wakil, S.J. (1978). The isolation of the two subunits of yeast fatty acid synthetase. Biochem. Biophys. Res. Commun. *84*, 225–231.

Stoops, J.K., Awad, E.S., Arslanian, M.J., Gunsberg, S., Wakilg, S.J., and Oliver, R.M. (1978). Studies on the yeast fatty acid synthetase. Subunit composition and structural organization of a large multifunctional enzyme complex. J. Biol. Chem. *253*, 4464–4475.

Stoops, J.K., Singh, N., and Wakil, S.J. (1990). The yeast fatty acid synthase. Pathway for transfer of the acetyl group from coenzyme A to the Cys-SH of the condensation site. J. Biol. Chem. *265*, 16971–16977.

Suburu, J., Shi, L., Wu, J., Wang, S., Samuel, M., Thomas, M.J., Kock, N.D., Yang, G., Kridel, S., and Chen, Y.Q. (2014). Fatty acid synthase is required for mammary gland development and milk production during lactation. Am. J. Physiol. - Endocrinol. Metab. *306*, E1132.

Sumida, C., Graber, R., and Nunez, E. (1993). Role of fatty acids in signal transduction: Modulators and messengers. Prostaglandins, Leukot. Essent. Fat. Acids *48*, 117–122.

Sumper, M., Riepertinger, C., Lynen, F., and Oesterhelt, D. (1969). Die Synthese verschiedener Carbonsauren durch den Multienzymkomplex der Fettsauresynthese aus Hefe und die Erklarung ihrer Bildung. Eur. J. Biochem. *10*, 377–387.

Suomalainen, H., and Keränen, A.J.A. (1963). The effect of biotin deficiency on the synthesis of fatty acids by yeast. Biochim. Biophys. Acta *70*, 493–503.

Suzuki, H., Inabe, K., Shirakawa, Y., Umezawa, N., Kato, N., and Higuchi, T. (2017). Role of Thiolate Ligand in Spin State and Redox Switching in the Cytochrome P450 Catalytic Cycle. Inorg. Chem. *56*, 4245–4248.

Tallorin, L., Finzel, K., Nguyen, Q.G., Beld, J., La Clair, J.J., and Burkart, M.D. (2016a). Trapping of the Enoyl-Acyl Carrier Protein Reductase–Acyl Carrier Protein Interaction. J. Am. Chem. Soc. *138*, 3962–3965.

Tallorin, L., Finzel, K., Nguyen, Q.G., Beld, J., La Clair, J.J., and Burkart, M.D. (2016b). Trapping of the Enoyl-Acyl Carrier Protein Reductase-Acyl Carrier Protein Interaction. J. Am. Chem. Soc. *138*, 3962–3965.

Tehlivets, O., Scheuringer, K., and Kohlwein, S.D. (2007). Fatty acid synthesis and elongation in yeast. Biochim. Biophys. Acta - Mol. Cell Biol. Lipids *1771*, 255–270.

Toomey, R.E., and Wakil, S.J. (1966). Studies on the Mechanism of Fatty Acid Synthesis: XVI. PREPARATION AND GENERAL PROPERTIES OF ACYL-MALONYL ACYL CARRIER PROTEIN-CONDENSING ENZYME FROM ESCHERICHIA COLI. J. Biol. Chem. *241*, 1159–1165.

Tripodi, F., Nicastro, R., Reghellin, V., and Coccetti, P. (2015). Post-translational modifications on yeast carbon metabolism: Regulatory mechanisms beyond transcriptional control. Biochim. Biophys. Acta *1850*, 620–627.

Tsumoto, K., Ejima, D., Senczuk, A.M., Kita, Y., and Arakawa, T. (2007). Effects of salts on protein-surface interactions: applications for column chromatography. J. Pharm. Sci. *96*, 1677–1690.

UniProt Consortium (2015). UniProt: a hub for protein information. Nucleic Acids Res. *43*, D204-12.

Vagin, A., and Teplyakov, A. (2010). Molecular replacement with MOLREP. Acta Crystallogr. D. Biol. Crystallogr. *66*, 22–25.

Vassylyeva, M.N., Klyuyev, S., Vassylyev, A.D., Wesson, H., Zhang, Z., Renfrow, M.B., Wang, H., Higgins, N.P., Chow, L.T., and Vassylyev, D.G. (2017). Efficient, ultra-high-affinity chromatography in a one-step purification of complex proteins. Proc. Natl. Acad. Sci. U. S. A. *114*, E5138–E5147.

Vickery, C.R., Kosa, N.M., Casavant, E.P., Duan, S., Noel, J.P., and Burkart, M.D. (2014). Structure, biochemistry, and inhibition of essential 4'-phosphopantetheinyl transferases from two

species of Mycobacteria. ACS Chem. Biol. *9*, 1939–1944.

Wakil, S.J., Pugh, E.L., and Sauer, F. (1964). the Mechanism of Fatty Acid Synthesis. Proc. Natl. Acad. Sci. United States *52*, 106–114.

Warburg, O. (1924). Uber den Stoffwechsel der Karzinomezellen. Biochem Z *152*, 309–344.

Ward, W., Geoffrey A. Holdgate, Siân Rowsell, Estelle G. McLean, Richard A. Pauptit, Edward Clayton, Wright W. Nichols, Jeremy G. Colls, Claire A. Minshull, David A. Jude, et al. (1999). Kinetic and Structural Characteristics of the Inhibition of Enoyl (Acyl Carrier Protein) Reductase by Triclosan‡. Biochemistry *38*, 12514–12525.

Wei, J., and Tong, L. (2015). Crystal structure of the 500-kDa yeast acetyl-CoA carboxylase holoenzyme dimer. Nat. 2015 5267575 *526*, 723–727.

Wenz, P., Schwank, S., Hoja, U., and Schüller, H.-J. (2001). A downstream regulatory element located within the coding sequence mediates autoregulated expression of the yeast fatty acid synthase gene FAS2 by the FAS1 gene product. Nucleic Acids Res. *29*, 4625–4632.

von Wettstein-Knowles, P., Olsen, J.G., McGuire, K.A., and Henriksen, A. (2006). Fatty acid synthesis. Role of active site histidines and lysine in Cys-His-His-type beta-ketoacyl-acyl carrier protein synthases. FEBS J. *273*, 695–710.

White, S.W., Zheng, J., Zhang, Y.-M., and Rock, C.O. (2005). THE STRUCTURAL BIOLOGY OF TYPE II FATTY ACID BIOSYNTHESIS. Http://Dx.Doi.Org/10.1146/Annurev.Biochem.74.082803.133524 *74*, 791–831.

WIELAND, F., RENNER, L., VERFURTH, C., and LYNEN, F. (1979). Studies on the Multi-Enzyme Complex of Yeast Fatty-Acid Synthetase. Reversible Dissociation and Isolation of Two Polypeptide Chains. Eur. J. Biochem. *94*, 189–197.

Wijffels, R., Kruse, O., biotechnology, K.H.-C. opinion in, and 2013, undefined Potential of industrial biotechnology with cyanobacteria and eukaryotic microalgae. Elsevier.

Woods, A., Munday, M.R., Scott, J., Yang, X., Carlson, M., and Carling, D. (1994). Yeast SNF1 is functionally related to mammalian AMP-activated protein kinase and regulates acetyl-CoA carboxylase in vivo. J. Biol. Chem. *269*, 19509–19515.

Worsham, L.M.S., Earls, L., Carrie, J., Keisha Gordon, L., M. Stephen, T., and M. Lou, E.-F. (2002). Amino Acid Residues of Escherichia coli Acyl Carrier Protein Involved in Heterologous Protein Interactions†. Biochemistry *42*, 167–176.

Worthington, A.S., and Burkart, M.D. (2006). One-pot chemo-enzymatic synthesis of reporter-modified proteins. Org. Biomol. Chem. *4*, 44–46.

Worthington, A.S., Rivera, H., Torpey, J.W., Alexander, M.D., and Burkart, M.D. (2006). Mechanism-based protein cross-linking probes to investigate carrier protein-mediated biosynthesis. ACS Chem. Biol. *1*, 687–691.

Wu, M., Singh, S.B., Wang, J., Chung, C.C., Salituro, G., Karanam, B. V., Lee, S.H., Powles, M., Ellsworth, K.P., Lassman, M.E., et al. (2011). Antidiabetic and antisteatotic effects of the selective fatty acid synthase (FAS) inhibitor platensimycin in mouse models of diabetes. Proc. Natl. Acad. Sci. *108*, 5378–5383.

Zhang, K. (2016). Gctf: Real-time CTF determination and correction. J. Struct. Biol. *193*, 1–12.

Zhang, F., Ouellet, M., Batth, T.S., Adams, P.D., Petzold, C.J., Mukhopadhyay, A., and Keasling, J.D. (2012). Enhancing fatty acid production by the expression of the regulatory transcription factor FadR. Metab. Eng. *14*, 653–660.

Zhang, Y.-M., Hurlbert, J., White, S.W., and Rock, C.O. (2006). Roles of the active site water, histidine 303, and phenylalanine 396 in the catalytic mechanism of the elongation condensing enzyme of Streptococcus pneumoniae. J. Biol. Chem. *281*, 17390–17399.

Zhang, Y.M., Wu, B., Zheng, J., and Rock, C.O. (2003). Key Residues Responsible for Acyl Carrier Protein and β-Ketoacyl-Acyl Carrier Protein Reductase (FabG) Interaction. J. Biol. Chem. *278*, 52935–52943.

Zheng, S.Q., Palovcak, E., Armache, J.-P., Verba, K.A., Cheng, Y., and Agard, D.A. (2017). MotionCor2: anisotropic correction of beam-induced motion for improved cryo-electron microscopy. Nat. Methods *14*, 331–332.

Zhou, Y.J., Buijs, N.A., Zhu, Z., Qin, J., Siewers, V., and Nielsen, J. (2016). Production of fatty acid-derived oleochemicals and biofuels by synthetic yeast cell factories. Nat. Commun. 2016 71 *7*, 1–9.

Zhu, Z., Zhou, Y.J., Krivoruchko, A., Grininger, M., Zhao, Z.K., and Nielsen, J. (2017). Expanding the product portfolio of fungal type I fatty acid synthases. Nat. Chem. Biol. *13*, 360–362.

Zimhony, O., Vilchèze, C., and Jacobs, W.R. (2004). Characterization of Mycobacterium smegmatis expressing the Mycobacterium tuberculosis fatty acid synthase I (fas1) gene. J. Bacteriol. *186*, 4051–4055.

Zivanov, J., Nakane, T., Forsberg, B.O., Kimanius, D., Hagen, W.J., Lindahl, E., and Scheres, S.H. (2018). New tools for automated high-resolution cryo-EM structure determination in RELION-3. Elife *7*.